FE Simulation Based Friction Coefficient Factors for Metal Forming

by

Xiang Ke

A Thesis Presented in Partial Fulfillment
of the Requirements for the Degree
Master of Science

Approved August 2013 by the
Graduate Supervisory Committee:

Jami Shah, Chair
Joseph Davidson
Steven Trimble

ARIZONA STATE UNIVERSITY

December 2013

ABSTRACT

The friction condition is an important factor in controlling the compressing process in metalforming. The friction calibration maps (FCM) are widely used in estimating friction factors between the workpiece and die. However, in standard FEA, the friction condition is defined by friction coefficient factor (μ), while the FCM is used to a constant shear friction factors (m) to describe the friction condition. The purpose of this research is to find a method to convert the m factor to u factor, so that FEA can be used to simulate ring tests with μ.

The research is carried out with FEA and Design of Experiment (DOE). FEA is used to simulate the ring compression test. A 2D quarter model is adopted as geometry model. A bilinear material model is used in nonlinear FEA. After the model is established, validation tests are conducted via the influence of Poisson's ratio on the ring compression test. It is shown that the established FEA model is valid especially if the Poisson's ratio is close to 0.5 in the setting of FEA. Material folding phenomena is present in this model, and μ factors are applied at all surfaces of the ring respectively. It is also found that the reduction ratio of the ring and the slopes of the FCM can be used to describe the deformation of the ring specimen.

With the baseline FEA model, some formulas between the deformation parameters, material mechanical properties and μ factors are generated through the statistical analysis to the simulating results of the ring compression test. A method to substitute the m factor with μ factors for particular material by selecting and applying the μ factor in time sequence is found based on these formulas. By converting the m factor into μ factor, the cold forging can be simulated.

DEDICATION

This research work is dedicated to my dear parents for their years accompanying and supporting in making my dreams possible and believing in my aspirations. This is also dedicated to my dear girlfriend who has so much understanding and always cheers me up in the low time. I also dedicate this to my friends, for their support.

ACKNOWLEDGEMENTS

I would like to express my sincere gratitude to my advisor Professor Jami Shah for his continuous encouragement, supervision and useful suggestions throughout the course of this research work. His vast knowledge, guidance and timely suggestions have been helpful in finding solutions to the problems encountered throughout this research endeavor.

My sincere thanks also go to Professor Joe Davidson and Professor Steven Trimble who provided a lot of valuable suggestions, and helped me to convert my research to a more valuable source for industry practical use.

I would also like to acknowledge the colleagues in the Design Automation Lab for their valuable support.

I would like to extend my sincerest thanks and gratitude to everyone who directly and indirectly supported me in the completion of this thesis.

TABLE OF CONTENTS

LIST OF TABLES

LIST OF FIGURES

1. Background

1.1   Introduction

Metalforming is defined as the process of converting raw materials into finished or semi-finished products with useful shapes and mechanical properties through processes such as forging, stamping, extrusion and rolling. The advantage of metalforming over cutting is that it changes the shape and dimensions of the workpieces without removing material. If used properly, it provides a greater benefit in saving materials as well as extra mechanical merits like higher structural strength gained through strain hardening. Metalforming techniques are progressing in the direction of net shape manufacturing, with more precise control on shape with no defects (Robinson, Ou, and Armstrong 2004, 54-59). According to Alting (Boothroyd and Alting 1994), metalforming involves three flows--material, energy, and information. When it is classified by stress systems, such processes are divided by six systems of stresses—compression, tension, tension and compression, bending, shear, and torsion. The upset forging process is one of the compression processes, in which there is no lateral constraint except for friction and consequently no three-dimensional confinement (Mielnik 1991).

Mechanical parts obtained through upset forging are very common in industrial practice, such as engine valves, coupling, bolts, and screws. They are stronger than an equivalent cast part or machined part. This is because the macrostructure of the material is continuous throughout the part, giving rise to a piece with improved strength

characteristics. To obtain this advantage, some specialized machines are required. Figure 1 (weiku.com) shows a 150kg pneumatic hammer which is a typical small size machine for the metal compression operation. It consists of an upper die, a lower die, and a power module that work together in the operation. During metalforming, the workpiece is placed between upper and lower die, and it is deformed under high compressing pressure provided by the power module when the two dies move towards each other. The die pair can be flat plates or a complex shape. The power module can be a fly wheel and slider crank or a hydraulic power module which includes hydraulic pumps and pipes. The compressing machine can be either a mechanical press or a hydraulic press, when it deals with small workpieces. Figure 2 shows a pennies press machine driven by human power; that is widely used to form souvenirs. When a penny is put in the machine, the user rolls the machine's handle and the penny is compressed into a much thinner plate with new marks on each side. When the workpiece with extremely large size is required to be compressed, the compressing machine with hydraulic power module is the only choice for such process. The hydraulic press machine, as shown in Figure 3 (koteco.co), which provides over ten thousands of tons compressing force, is a remarkable symbol of the manufacturing capability. It can be used in manufacturing of large components such as crankshafts for ocean-going cargo ships, and pressure containers for power generation systems.

Figure 1. Pneumatic hammer(weiku.com ; koteco.co)

Figure 2. Pennies press machine

Figure 3. 10,000 tons hydraulic press machine(koteco.co)

In the compression process, the friction affects the shape of the workpiece. When the workpiece contacts with the die, the workpiece is deformed mainly under the pressure normal to the interface, and at the same time the workpiece flows in the tangential direction as well. Such tangential flow depends on the friction condition of the die-workpiece interface. It would lead to higher equivalent stress, which reduces the workability of the metal block and generates failure such as cracks so that the metal block is rejected. Thus for controlling the quality of the product obtained through the compressing process, the friction condition on the die-workpiece interface is required to be controlled. In this research，the friction condition that is related with compressing process will be discussed.

1.2   Mechanics behavior related to upset forging

In upset forging process, the workpiece is under a uniaxial stress-strain state ideally. The calculation method of the stress and strain is important, especially for large strains in the plastic range. Two methods frequently used in calculation, are engineering stress and engineering strain, and true stress and true strain. The engineering stress is

$$\sigma_E = \frac{P}{A_0}$$

and the engineering strain is

$$\varepsilon_E = \frac{\delta}{L_0}$$

where A_0 is the original area, δ is the extended length, and L_0 is the original length. The true stress is

$$\sigma_{T} = \frac{P}{A}$$

where A is the instant area. The true strain is

$$\varepsilon_{T} = \int d\varepsilon = \int_{L_0}^{L_f} \frac{dl}{l} = \ln\frac{L_f}{L_0}.$$

where L_f is the final length of the test bar.

The calculation of engineering stress and engineering strain is easy in practice because only simple measurement data is required, but the results from tension and compression testing do not match well with each other. In contrast, the true stress and true strain are difficult to obtain, but they have a better consistency between tension and compression for applications involving large strain. The results are more convenient for accumulating strains, and are more accurate with the instantaneous area value used in the calculation. Therefore they are used commonly in research work. Since the engineering stress or strain and the true stress or strain can be easily converted, the investigation on the mechanical properties of material often is carried out in two steps. First, calculate the engineering stress and strain under particular test conditions; second, convert the engineering stress and strain to true stress and strain; where the true stress is

$$\sigma_{T} = \frac{P}{A} = \frac{P}{A_0} \cdot \frac{l}{l_0} = \sigma_E(1 + \varepsilon_E),$$

and true strain is

$$\varepsilon_{T} = \ln\frac{L_f}{L_0} = \ln(1 + \varepsilon_E)$$

The comparison between the engineering stress-strain curve and the true stress-strain curve is shown in Figure 4. These two curves overlap each other at the beginning, which indicates that their differences are small during the elastic deformation period.

Then the deviation between true stress and engineering stress grows with the increase of the strain; σ_T is to grow continuously, and σ_E grows slowly and then drops because of the necking phenomenon during the plastic deformation,. Figure 5 shows a typical engineering stress and strain curve. Elastic Modulus, yield strength, and ultimate stress are shown on the curve. Sometimes, the yield strength point is not obvious on stress-strain curve, and 0.2% strain is used as the division between elastic deformation and plastic deformation.
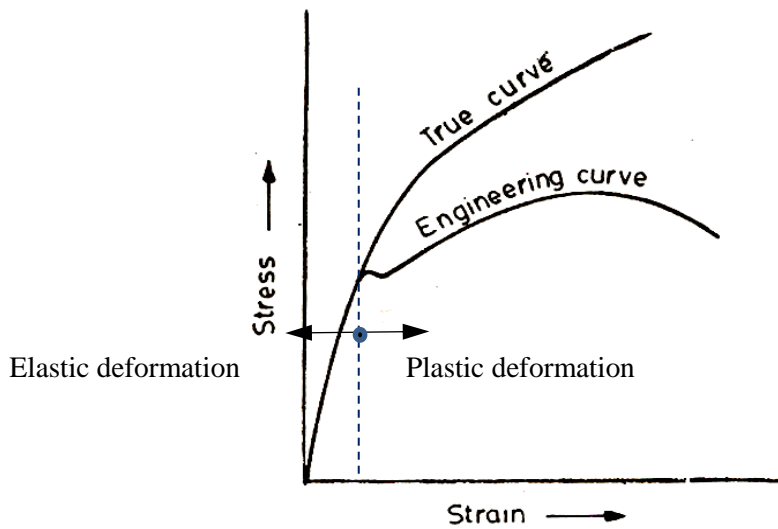
Figure 4. Engineering stress-strain vs. true stress-strain
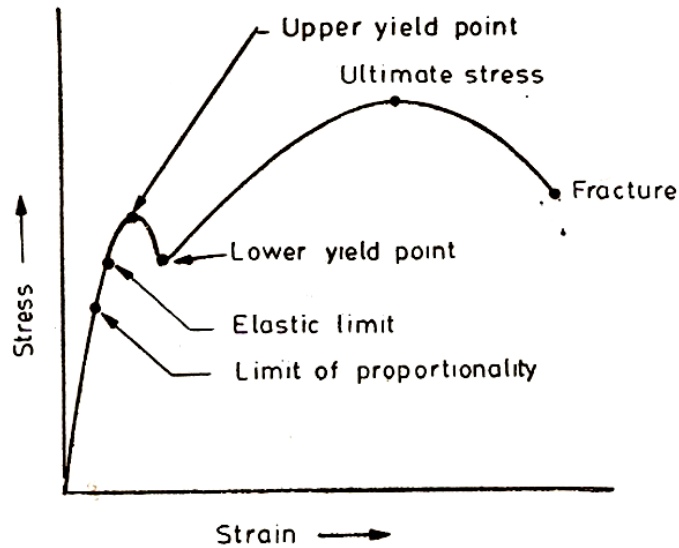
Figure 5. Typical engineering stress strain curve

Idealized stress-strain curves with plastic deformation are shown in Figure 6 (Mielnik 1991). There are four types of curves: type I, rigid-perfect plastic curve; type II, elastic-perfect plastic curve; type III, rigid-linear plastic curve are shown; and type IV, elastic-linear plastic curve.

a. Rigid-perfect plastic

b. Elastic-perfect plastic

c. Rigid-linear plastic   d. Elastic-linear plastic
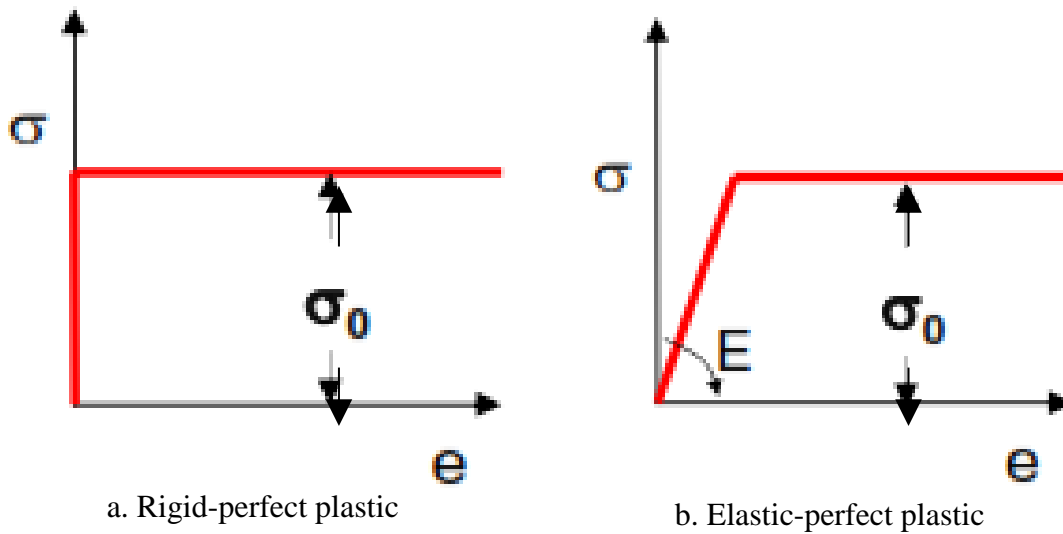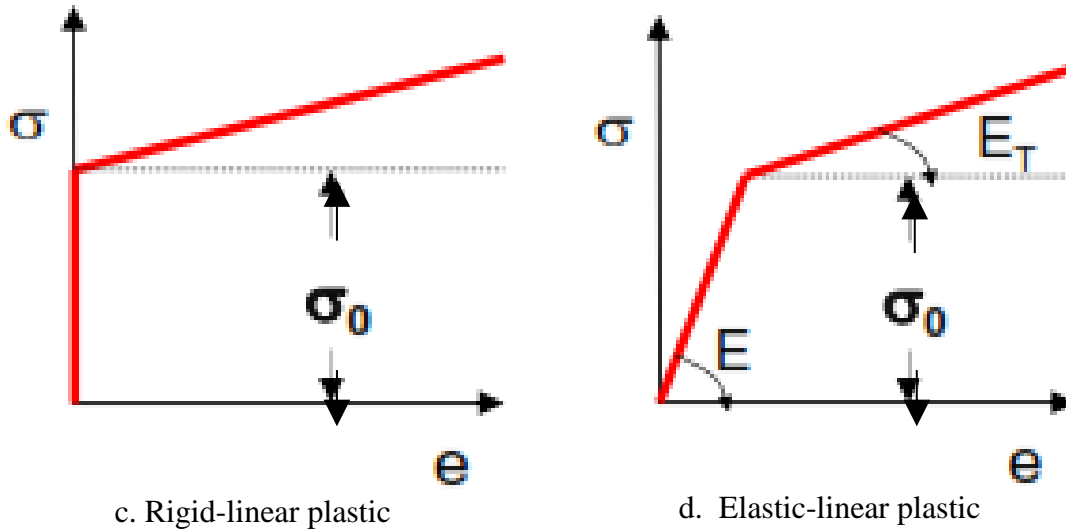
Figure 6. Idealized stress-strain curves (Mielnik 1991)

The engineering stress-strain curves of three typical ductile materials, aluminum 7075, carbon steel 1020, and stainless steel 303 are shown in Figure 7, Figure 8, and Figure 9 respectively (ASM International 2002). These materials can be simplified with an elastic-linear plastic material model and represented by three parameters, the Elastic Modulus (E), Yield Point (σ_0) and Tangent Modulus (E_T) for linear plastic, as displayed in Figure 6d.

Metalforming, such as upset forging, involves large strains and plastic deformation. In engineering practice, the period of elastic deformation is often neglected and the corresponding true stress after the yield point is named as flow stress for the large strain situation. As the elastic deformation is neglected and the plastic behavior of a workpiece is considered as incompressible, the Poisson's ratio of materials in all metalforming processes approaches 0.5.
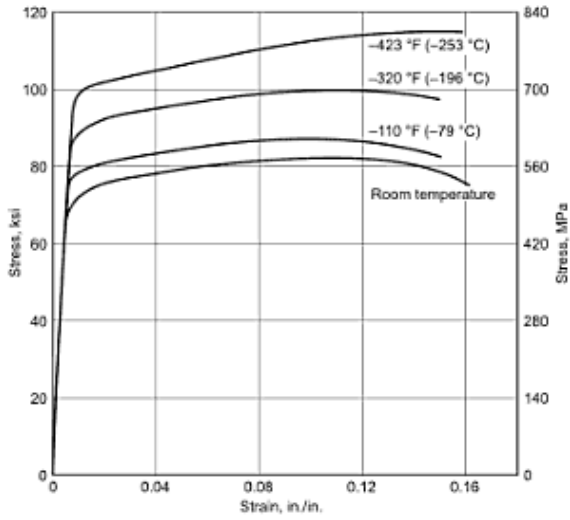
Test at room and elevated temperatures

Figure 7. Stress-strain curve of Al 7075-T6
at room and elevated temperatures (ASM
International 2002)
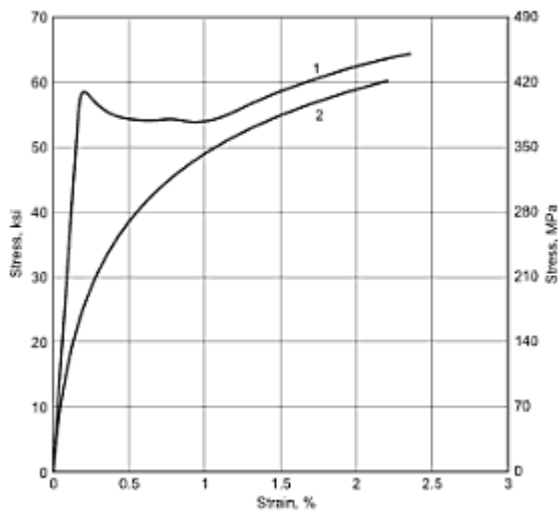
Curve 1 specimen is pre-strained at 250
and test in compression at room
temperature
Curve 2 specimen is pre-strained at room
temperature and test in compression at
room temperature

Figure 8. Stress-strain curve of Carbon
1020 steel
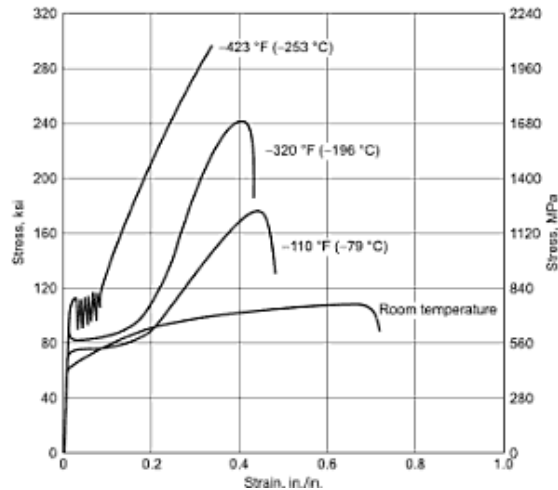
Annealed stainless steel bar and test at room and low temperatures

Figure 9. Stress-strain curve of Stainless 303

In the upset forging process, flow stresses in the workpiece depend on the strain path, temperature, and mechanical properties of the materials (Mielnik 1991). The strain path refers to the plot of consecutive strain state, in which a curve is joining two strain states, and it may be existing different strain paths between two states, and different process conditions result in different strain paths. Also, the strain path is sensitive to the geometry of workpiece (Shah and Kuhn 1986, 255-261). In the ring compression test, the cylinder workpiece is subjected to uniaxial load. The cubic element used for stress-strain state analysis in the block is subjected to biaxial stresses in the cylindrical coordinate system. Then the stress state can be represented by a axial compression stress σ_A and hoop tension stress σ_θ; and the strains corresponding to them are axial strain ε_A, and hoop strain ε_θ.

Figure 10 shows the strain paths from some deformation processes (Kuhn, Erturk, and Lee 1973, 213-218). The fracture locus is a plot on the axial strain-hoop strain

10

diagram which indicates the strain state when fracture happens during the analysis of the forging process. It only depends on the material and not on the strain path. The slope of the fracture locus has been shown to be ½, because the Poisson's ratio is 0.5 during the plastic deformation.

Relations between strain path and fracture locus is shown in Figure 11 (Shah and Kuhn 1986, 255-261) in which one can see how the strain path and fracture locus are related. The y-intercept on each fracture locus is a characteristic point. At this point, the fracture of the material occurs when only hoop strain is applied. According to M. C. Shaw (Shaw and Avery 1983, 247), it is a constant and should be ¾ of the observed strain when fracture happens in a uniaxial tensile test. So as shown in Figure 11(Shah and Kuhn 1986, 255-261), when fracture occurs in the plastic deformation period, all fracture locus from different materials are parallel to each other, with slopes at -0.5 and different y-intercepts.

For a particular process, when its strain path intersects with the fracture locus, the workpiece fractures at that particular point, that is, the stain the workpiece could bear reaches its limit. For material blocks with the same geometry, under different compression conditions, such as friction, temperature, there are two strain paths, path 1 and path 2. There are two different fracture locus for material A and material B. For each material, when the strain path rises above the fracture locus, fracture occurs.
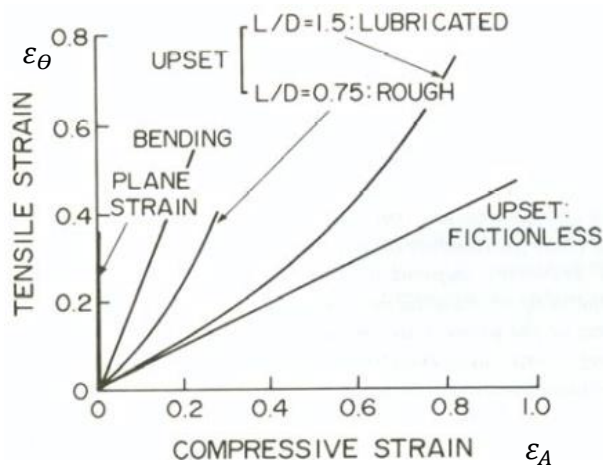
Figure 10. Strain paths for some deformation process (Kuhn, Erturk, and Lee 1973, 213-218)
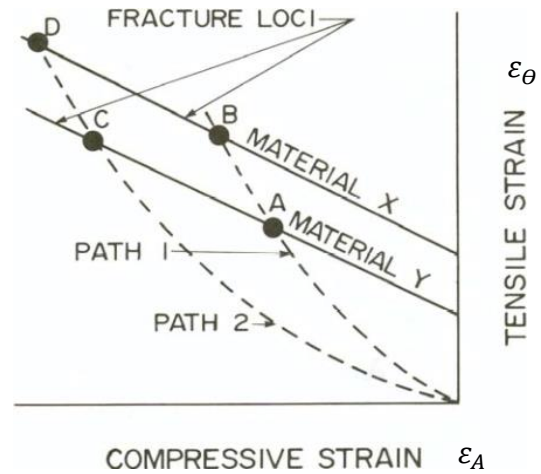
Figure 11. Superposition of fracture loci and strain paths (Shah and Kuhn 1986, 255-261)

Typical deformation states of the cylindrical specimen in compression test are shown in Figure 12. Figure 12a shows the initial geometry of the workpiece. The shape shown in Figure 12b happens when there is no friction between the die-workpiece interfaces. The upper and lower surfaces workpiece slide along the die surface during the axial reduction, and the side surface hold straight at all times. The deformation shown in Figure 12c happens when there is some friction on the die-workpiece interface. The upper and low surfaces of the workpiece slide a little along the interface, but frictional force holds the contact surfaces, so the material near the interface in the workpiece flows slower than the material in the middle. So slight barreling occurs in the cylindrical specimen. Figure 12d shown greater barreling happens when a very high friction factor is applied on the interface. From the deformed grid pattern, the flow of the material can be observed.
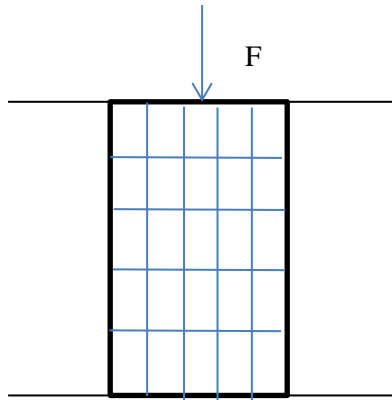
a. Uniaxial compressive set up of cylinder specimen
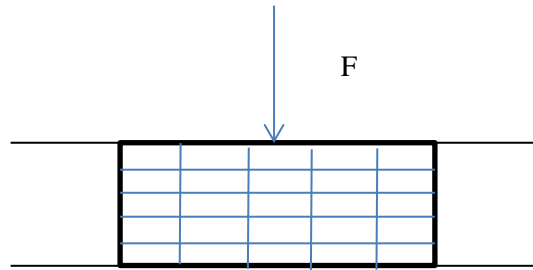
b. Compressed material with no friction
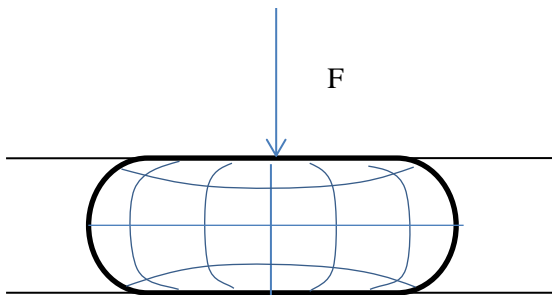
c. Compressed material with low friction
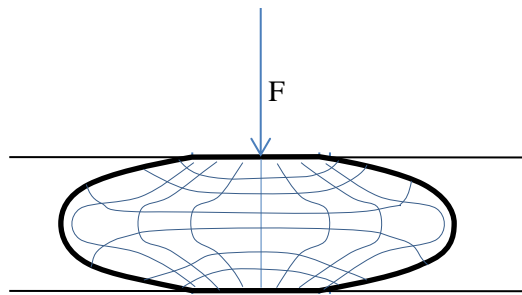
d. Compressed material with high friction

Figure 12. Compression of a cylinder material block

1.3 Problem statement

During the designing of cold upsetting process, we need to ensure that the desired deformation of the workpiece for certain material will be achieved without fracture. This is related with the material properties and the strain path for a certain process. It can be

adjusted by the friction condition on the contact interface between the die and workpiece. Traditionally, the friction condition is calibrated with the FCM, which is generated with constant shear friction factors, usually called m factors, by means of the ring compression test and it matches the actual manufacturing process well. However, the physical ring compression test is costly and time consuming. If friction factors can be obtained from numerical simulation by using the finite element method (FEM) software, such as ANSYS, such factors can be obtained easily and economically. However, in standard FEA, the friction condition is defined by the Coulomb's friction law with friction coefficient factor (μ), which is related with the normal stress on the contact interface and is different from the m factor. As the FCM generated by the constant μ do not have a good match with the FCM generated by the constant m, the problem is whether FEA can be used to simulate ring tests with μ and then generate a FCM in which m factor can be extracted for the cold upsetting process. In this thesis, numerical simulation and the reverse analysis method are used to map μ values with strain to find the best matches.

2. Literature review

    In this chapter, we will review four areas relevant to this thesis: characterization of interface friction condition, experimental studies of cold upsetting, computational simulation, and design of experiments.

2.1.   Ring compression test

2.1.1   The principle of the ring compression test and its application

    In upset forging, the shape of the slab, the interface condition, and the state of stress interact with each other dynamically. Thus the prediction of the stress-strain state and shape of the workpiece is complicated. A set of test methods for material mechanical properties has been designed traditionally to simulate the actual compression conditions for products. Among them, three commonly practiced property tests which involve uniaxial compressive stress are: conventional solid cylinder axisymmetric compression test, Polakowski's compression test and axisymmetric ring compression test (Polakowski 1949, 250-276). The two main drawbacks of the conventional solid cylinder axisymmetric compression test are the characterizing bulging of the cylinder side surface and the friction on the die-workpiece interface. The bulging effect does not simply accumulate but exaggerate the data obtained step-by-step during the compressing process, so it was necessary to eliminate it in each intermediate stage. Polakowski made great efforts in avoiding such inhomogeneous deformation and proposed a different method to deal with these issues (Mielnik 1991). It is also to compress a cylinder specimen but with more treatments on it. The process of Polakowski's compression test is divided into many

steps involving several cycles of loading and machining the cylinder specimen. The cylinder specimen was re-machined at each load step to keep the cylinder shape at the same height-diameter (*H/D*) ratio. Not only is the process of this method tedious but some critics pointed out that such a process can lead to errors up to 30 percent in data obtained (Mielnik 1991).

The axisymmetric ring compression test is a more commonly used test than the former two tests. A standard ring (Figure 13) made of the workpiece material is compressed between two flat dies. Lubricant is applied to the die-workpiece interface to provide the desired friction condition. Figure 13a is the top view of the ring specimen, Figure 13b is the cross-section view of the ring specimen with the standard ratio of outer diameter: internal diameter: height of the ring specimen as 6:3:2. If the die-workpiece friction factor is zero, the ring deforms the same way as a solid disk, that is, the internal diameter (ID) will increase. If friction is slightly more than zero, the ID increase is less up to some threshold value. Friction beyond this threshold results in the outer part of the ring flowing outwards and the internal part flowing in the opposite direction i.e. the ID decreases, as shown in Figure 14. This phenomenon is employed to quantify the friction value at the interface. The true advantage of the ring compression test compared to Polakowski's method is the way the barreling problem is treated and no force measurement is required.
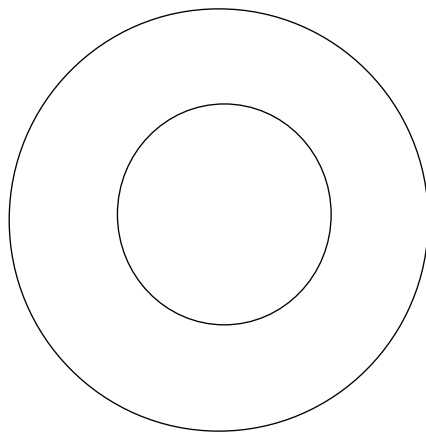
| a. Ring specimen's top view | b. Ring's intersection view |
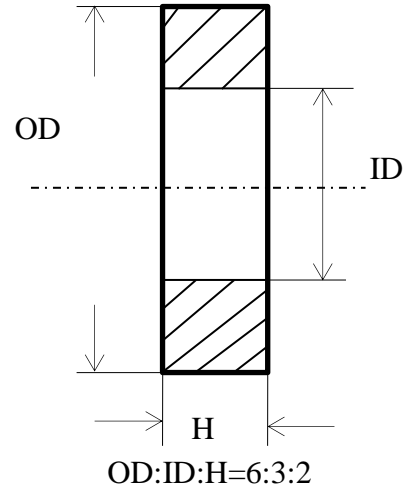
Figure 13. Ring compression test

| a. Good lubrication | b. Poor lubrication |

Figure 14. Compressed ring subjected to different friction condition

2.1.2 The description of the friction condition

In ring compression test, the friction condition on the interface between the die and ring specimen can be described in two ways, one is friction coefficient factor μ, according to the Coulomb friction law; another is shear friction factor m according shear friction law. In the Coulomb friction law, μ is defined as

17

$$\mu = \frac{F}{N} = \frac{\frac{F}{S}}{\frac{N}{S}} = \frac{\tau}{\sigma};$$

where τ is tangential stress; σ is normal stress; F is the sliding force on the interface along the interfacial direction; N is normal force on the interface along the normal direction.

While in the shear friction law, shear friction factor m is defined as

$$m = \frac{\tau}{\tau_0};$$

where τ is the shear stress on the interface along the interfacial direction; τ_0 is the shear strength of the material. Shear friction factor m is also referred to as 'constant shear friction factor', indicating that m is independent of interfacial stress (Hartley, Cloete, and Nurick 2007, 1705-1728).

According to the von Mises criterion, the tensile and shear yield stresses are related in the uniaxial stress condition as follows:

$$\sigma_0 = \sqrt{3}\tau_0$$

where σ_0 yield strength, and τ_0 shear strength.

Thus

$$m = \frac{\tau}{\tau_0} = \frac{\sqrt{3}\tau}{\sigma_0};$$

As it is discussed in Avitzur's work (Avitzur 1968), the average Coulomb friction coefficient factor, μ, can be calculated with measured m friction factors using the following relation:

$$\mu = \frac{m}{\sqrt{3}}\left(\frac{\sigma_0}{P_{ave}}\right),$$

where P_{ave} is the average surface pressure on the deformation specimen (Avitzur 1968).

In the metal compression process, the die would interact with the specimen to provide the internal force for shape change. It is desired to have the shape change controllable. Therefore, the internal force that causes the unrecoverable deformation would be of interest. When the material of the structure is at its yield point, the σ is equal to σ_y, thus the m factor would be

$$m = \sqrt{3}\mu.$$

For materials that do not show strong strain hardening behavior, the axial stress would keep the level at the yield strength, after the axial stress reaches the yield point, then the shear friction factor m would remain as $\sqrt{3}\mu$.

2.1.3 Established method for the friction calibration curve

As mentioned above, the interface friction condition has an important influence on the actual shape deformation of the specimen in the upsetting process. In order to evaluate the friction condition on the interface of the die and specimen, the friction calibration curve (FCC) is standardized into plots that represent the deformation in the ring as it is compressed. To plot the FCC, two parameters, the heights of the ring (H), and the internal diameters of the ring (ID), are measured in the ring compression tests. Both parameters are transformed into shape change ratios. The height reduction ratio is

$$h\% = \Delta H/H \times 100\%,$$

which becomes the x coordinate in FCC.

The internal deformation ratio is

$$id\% = \Delta ID/ID \times 100\%,$$

which becomes the y coordinate in FCC. The internal diameter response to the height

deformation is sensitive to the initial shape of the ring specimens. Figure 15 presents a

typical FCC plot. It shows the percentage decrease in internal diameter as a function of

the percentage of height reduction when a constant friction factor is applied on the

interface of the die and workpiece. FCC is plotted when dots on the chart are jointed to be

a curve. When a series of FCC are plotted on the same chart, the resultant chart is called a

friction calibration map (FCM). The friction factor can be obtained simply by measuring

the compressed ring and referring to the FCM for a certain material, as long as the

interface friction condition is considered constant.
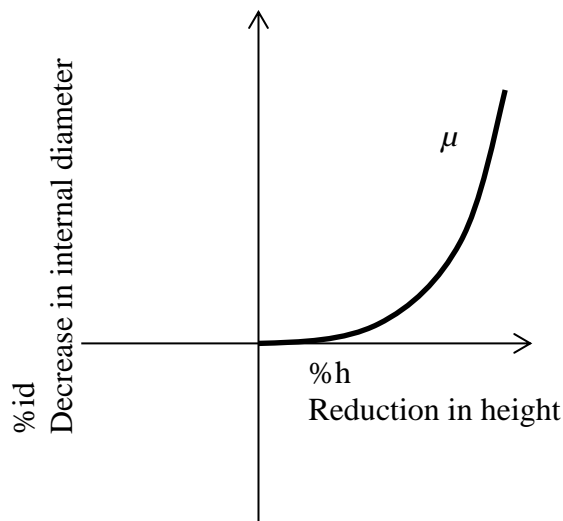
Figure 15. Typical FCC plot

The dimension ratio on outer diameter (*OD*): internal diameter (*ID*): height (*H*) is critical

in the ring behavior. Male's research (Male and DePierre 1970, 389) illustrates the

influence of the initial dimension ratio on ring compression test by carrying out

simulations on aluminum with initial dimension ratio at 6:4:2, Figure 16, and 6:1.6:2, Figure 17. The obvious difference is found by comparing Figure 16 & Figure 17. As long as the initial dimension ratios of ring specimens were the same, the FCM were the same.
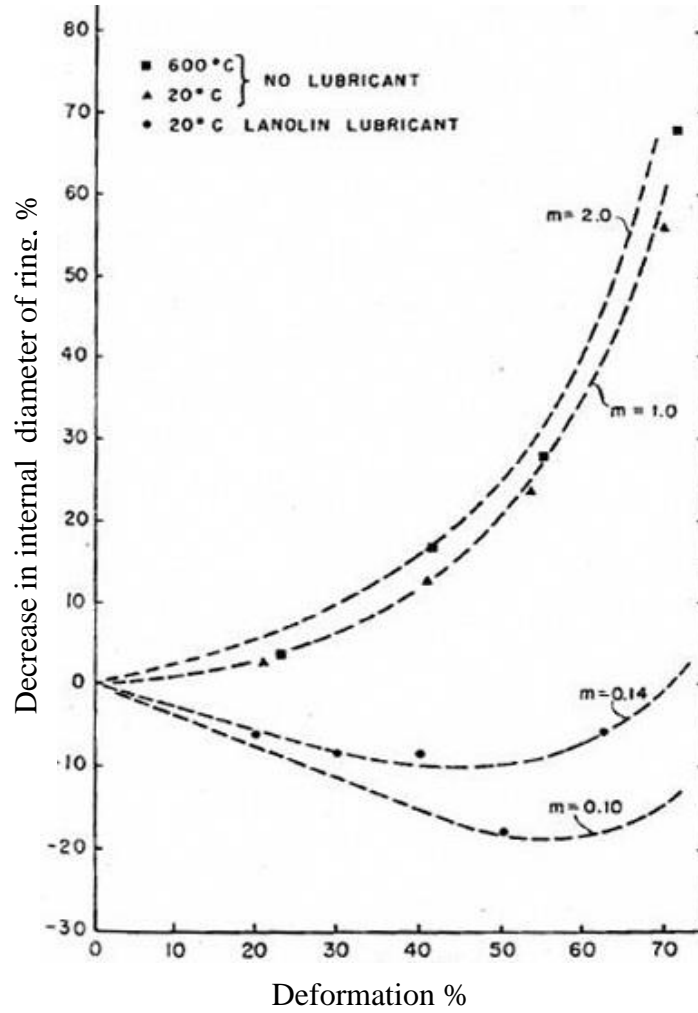
Figure 16. Aluminum deformation curves with initial ratio at 6:4:2
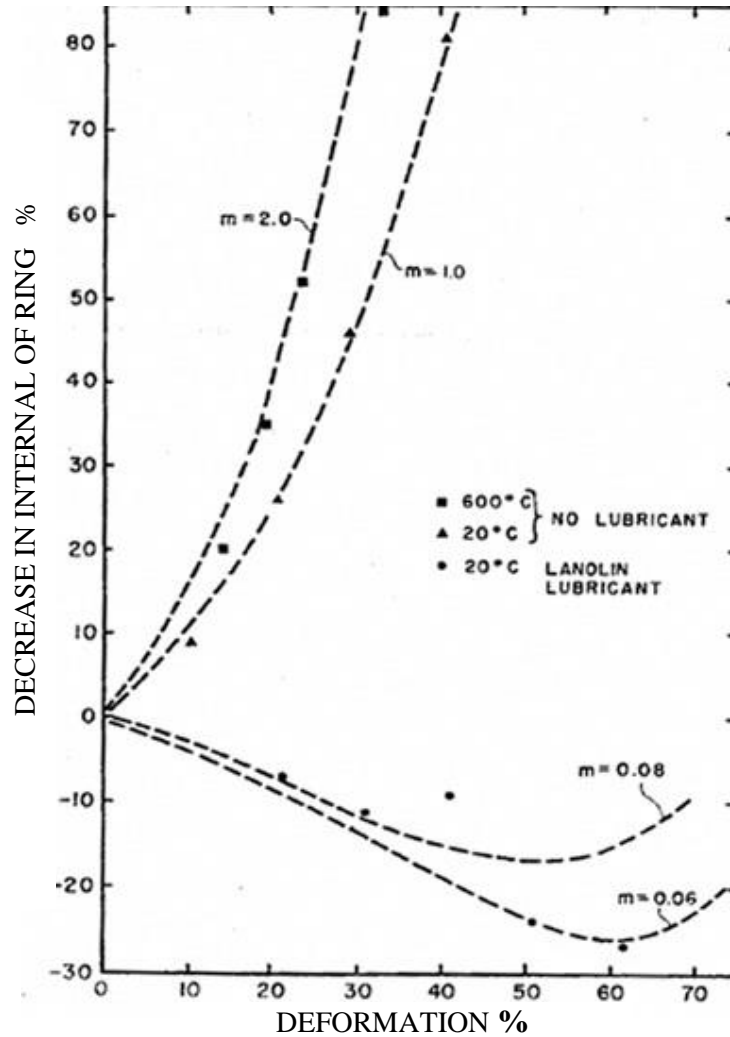
Figure 17. Aluminum deformation curves with initial ratio at 6:1.6:2

The *OD: ID: H* with 6:3:2 is widely accepted as standard specimen geometry in the ring compression test. Avitzur's (Avitzur 1964, 295-304) theoretical analysis was used to generate FCM Figure 18 (Male and DePierre 1970, 389). To find the friction condition, one conducts a ring test and then matches the results to calibration curves. Two alternative but equivalent measures can be used for FCC: friction coefficient factors, μ

22

(Coulomb's friction law) as shown in Figure 19 (MALE 1964, 38-46), and shear friction

factors, m (shear friction law) as shown in Figure 18.
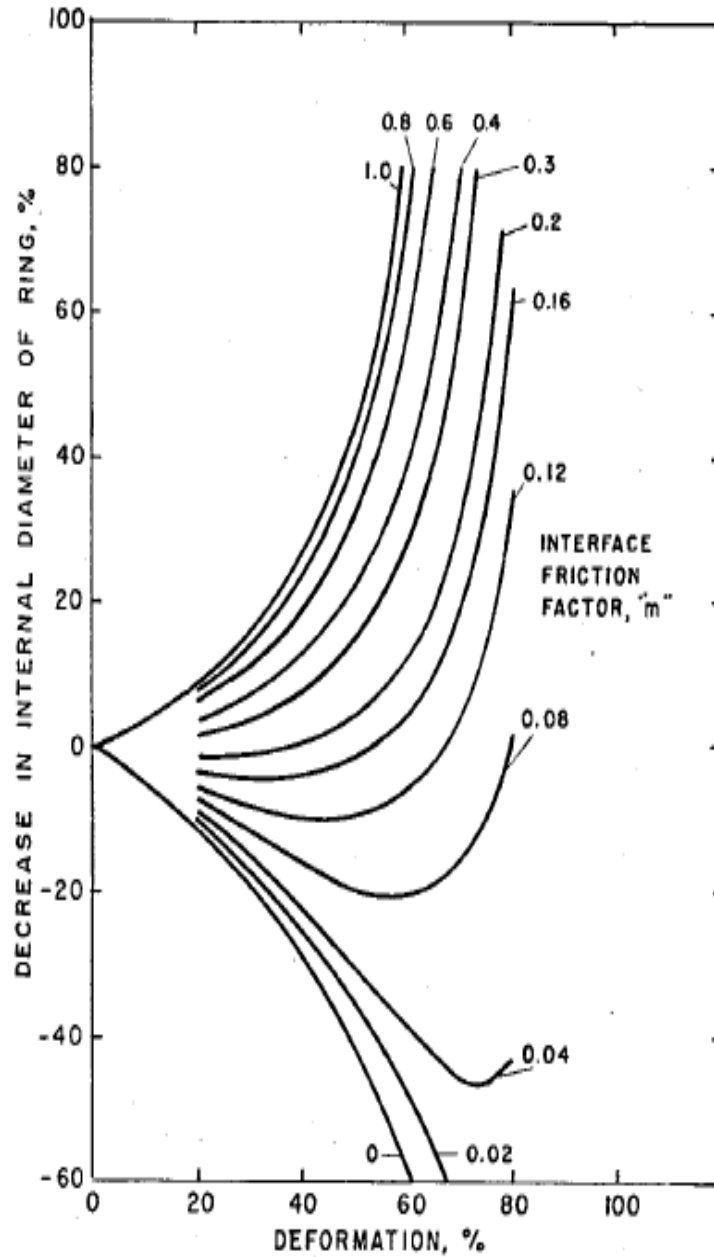
Figure 18. FCC by m friction

23
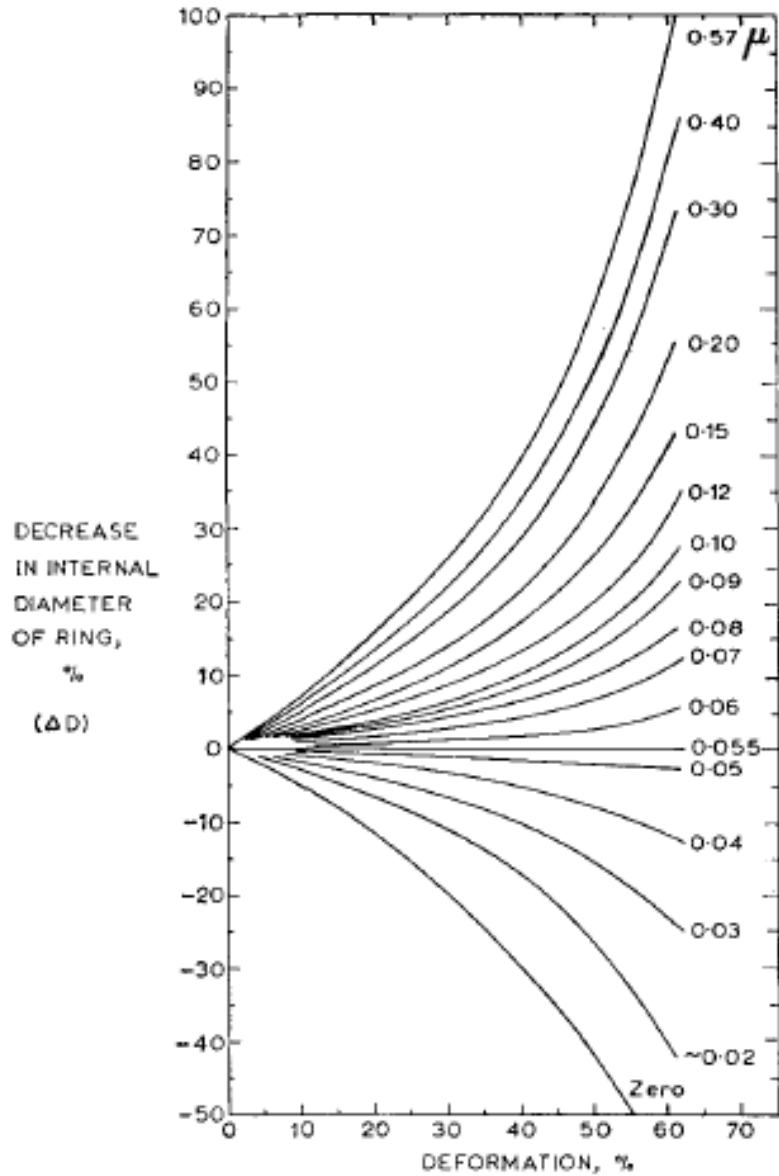
Figure 19. FCC by *u* friction (MALE 1964, 38-46; DePierre and Male 1969)

2.2   Experimental studies

2.2.1. The influence of the experimental parameters on the FCC

In Male's research (MALE 1964, 38-46), ring compression tests were calibrated with μ experimentally at different geometry, strain rates, and temperatures. He also standardized the initial geometry of the specimen as 6:3:2 (OD: ID: H) (MALE 1964, 38-46). The deformation of the specimen would vary at a different initial geometry ratio even if the friction factors were the same. When the rings took the standard geometry as initial geometry, the shear friction is 1 at the sticking condition. Annealing treatments were applied in preparing the testing materials such as Aluminum, Copper, α-Brass, Mild-carbon steel, and Titanium. Three strain rates (10^{-2}/sec, 10/sec, and 1.2×10^{3}/sec) were applied to specimens by a 50-ton hydraulic testing machine, a 60 ton vertical hydraulic press and an experimental drop – hammer respectively. The dies in the experiments were hardened to 470 VPN. Their surfaces were ground to get a similar surface profile. The specimens were treated at elevated and low temperatures. An open tube-furnace was used to pre-heated the specimens and liquid nitrogen were used to cool the ring to as low as sub-zero temperature. The analytical solution from Schroeder and Webster (Schroeder and Webster 1949, 289-294) was used to treat Male's experimental deformation data for μ to obtain the FCM.

Rudkins (Rudkins et al. 1996, 349-353) conducted the ring compression tests especially focused on the effects of the elevated temperatures on FCM and compared it with Hansen's theoretical calibration curves (Hansen, Bay, and Christensen 1988), which were based on another friction theory. The specimens were pressed by the 3000kN

hydraulic press machine. Medium carbon steel and a lead free cutting steel was manufactured into standard geometry for ring test, and a borehole was drilled which enabled the temperature measurement by means of thermocouple. Three reductions of height were used and no lubricant was applied on the interface. Force, displacement, and temperature were measured and recorded by means of Siemens data logging system.

Sanctis (de Sanctis et al. 1997, 195-200) compared experimental data and calibration curves and declared that that the shear friction can be a function of surface roughness, temperature, and strain rate. Al359/SiC/20P was the material used in their experiments. The turning machine and electrical discharge machining (EDM) were used to get the surface roughness of the ring specimens at 0.75 μm, and 0.25 μm respectively. Rings were compressed by servo-hydraulic computer-controlled test machine under isothermal and non-isothermal conditions and the strain rate provided by the test machine were 0.01/s-1 and 1/s. A graphite-based lubricant was applied on all the surfaces. When checking deformations of rings under elevated temperatures, a resistance furnace was used to heat the specimens to 300 and 450 $^{\circ}$C.

Li (Li et al. 2000, 138-142) studied Ti-6Al-4V alloy's friction behavior under various temperatures and strain rates. Hot-rolled commercial bar with 20mm diameter were machined to the standard geometry ratio, 15mm (outer diameter), 7.5mm (internal diameter), and 5mm (height). A computer-controlled, servo-hydraulic Gleeble testing machine was used to compress specimens lubricated by A5 glass lubricant. The ends of specimens were recessed 0.2mm to entrap the lubricant. Final true stains were kept below 0.7, so that the errors which are brought on by the recessed ends were expected to be

insignificant. Accurate temperature control and measurement were realized with thermocouples which were welded at the mid-span of the ring. He concluded that the temperature has greater influence on the interface friction when it is lower than 950 $^{\circ}$C and the strain rate has greater influence when the temperature goes over 950 $^{\circ}$C.

Robinson (Robinson, Ou, and Armstrong 2004, 54-59) provided physical experiment with clay to get μ factors with several lubricants. The clay was much softer than metal, so that the compression experiment was much easier and less expensive. FCM were provided by FE simulation. After the rings were compressed with different lubricants, deformation data was compared with the FCM to get the μ.

Split Hopkinson pressure bar (SHPB) was used to measure stress pulse propagation in a metal bar, and Hartley (Hartley, Cloete, and Nurick 2007, 1705-1728) conducted research which combined the ring compression test with the SHPB test scenario with the aim of understanding the influence of the friction condition on stress-strain in the compact problem. The schematic diagram is shown in Figure 20 (Hartley, Cloete, and Nurick 2007, 1705-1728). In the original SHPB test, a short cylindrical specimen was sandwiched between two metallic bars. A striker was fired as a first (incident) bar to compress the specimen at a strain rate over 10^3/sec. Strain gauges were attached to each bar to catch the stress waves. In Hartley's study, the ring shaped specimens were also compressed in the SHPB, and it was shown that the stress-waves change due to different interfacial friction.
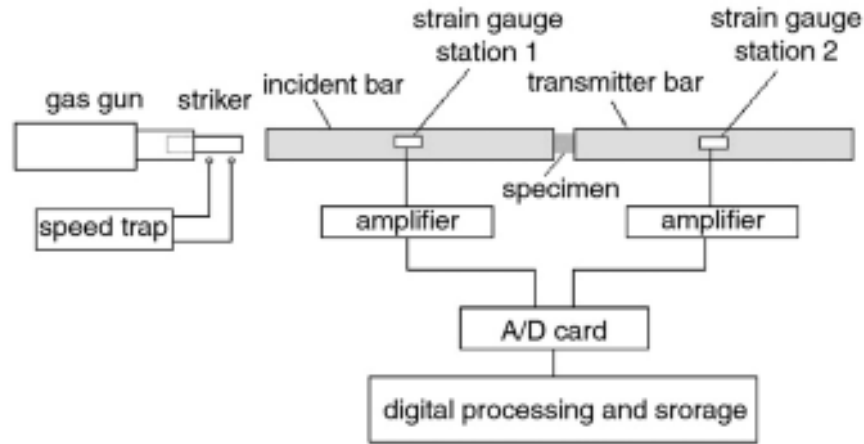
Figure 20. SHPB test schematic diagram (Hartley, Cloete, and Nurick 2007, 1705-1728)

Rao (Rao et al. 2009a, 128-136; Rao et al. 2009b, 1298-1309) conducted upset forging of cylinders to determine the ability of material to be forged for Al-4Cu-2Mg alloy. Lubricants and specimen aspect ratios were used to study the effects of these factors on the strain paths, and the failure locus is also found for this material. It is shown that when ductile fracture happens, the ratio between hoop strain and axial strain comes to the maximum point on the strain path. Ring specimens and cylindrical specimens were obtained from the same casted ingots.

2.2.2.   The intuitive method in deformation study

The grid pattern carved on the surface of a deformed metal is a very good method to evaluate the amount of metal deformation. For the cylinder specimen, a uniform grid pattern was marked on the lateral surface of the specimen before compressing. A load was applied on the plane surface of the specimen to observe the metal flows on macro scale. In Rao's experiment, ring specimens and cylindrical specimens were obtained from

the same casted ingots. The ring specimens were compressed to get the friction condition. The cylindrical specimens with gridded pattern on the cylindrical surface were compressed. The varied grid patterns were recorded by a machine version system continuously during the compression. Figure 21 (Valberg 2010) is a typical example of compressed cylinders with well lubricated and rough interfaces. It indicates that the hoop strain at the middle is larger than the hoop strain at the upper or lower position of the cylinder when frictions are applied on the interface. Good lubrication on the friction surface would reduce the difference of the hoop strain between the middle and upper or lower part of the cylinder. Thus it is concluded that the friction condition on the friction surface will affect the deformation state of the cylinders. Furthermore, the upset forging would be affected by the friction factors on the contact interface between the die and product. Of course, this kind of grid pattern method can be applied in the ring specimen in order to get the strain on the surface of the hollow cylinder.
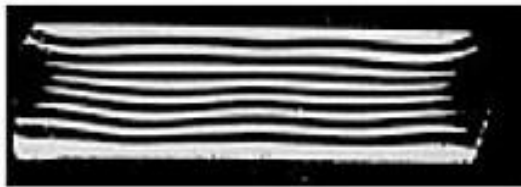
| a Lubricated specimen with lather grid pattern | b Lubricated specimen with lather grid pattern |
| a Un-lubricated specimen with lather grid pattern | a Lubricated specimen with lather grid pattern |
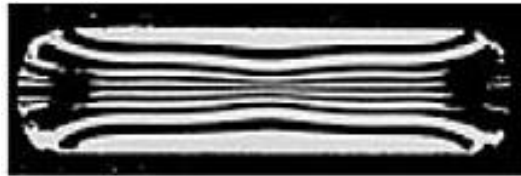
Figure 21. Deformed grid pattern after compression (a,b) graphite-oil lubrication; (c,d)unlubricated (Valberg 2010)

29

2.3   Computational studies of FCC

2.3.1 Classification of computational studies

The non-linearity of the plastic deformation is the problem to be solved in metal

forming calculation. According to Lange K. (Poꞌhlandt and Lange 1985), as shown in

Figure 22 (Poꞌhlandt and Lange 1985) plasticity theory falls into two types, elementary

theory, and technical theory of plasticity. The Elementary theory provides exact

equations for a particular metalforming process with a number of simplifying

assumptions. The technical theories of plasticity, especially those which could provide

the approximate solutions, are widely used in the computer-aided evaluation (CAE). As

early as 1969, Male (DePierre and Male 1969) solved the friction calibration problem by

writing a program with Fortran 4 and using an IBM Digital Computer. The algorithm of

the FORTRAN program took Avitzur's analysis (Avitzur 1964, 295-304) which was

based on the method of upper and lower bounds. Recently, more numerical methods were

applied in solving the metalforming processes. Dixit (Dixit, Dixit, and SpringerLink

(Online service) 2008) summarized the approximation methods applied in metalforming

and machining. Two main difficulties which restrict the application and accuracy of the

computational solutions are the uncertain mechanical properties of the material and the

uncertain friction condition during the manufacturing processes. These two difficulties

are the major causes of non-linearity in computation for solving the upset forging. Dixit

divided the computational modeling for manufacturing process into finite element

modeling and soft computing modeling to deal with non-linearity as mentioned above.

Finite element modeling needs proper material models and friction models through

30

assumptions so that the relation between shape deformation and loading in simulation has better consistent with the physical experiments. The soft computing modeling indicates that the uncertain material properties and friction conditions are not going to be fixed at the very beginning of the calculation, but will be calculated by the measurement of the loading and deformation. So some researchers referred to such a method as inverse method.
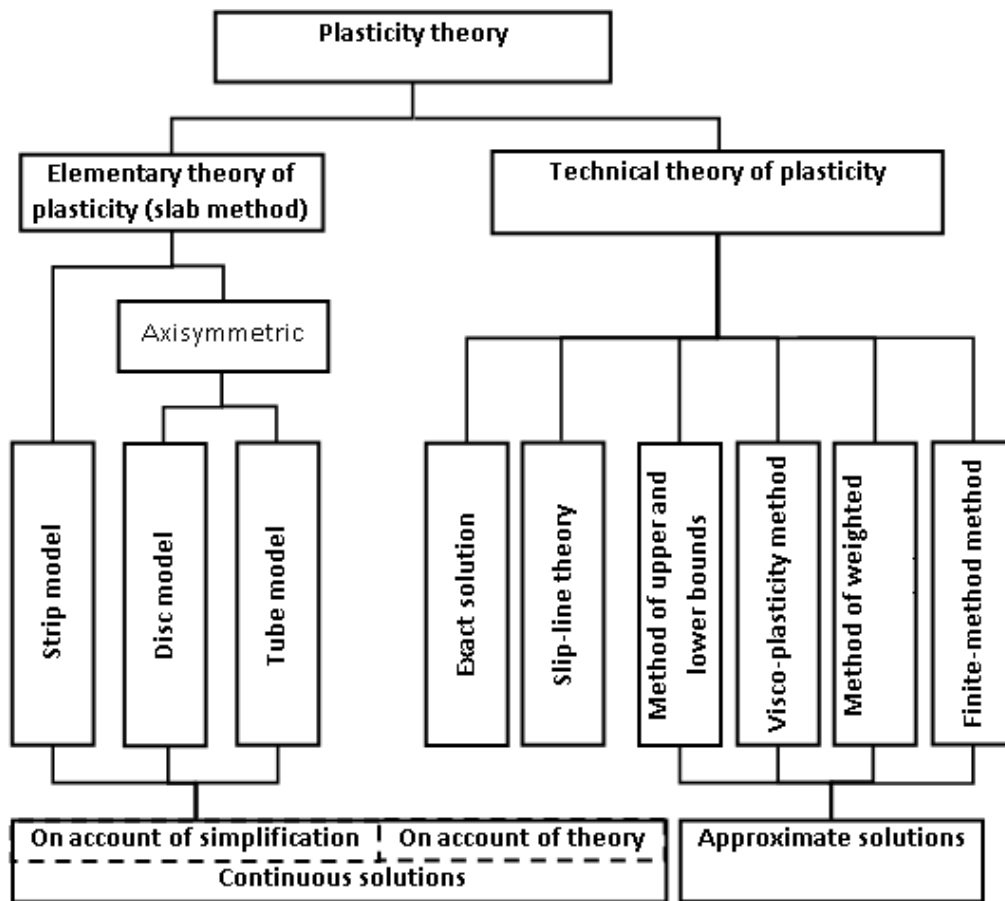
Figure 22. Flowchart showing various theoretical solution methods for metal forming problems (Po ̈hlandt and Lange 1985)

31

2.3.2   Soft computing technique

In the soft computing model, including fuzzy set theory, neural networks and genetic algorithm, the experimental data are taken as input to predict those uncertain parameters that affect the results, such as, plastic mechanical properties of the workpiece. Actually, the varied material mechanical properties (constitutive relations) and friction condition during the upset forging can be obtained in this way. This is especially useful to obtain these parameters which cannot be measured precisely.

Many researchers follow the soft computing methods to study upset forging. Lin and Chen (Lin and Chen 2005, 1059-1078; Lin and Chen 2006, 297-306) applied the Levenberg-Marquardt method in inversing calculation with experimental data to get the interface friction coefficient factor, μ, in the upsetting process. The resultant friction factor μ from the inverse calculation, is substituted back into a thermo-elastic-plastic finite element model, and the simulation results are close to Lin's (Lin 1999, 666-673) experimental data. Szeliga (Szeliga, Gawad, and Pietrzyk 2006, 6778-6798) conducted direct and inverse simulation for the forging process and used the inverse algorithm with sensitivity analyses. Through the sensitivity analysis, the mechanical properties of the material and process parameters obtained are very close to the actual ones. Behrens (Behrens and Schafstall 1998, 298-303) studied the stresses in the die in multistage cold forming processes. By using accurate μ on the contact interface he predicted the stresses in the die to avoid early damage. Neural network techniques were used to generate the dependency of friction values on contact conditions such as normal contact pressure,

sliding velocity, plastic strain and temperature, and then to obtain an adaptive friction factor *m*. Such adaptive friction factors are verified in a combined cup-backward full-forward extrusion process by comparing the measured data with simulation results from FEM analysis (FEA).

2.3.3   Introduction of FEA

The FEA technique was first developed for solving complex elasticity problems and structural analysis problem in civil and aeronautical engineering; however, it has been applied to problems such as thermal, electromagnetism and fluid dynamics. The FEA is a numerical technique for finding approximate solutions to differential equations. It is achieved by dividing up a continuum into small elements that can be solved in relation to each other (Finite element method), replacing the continuous problem by a discontinuous element network. Especially for static problems, the FEA can provide precise simulation of the physical experiment. These days, the FEM is used to simulate the physical experiment in order to save the expensive investment in the physical trials. Many commercial tools have made the FEA easier to be carried out in industry with reliable solutions. FEA solvers have already been used in the ring compression tests in previous research. Hatzenbichler (Hatzenbichler et al. 2012, 75-79) compared the simulation solutions of the ring compression tests with several commercial solvers, and observed differences in FCM among them. The differences were not negligible, and they suggested that the friction coefficient has to be calibrated for the software used for simulation.

2.3.4   FEA with different material modeling techniques

Generally speaking, FEA simulation of the metal forming process is a non-linear problem. It may involve geometry nonlinearities (GNL), material nonlinearities (MNL) and boundary nonlinearities (BNL). In the simulation of ring compression, the specimen is standardized to be an axial-symmetrical structure. The loading keeps symmetry to the middle plane, so that the geometry will not be a dominant issue. Due to the large deformation, the specimen will involve elastic deformation and plastic deformation, thus the material model is nonlinear. Also because of the involving of friction on the die-workpiece interface, the boundary condition is also nonlinear. The contact areas, contact pressures are changing during the simulation.   Thus the simulation of the ring compression test is a combination of MNL and BNL. Such a nonlinear problem is solved approximately in FEA in several ways. In the Newton-Raphson iteration approach, the tolerance error is defined as a convergence value, and this value is used to determine the size of each load step in each iteration. The convergence value can be displacement or force according to the convergence type. Also, the stiffness matrix is an important factor. If the stiffness matrix is updated in each iteration, it would take a lot of effort to generate the new stiffness matrix.

The FEA input parameters include material models and friction models. Because of the uncertainty of these models, proper selection and definition of the material and friction models is critical for the FEA simulation. Elastic-plastic (E-P), Rigid-plastic (R-

P), and Rigid- viscoplastic (R-V) are the commonly used material models as shown in Figure 23 (Mielnik 1991).
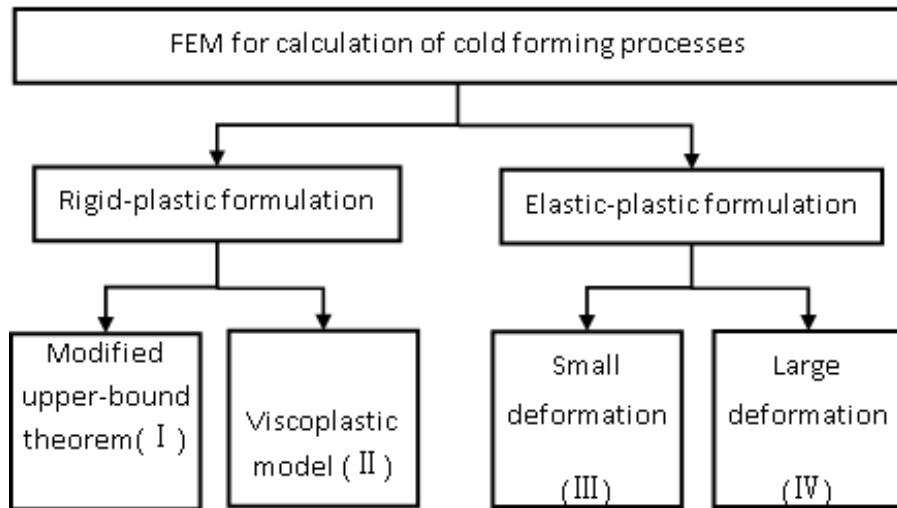
Figure 23. Flowchart showing some FEMs for analyzing cold forming processes
(Mahrenholtz and Dung 1987, 3-10)

2.3.5   FEA with different friction modeling techniques

Similar to the material model, many friction models were proposed and studied. Hayhurst (Hayhurst and Chan 2005, 1-25) proposed the use of a combined Coulomb and friction factor model to describe the frictional behavior between the workpiece and the die. He claimed that with the aid of accurate stress-strain curves, the friction model would provide an accurate prediction of upset forging. Danckert (Danckert and Wanheim 1988, 217-220) also tried to set up a better friction model for the FCM. He claimed that neither μ nor m friction is generally valid. While μ factor is only valid at low normal surface pressures and m factor is only valid at high normal surface pressures.

Sahi (Sahi et al. 1996, 286-292) proposed a semi-analytical model for the ring test with a visco-plastic material model to evaluate the friction factor m. The relationship

between the strain-rate sensitivity exponent *n* and friction factor *m* was shown in this analysis.

Yang (Yang 2007, 289-300) proposed a refined friction model that works for steady or unsteady three-dimensional processing, such as the axisymmetric and plane strain cases. With the help of simulation, Joun (Joun et al. 2009, 311-319) with the help of simulation, observed the difference between two friction laws, the Coulomb's friction law and the shear friction law, in ring compression test and other processing methods. Cristino (Cristino, Rosa, and Martins 2011, 134-143) studied the influence of surface roughness and material strength on μ factor. He proposed an operator based on the sigmoid function. He incorporated the combined influence of both phenomena in a modified version of the Amonton-Coulomb's friction law by carrying out ring compression experiments and simulations.

From 1990 to 1999, Lin (Lin 1995, 239-248; Lin 1999, 666-673; Lin and Lin 1990, 599-612) adopted the thermo-elastic-plastic model for material definition, and developed a hydrodynamic lubrication model for the description of interface friction. FEM was applied and the experimental data from the forming process under a warm forming condition was adopted as input to the deformation simulation for the inverse methodology. Full film lubrication, and mixed and boundary lubrication were applied. He noticed that the die-workpiece <u>interface friction was not constant during the loading and could be regarded as a function of deformation of a workpiece</u>*[1]. The calculated forging load and the deformed shape of the workpieces were in good agreement with the results

---

[1] This observation will be exploited in this research

obtained from the upsetting experiments. He also considered the difference between different regions on friction condition.

In Guerin's research (Gu érin et al. 1999, 193-207; Wagener and Wolf 1995, 22-26), Bay-Wanheim's friction model (Bay 1987, 203-223) was adopted in the simulation on the upsetting slide test (Figure 24). He also mentioned the limitations of Coulomb's friction model in the single coefficient μ, and the advantage of Bay-Wanheim's friction model over the Coulomb's friction model was discussed by comparing the experiments, analysis and simulations. In his work, when reduced contact pressures become greater, the μ will decrease with the increase of contact pressure.
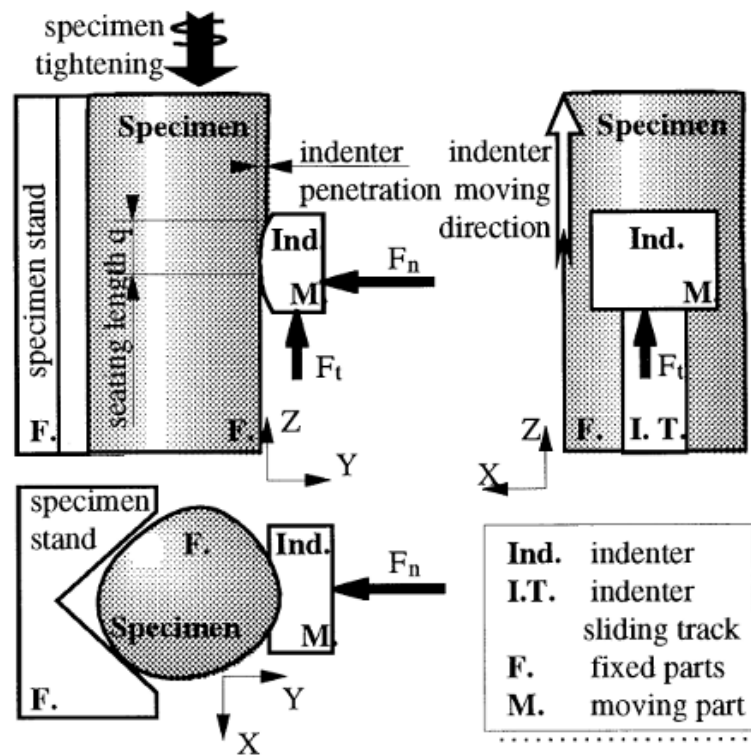
Figure 24. Layout of upsetting slide test (Gu érin et al. 1999, 193-207)

Noh (Hoon Noh, Ho Min, and Bok Hwang 2011, 947-955) observed the deformation characteristics for the tool/workpiece interface. He studied surface expansion, its velocity, and pressure distributions exerted on the die surface, relative sliding velocity between die and workpiece, and the sliding distance along the die surface. As mentioned previously, several friction models (Danckert and Wanheim 1988, 217-220; Hayhurst and Chan 2005, 1-25; Hartley, Cloete, and Nurick 2007, 1705-1728) were proposed, however, μ friction and m friction are still the most adopted indicators applied in the ring compression test study.

Sofuoglu (Sofuoglu, Gedikli, and Rasty 2001, 338-348; Sofuoglu and Gedikli 2002, 27-34; Sofuoglu and Rasty 1999, 327-335) developed a technique, which is called the open die backward extrusion test (ODBET) to calibrate the friction with simulation. Figure 25a shows the layout of the test. A cylinder specimen is placed between flat upper and lower platens. On the upper platen, a through hole is drilled and the specimen is placed concentric with the hole where the material can flow out during the compression process. Figure 25b shows that during specimen compression, material is extruded from the hole on the upper platen. With this technique, μ is calibrated with the height reduction and extrusion height of a cylinder specimen and the calibration plot is shown in Figure 25c. In this plot, the x axis is the reduction ratio, and the y axis is the material extrusion height ratio. Sofuoglu pointed out that the friction calibration curves (μ) are affected by the material properties and test conditions after conducting physical ring compression test as well as simulation with elastic-plastic material model.

upper platen

cylindrical
specimen

Ux=0

lower platen

symmetry axis
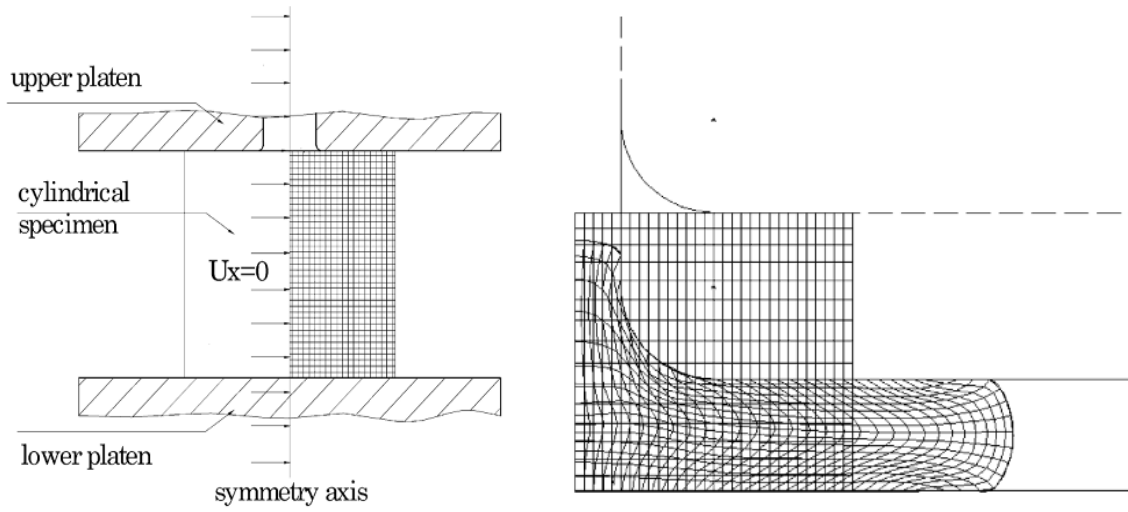
a. Layout of ODBET

b. Simulation of ODBET
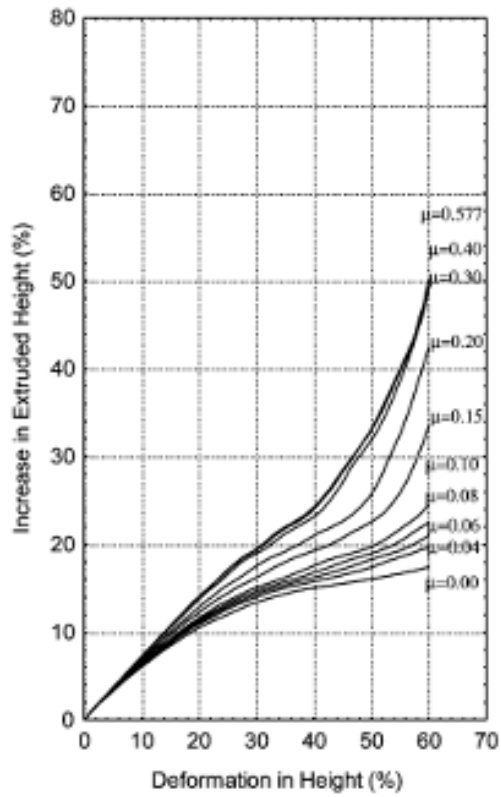
c. Calibration of μ

Figure 25. Sofuoglu's ODBET

39

3. Research overview

The die-workpiece friction condition in upset forging is an important factor which will influence the deformation of the workpiece, stress on the die, and fracture of the workpiece. In the upset forging process, such friction is described by the m factor according to the shear friction law. In ANSYS's solver, the friction is defined by μ factor according to the Coulomb's friction law. Ring compression test is widely used to calibrate the friction factor by measuring the changes of internal diameter and reduction of the ring. To determine the friction factor, workpiece material is used to manufacture a ring specimen and m factor is obtained by a ring compression test using the same die and lubricant. The purpose of this research is to find a way to use a proper setting of μ to simulate the compression process in the FEA software, so that the setting of μ can be used to replace the specific m for a particular material in simulation.

3.1   Alternative Strategies

Two possible strategies are considered to replace the m factor by the μ factor. One is applying different regions with different μ factors, i.e., a multi-regions strategy (Figure 26); the other is applying different μ factors according to the axial reduction volume, i.e., a multi-stages strategy (Figure 27). Before conducting detail treatment on μ, decision making is carried out by comparing the advantage and disadvantage of these two strategies.

a. The multi-regions strategy: The reason that it is possible to apply the multi-regions strategy is that the ratio between areas with a different μ will influence the

40

deformation. When the ring specimen is compressed, the total contact regions will change in size, so the ratio between areas with different values of μ would change. After the initial contact region is divided, the friction coefficient factors in the sub-regions are assigned with different values of μ, such as μ_1, μ_2 as shown in Figure 26. The area ratio of different regions is uncertain during the compression. When a combination of μ_1, μ_2 can correctly simulate the deformation equivalent to the value of m, then the m is obtained. However, this cannot provide useful information to generate new combination of μ values for another m value.
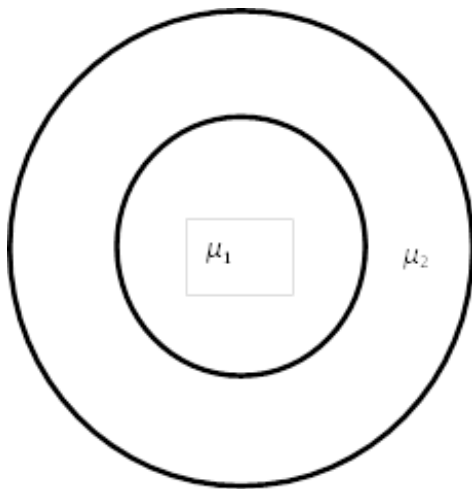
Figure 26. Apply different regions with μ_1 and μ_2
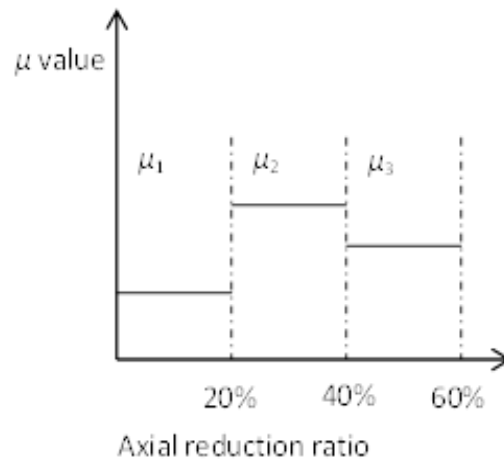
Figure 27. Apply $\mu 1$, $\mu 2$ and $\mu 3$ in sequence

b. The multi-stages strategy: Since the friction condition on the interface between the die and specimen influences the sliding of the interface, and then influences the variation of the internal diameter of the ring specimen, it is possible that the incremental quantity of the diameter of the ring specimen corresponding to the axial reduction changes when the boundary conditions change. Also, the material deformation that has

41

already happened would not be influenced; the variation of internal diameter of the ring specimens is accumulated during the axial reduction of the ring. Thus the deformation, that is, the change of the diameter can be accumulated stage by stage. Therefore, it is possible to find out the friction condition on the contact interface between the die and the specimen by measuring the deformation of the ring specimen. That is to say, at each stage of the deformation, a friction factor, μ, can be found through the variation of the diameter of the specimen, and several values of μ can be obtained through the different deformation at different stages. The advantages of this strategy are that, if it works for one scenario, it would be as simple as curve fitting for other scenarios. Data, such as those related with the influence of friction on deformation for a particular compressed material, can be reused. Therefore, this is a better approach because we can obtain a set of new μ factors to replace another equivalent m factor.

Based on above discussion, it is the multi-stages strategy that was investigated in this research.

3.2   Research procedure

The quantitative relationship between friction factor and deformation for the selected material is needed for the multi-stage strategy. The design of experiment (DOE) method can be used to get such a relationship. Before carrying out experiments on the simulation for statistical analysis, it is important to establish a reliable FEA model. This process is shown as a flowchart in Figure 28.

The first step is to set up a non-linear baseline FEA model and use this model to simulate the compressed ring to get a FCC with a constant μ factor, and compare the simulation with existing data from the recent research. The second step is to verify the FEA model with mechanical properties of different materials to make sure that the established FEA geometrical model's deformation corresponds to the change in the material. The third step is to observe the barreling in the FEA simulation to get the detailed contact condition in the FEA. The fourth step is to carry out a simulation with a three-stage (just pick a 3 stage process for example) compression process by using three μ in sequence to see how the variation of μ influences the deformation of the ring. With information gained from the experiments listed above, modifications will be required for the baseline model, and then a reliable FEA model will be established for the multi-stage μ model.
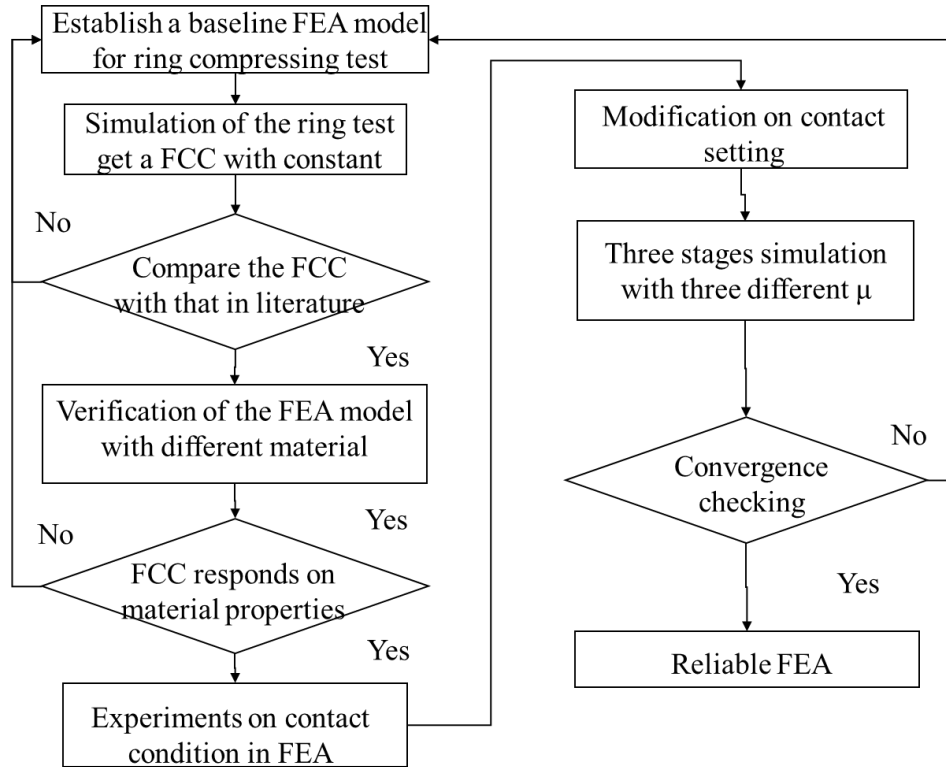
Figure 28. Flow chart of the research procedure

To devise the multi-stage μ model, a DOE must be carried out through FEA simulation to establish the relationship between material properties and deformation when a particular μ factor is applied to the interface. This can be further broken down to 4 sub-steps as it is shown in Figure 29.

a. Use DOE method to get the factor combinations for experiments in statistical analysis. The material model is adopted an elastic-plastic material. Thus the deformation pattern of the material is relevant to elastic-plastic analysis criterion by Elastic Modulus, Yield Strength, and Tangent Modulus.

b. Run FEA simulation with all material property combinations defined by DOE method for selected μ factor.

c. Carry out DOE analysis with different materials at each selected reduction ratio, so that the quantitative relationships between deformation and material properties are obtained at the selected reduction ratio and at a particular μ factor.

d. Go through sub-step b and c for all μ factors
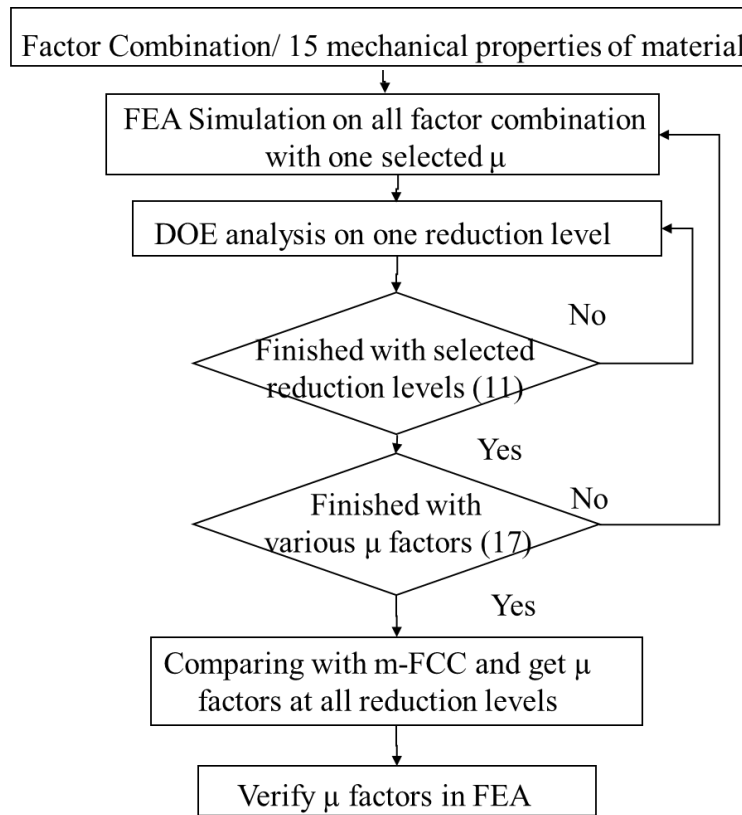
Figure 29. Flow chart of selection of μ factors

After these steps are done, quantitative relations between deformation and material properties are obtained for all reduction ratios and μ factors which are of interested. When the *m* factor for the interface and the workpiece material are determined, the μ factors whose deformations are closest to the deformation of FCC with m factor at

45

each reduction division point are used. The one applies the set of μ factors stage by stage in sequence in the FEA and compare its deformation with the deformation by the m factor, so that the correctness of the substitution would be verified.

3.3   Design of experiment

The quantitative relationships between material mechanical properties and deformation at a particular μ factor and the particular reduction ratio are to be obtained from statistical analysis through FEA simulation through DOE analysis. When analyzing properties with the statistical method, good experimentation planning is important in improving the computation efficiency by reducing the number of runs required. DOE became an important science topic, along with the development of technology, commercialization, and product realization activities. Applications of DOE include: evaluating physical objects, chemical formulations, structures, components, manufacturing process improvement. Today, the usage of DOE even extends to the non-product-development setting (Montgomery 2009).

The FCM developed from ring compression reflects the material behavior obtained in the manufacturing process. DOE can be used to find the relationship between material properties and the FCM.

Properties of the actual materials and some other parameters in the ring compression process are not controllable in physical tests. Material properties used for iterations can be suggested through DOE, but not all iteration of material properties is

possible due to material availability. However, software can work well in simulating any material property combinations because of the development of FEA simulation software. It is reliable to carry out a series of simulations with controllable parameters in the material compression problem. In this research, simulations were organized and carried out with a DOE strategy.

Generally, 7 steps are needed to carry out the DOE. The first one is the recognition of problem statement. In this research, DOE is applied for establishing the relationship between material properties and deformation under different friction factors. The second step is the selection of the response variable. The third step is the choice of factors, levels and ranges. The fourth step is the choice of the experimental design. The fifth step is the performance of the experiment. The sixth step is the conducting a statistical analysis of the data. The seventh step is drawing conclusions and recommendations (Montgomery 2009). This research uses the strategy discussed above. Following such procedures, Davim (Davim and MyiLibrary 2012) also carried out case studies on free-forming of a conical cup, chip formation in machining, and drilling numerically with the help of DOE. DOE is done according to the standard DOE procedure for the FEA simulation on ring tests in this research.

3.3.1   Objective of the experiment

The friction factors and material properties have important influence on the actual shape deformation of the specimen in the upsetting process. The purpose in this research is to find a method to determine the proper μ in different stages of the upsetting process

to reach the desired shape deformation. The desired deformation refers specifically to curves plot in FCM under the constant shear friction. Through the DOE, relationship between deformation, material properties, and the μ factors are determined quantitatively.

3.3.2 Selection of response variables

The concern of the ring compression test is that the diameter variation of the internal cylinder of the ring specimen corresponding to the axial reduction in the compression process. As the diameter variation and axial reduction are presented in the form of friction calibration curve, the characters of the curve can be also treated as the characters of the ring compression test. The slope of the FCC curve is one of them, and is used as the response variable in the DOE simulation. Details of the usage of the deformations are discussed in the next chapter.

3.3.3 Potential factors to be used

In this research, DOE analysis is used extensively, and the research consist of a serial of DOE analysis. μ factors and reduction ratios of the ring are important factors that determine the shape of the ring sample after compression process, and they are used as constants in each DOE analysis. After recording the shape of the ring samples at various conditions during the compressing procedure, the data from the same factor and same reduction ratio are grouped for one of the DOE analysis in the research. The range of the μ factor used in this research is from 0 to 0.57. The selected μ factors are 0, 0.02,

0.03, 0.04, 0.05, 0.06, 0.07, 0.08, 0.10, 0.12, 0.15, 0.20, 0.30, 0.40, and 0.57. The selected reduction ratios are 5%, 10%, 15%, 20%, 25%, 30%, 35%, 40%, 45%, 50%, and 55%.

The Poisson's ratio represents the strain ratio of the workpiece in the transverse direction to the axial direction. The plot in the FCC is based on the measurement of axial reduction and diameter dilation of a ring specimen. The Poisson's ratio affects the FCC plot. In previous research, it has been shown that the strain rate of the processing and temperature will affect the deformation of the compressed ring.

The hardness of the surface is used to represent how difficult it is to deform the surface of a material within a small region. So it will affect the interface's micro-topology resistance to the compressing. The friction condition is related to the micro-topology of the interface. It is said that the friction on the interface is different along the area during a compression process and so the hardness can also be a potential factor.

The material is described by a bi-linear elastic-plastic model. Smooth constitutive curves are converted to a bi-linear curve with three parameters: the elastic modulus, the yield strength, and the tangent modulus. So the factors that may affect the deformation results are Poisson's ratio; temperature; strain rate; hardness of surface; elastic modulus; tangent modulus; and yield strength.

3.3.4   Selection of potential factors

The Poisson's ratio is assumed to be a constant, so it is a not one of the variable factor for the DOE. The data of hardness is not available in previous physical experiments. Hence, though the surface hardness is considered in the FEA simulations

and considered as contact stiffness, the model cannot be validated as no comparison can be done between FE simulation and experimental results. Therefore, the contact stiffness is assumed to be a constant. It is assumed that the temperature and strain rate's effects on the FCC are because of their influence on material constitutive relations. So these two factors are taken care of in the constitutive relationships. The bilinear constitutive relationships are used to simplify the general constitutive curves. The linearized relation of points on the constitutive curve before yielding was used for elastic modulus. The linearized relation of points after yielding was used for the tangent modulus. The intersected point of these two lines was considered to be the yield point. Thus factors which are going to be used in the experiment are the three characteristic performances of a material, that is, Elastic Modulus, Tangent modulus, Yield strength.

3.3.5   Factor levels

The elastic modulus is the slope of the first section of the bi-linear curve. The yield strength is the intersection point of the first linear section and the second linear section. The tangent modulus specifies the slope of the second section, where plasticity is the dominant cause for deformation. By checking the material handbook(United States. Dept. of Defense 1966), 28 constitutive curves of metals were selected from common material catalogs such as steel, aluminum, magnisum, nickel, at various temperatures, from room temperature to 700 F (Table 1). Four point data were picked from the constitutive curves, as shown in Figure 30. The x axis is strain value and y axis is stress.
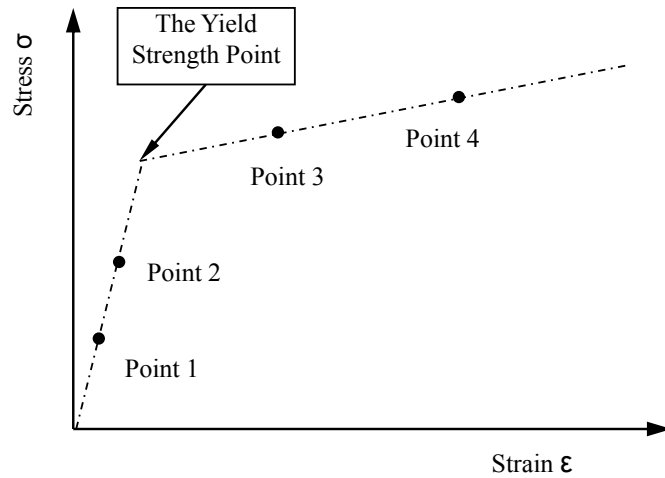
Figure 30. Schematic diagram for the picking of special point on the Stress-Strain Chart

The elastic modulus was estimated by the first two points, while the tangent modulus was estimated by the other two points. The intersection point of the two lines was the yield strength point. After processing all these constitutive curves, the ranges of the elastic modulus, yield strength, and tangent modulus were obtained. According to the selected 28 metals' linear constitutive relations, the range of the elastic modulus was from 6490ksi to 30800ksi; the range of the tangent modulus was from 0ksi to 13000ksi; the range of the yield strength was from 17.14ksi to 268ksi. In Table 2, 'a' & 'b' are slopes of σ/e which are the elastic modulus and tangent modulus respectively; while 'c' is the yield strength (σ).

Table 1 Selected materials properties (United States. Dept. of Defense 1966)

Material	Elastic Modulus	Tangent Modulus	Yield Strength	Temperature
Al6061-T6(*1)	9671.933	718.638	39.216	
Al 2024-T62(3)	10887.502	984.716	55.798	
Al 2024-T62(3)	10887.502	984.7156	55.798	
Al 6061-T6(*2)	10037.907	745.025	38.949	

51

Al 7175-T74(*2)	10816.052	854.3526	73.645	
Al 2024-T851(*2)	10946.432	1405.523	64.523	
5086-H34(*2)	10319.436	1399.792	31.973	
AZ31B-O(*3)	6490.620	242.516	17.140	
ZK60A-T5(*2)	6805.987	93.347	35.670	
Ti-8Al-1Mo-1V(*3)	6490.620	242.516	17.140	
Ti-8Al-1Mo-1V(*2)	14183.227	1231.820	106.676	550F
Ti-8Al-1Mo-1V(*2)	18262.367	1205.335	137.258	
duplex-annealed Ti-8Al-1Mo-1V(*2)	15569.491	1674.801	89.767	550F
solution-treated and aged Ti-6Al-4V(*2)	16592.885	2635.839	163.4419	
	9969.6789	3634.254	74.183	550F
annealed Ti-4.5Al-3V-2Fe-2Mo(*2)	16448.181	2641.263	136.915	
annealed Inconel 625(*2)	29884.702	703.955	72.534	
solution-treated and aged Inconel 718(*3)	30791.226	3295.781	179.969	
Steel 18-8(*2)	13139.903	984.128	66.865	
	9656.364	583.559	36.900	1400F
Al 2024-T3, aramid fiber-reinforced(*2)	9401.753	1482.666	35.430	
9Ni-4Co-0.20C(*2)	28096.026	4247.457	194.433	
250 grade maraging(*2)	28873.084	3847.579	268.131	
AM-350 (SCT 850) stainless steel(*2)	30148.513	8093.001	170.267	
	23799.019	7004.366	128.326	800F
17-7PH (TH1050) stainless steel (*2)	23187.166	4045.003	104.0378	
12.5Cr-1.0Ni-15.5Co-2.0Mo stainless steel (*2)	30727.484	12965.466	169.017	

*1: tensile stress-strain

*2:compressive stress-strain

*3: tensile and compressive stress-strain

Table 2 Range of factors (material properties)

		a	b	c
Factors		Elastic Modulus (ksi)	Tangent Modulus(ksi)	Yield Strength(ksi)
Levels	Low level	6490	0	17.14
	High level	30800	13000	268

3.3.6   Constraints on factor combinations

Since the elastic modulus, tangent modulus, and yield strength are related, the tangent modulus is always smaller than the elastic modulus. Thus for each constitutive relation, when designing the experiment, there should be a constraint between these two factors. By checking all the metals' data selected in Table 1, the smallest ratio between elastic modulus and tangent modulus of all metals is 2.4, so this is set as one constraint. Also, the smallest ratio between the elastic modulus and the yield strength of all metals is 100, and this is considered as another constraint.

3.3.7   The experiment plan

With factors, levels, and additional constrains determined as input information, the experiment is designed using the software "Design Experts". It is used because the classical factorial design cannot deal with experiments with factors not completely independent to each other. But in the "Design Experts", the optimal design with response surface is a good choice when there are constraints between factors.

With three factors, 15 combinations are needed for an optimal design as there is no need to have replicate runs in the computer aided experiments. Thus 15 runs are

performed for statistical analysis. In Table 3, the coded factors 'A', 'B', and 'C' were generated from the 'Design of Expert' for statistical analysis. They are normalized factors representing elastic modulus, tangent modulus, and yield strength respectively. These coded factors have to be linearly converted to actual factors 'a', 'b', and 'c' for simulation runs by applying the ranges of each actual factor with following equations, where 'a' is Elastic modulus, 'b' is Tangent modulus, and 'c' is Yield strength respectively, which are corresponding to the definition in section 3.3.5.

$$a = \frac{30800 - 6490}{2} * (1 + A) + 6490;$$

$$b = \frac{13000}{2} * (1 + B);$$

$$c = \frac{268 - 17.13962}{2} * (1 + C) + 17.13962.$$

The new experimental parameters generated in the "Design Expert" are given in Table 3. Parameters, which are mechanical properties of elastic-plastic materials, in both coded form for statistical analysis and actual form for simulation runs, are listed together.

Table 3 The coded and actual factors

Combina tion	Coded parameters			Actual parameters		
	Elastic Modulus	Tangent modulus	Yield strength	Elastic modulus(ksi)	Tangent modulus(ksi)	Yield strength(ksi)
code	A	B	C	a	b	c
1	1	-0.3	-0.5	30800	6363.636	79.85472
2	1	0.43477	-1	30800	13043.44	17.13962
3	1	-1	-1	30800	0	17.13962
4	0.02657 3	-0.28	0.00025 6	18968	6545.455	142.6019
5	0.44	0.19	-0.4	23993.2	10818.18	92.39773
6	0.3	-0.24	-1	22291.5	6909.091	17.13962
7	-0.4	-0.53	-1	13783	4272.727	17.13962
8	-1	-1	-1	6490	0	17.13962

9	1	-1	0.00999	30800	0	143.8229
10	-1	-1	-0.01001	6490	0	141.3143
11	0.612574	-0.50763	-0.03	26090.84	4476.088	138.8069
12	1	0.434778	0.00999	30800	13043.44	143.8229
13	-1	-0.43479	-0.5	6490	5138.3	79.85472
14	0	-1	-0.5	18645	0	79.85472
15	0.628111	-0.96	-0.49263	26279.69	363.6364	80.77871

4.   Development and validation of FEA model for ring compression tests

As mentioned in chapter 3, a reliable FEA model is established first before the DOE is carried out on the ring compression test with various material properties. The first part of this chapter discusses the establishment of FEA model. The second part of this chapter covers the simulation results and final solution for the FEA model.

4.1   Introduction of ANSYS

The general working procedure for ANSYS is in four steps. The first step is pre-processing, in which the problem type is defined to determine whether the problem is structural analysis, thermal analysis, magnetic analysis, or coupled fields' analysis type. Then the element types used in the simulation, material properties, contact, elements meshing, boundary condition and loading are defined. The third step is solving the model. In this stage, a solver is chosen (e.g. linear solver or non-linear solver); load steps and sub-steps are determined, and the numerical solution for the problem is given. The fourth

step is post-processing. In this stage, the solutions are reviewed, and are in forms of tables, charts to present stresses, strains and displacement and etc.

There are three sources of non-linearity in static structural problems: material non-linearity (MNL), boundary non-linearity (BNL), geometry non-linearity (GNL). Of these, the first two are present in ring compression simulation. In this situation, the material model and contact model are two of the most critical issues that affect the credibility of the simulation results.

4.2   Contact modeling

When modeling contact phenomenon in a problem, such as in the upset forging process, boundary conditions such as friction factor, contact area, contact pressure and material properties on the\ contact interface are changed during the process; therefore, the numerical simulation of contact phenomenon is a non-linear problem. Boundary non-linear (BNL), which is so called contact problem, needs to be well defined, that is, the numerical characters of the interface friction condition should be defined properly. In the ring compression test, the interfacial friction condition has significant influence on deformation, and cannot be measured precisely. Therefore, the simulation of ring compression test is a typical contact problem with all the boundary conditions actively changing; the contact condition should be defined very carefully.

In ANSYS, the contact interface is defined by contact pair, in which one side of the interface is the target, and the other side is the contact. Generally, the side with the larger surface or the surface with higher stiffness will be defined as the target, and the

contact is the deformable surface. For the upset forging, the die is much more rigid than the workpiece, so the surface of the die is treated as undeformable surface in FEA.

In reality, there is no penetration of one material into the other, but in FEA, this condition is approximated by a contact algorithm. Several contact algorithms are available in ANSYS such as penalty method, Augmented Lagrange, Lagrange multiplier on contact normal and penalty on tangent direction, and pure Lagrange multiplier on contact normal and tangent direction. The Augmented Lagrange method usually leads to better stiffness matrix conditioning and is less sensitive to the magnitude of the contact stiffness compared to the pure Lagrange. It is the default algorithm in ANSYS, and is adopted in this research. The Augmented Lagrange method actually combines the Lagrange multiplier method and the penalty method when solving the contact problem. When the element penetration is less than 0.1 of the contact element thickness, the penalty method would work; however, in other situations, the Lagrange multiplier method works better. The stiffness matrix is also an important parameter. Higher stiffness values decrease the amount of penetration, but would lead to ill-conditioning global stiffness matrix and convergence. Ideally, the stiffness is high enough, while the contact penetration is acceptably small. In the pure penalty method, the normal stiffness is defined as (Guide 2007)

$$F_n = k_n \cdot x_p,$$

where F_n is the normal force, k_n is the normal stiffness factor, and x_n is the penetration; while in the Augmented Lagrange method, the stiffness is defined as

$$F_n = k_n \cdot x_p + \lambda,$$

57

where λ is an extra term to make the normal force less sensitive to the contact stiffness k_n (Guide 2007). In the simulation such as the ring compression problem, the convergence is often a challenge. Due to its insensitivity on the stiffness matrix, the adoption of Augmented Lagrange algorithm would make the simulation convergence easier. Thus in this research, the Augmented Lagrange algorithm is selected.

4.3   Material modeling

In upset forging, material plasticity will dominate the deformation. So in ANSYS, any selected material will be simplified to elastic-plastic material model. Material plasticity can be modeled by bi-linear elastic-plastic curve, multi-linear curve. Multi-linear curve can be used to reconstruct the constitutive relation as close to the accurate constitutive relation as possible, but it's not easy to find comparative parameters between two multi-linear constitutive curves. The bilinear elastic-plastic model is chosen because only three characters (elastic modulus, tangent modulus, and yield strength) are required for such a model. Then constitutive relations of different materials can be compared by comparing these three characters.

T. S. Robinson's simulation results are used for comparison. In Robinson's research, clay was used to find the relationship between friction and deformation. The clay is much softer than general metals, so on one hand, physical experiments cost less to be conducted; on the other hand, such soft material's constitutive curve is several times lower in order than the general constitutive curve of the metal so that less errors would be

58

brought in when simplified the materials. Material used in FEA is as close to the Robinson's material as possible. At first, the material model in ANSYS is set as multi-linear model for verification tests. Once the multi-linear material model worked, the material model was changed to the bi-linear material model, while keeping all other settings fixed. In ANSYS, the maximum number of input data points for the multi-linear material model is 100. The constitutive curve is implemented point-wise with one hundred input data from Figure 31 (Robinson, Ou, and Armstrong 2004, 54-59).
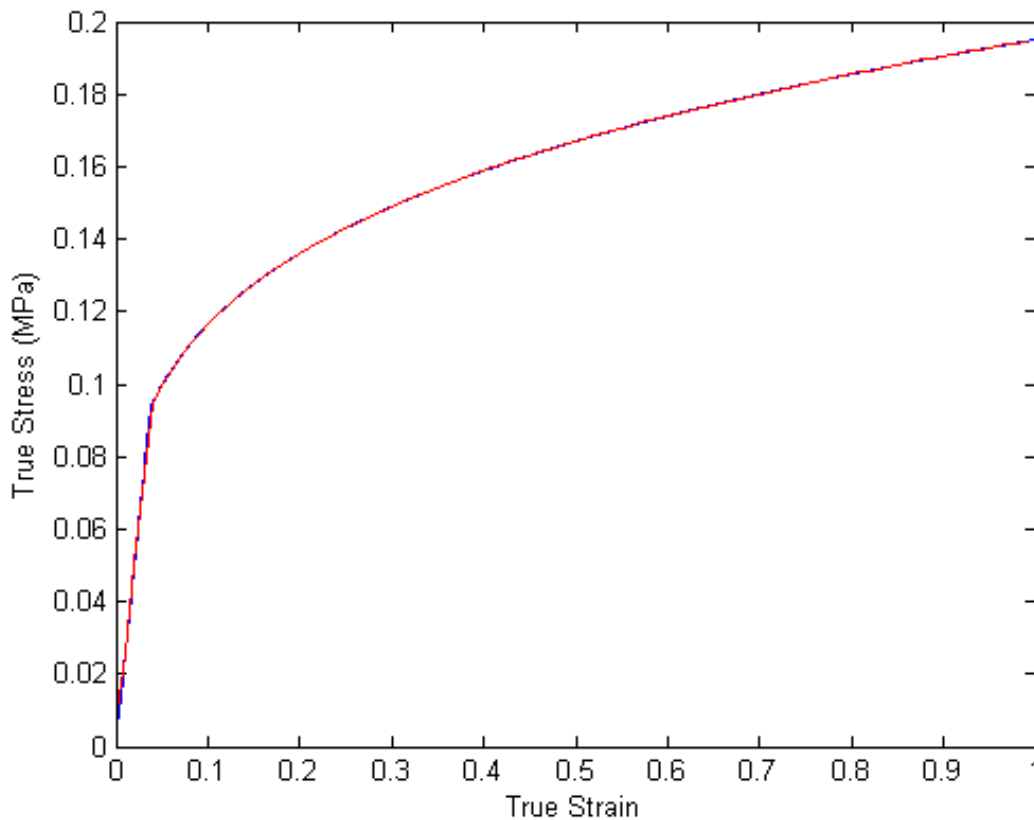
Figure 31. Constitutive curve of clay material (Robinson, Ou, and Armstrong 2004, 54-59)

In the multi-linear material model of ANSYS, even though multiple precision points were picked from constitutive curve, an elasticity module was still required. The

59

elasticity module was acquired from the slope of the initial section of the curve as 2.5MPa (Robinson, Ou, and Armstrong 2004, 54-59). Also, the material was set as isotropic material.

The Poisson's ratio is a property which takes significance in the elastic deformation. It is a constant that defines the ratio of the material's deformation in the transversal direction to the axial deformation when the specimen is deformed under the axial load. The value of Poisson's ratio would be an influential factor, since a strong relationship between the deformation of the ring's internal diameter, which is in the transversal dimension, and the axial deformation were observed in the ring compression test. The range of the Poisson's ratio is from 0 to 0.5. When an ideally compressible material is subjected to axial load, it won't have any dilatation in the transversal plane. The Poisson's ratio is zero, and even the total volume of the specimen would be shrunk. For an ideally incompressible material, when it is subjected to a uniaxial compression, the total volume of the specimen would be constant and the deformation in the axial direction would reflect on the transversal plane directly.

Whether the Poisson's ratio is automatically changed to 0.5 when the material starts the plastic deformation in ANSYS simulation is not shown in literature. So one of the verification tests were carried out to determine the Poisson's ratio's set up in this research.

4.3.1   Element type and meshing

In numerical calculation, the simpler the geometry is, the easier the numerical computation would be. In the ring compression test, the geometry of the ring shaped cylinder is axisymmetric, and the load is uniformly distributed on the contact interface between the die and the ring. Therefore, the geometry of the ring was established with cylindrical coordinates in ANSYS, and was simplified to a 2D plot by using half of the cross-section of the ring (Figure 32). The 'PLANE 182' was used to define the element of the ring specimen, and took "Full integration" for the element technique, 'Axisymmetric' for the element behavior, and 'Pure displacement' for the element formulation. The element type used was axisymmetric element. Also in the upsetting process, the upper and the lower die are simply flat plates, thus the loading conditions are exactly the same on two sides. The response to the upper and the lower die is mirrored by the plane of symmetry in the middle. So a quarter of the cross section of the ring was established as it is shown in Figure 32.
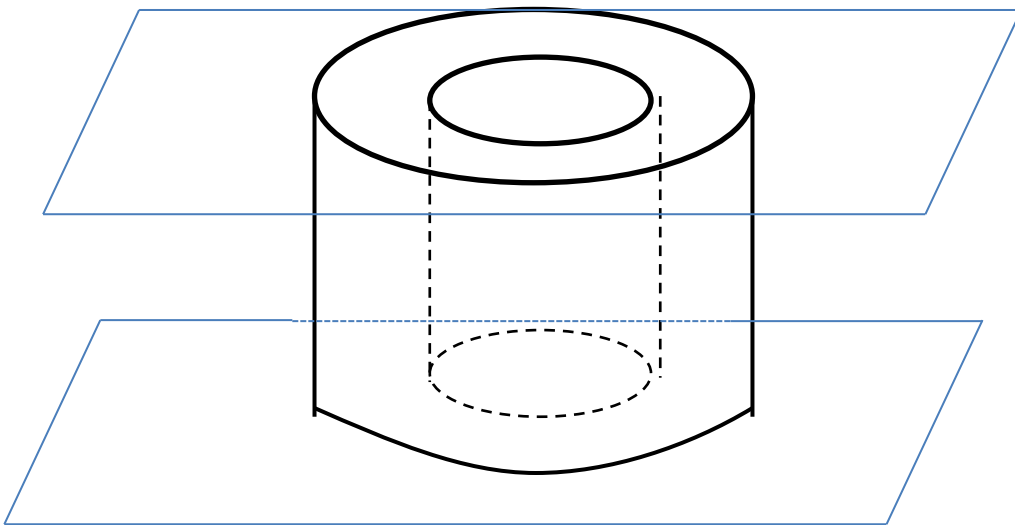
a. Ring specimen and its layout with die

b. Cross section of the ring

c. Quarter elements model
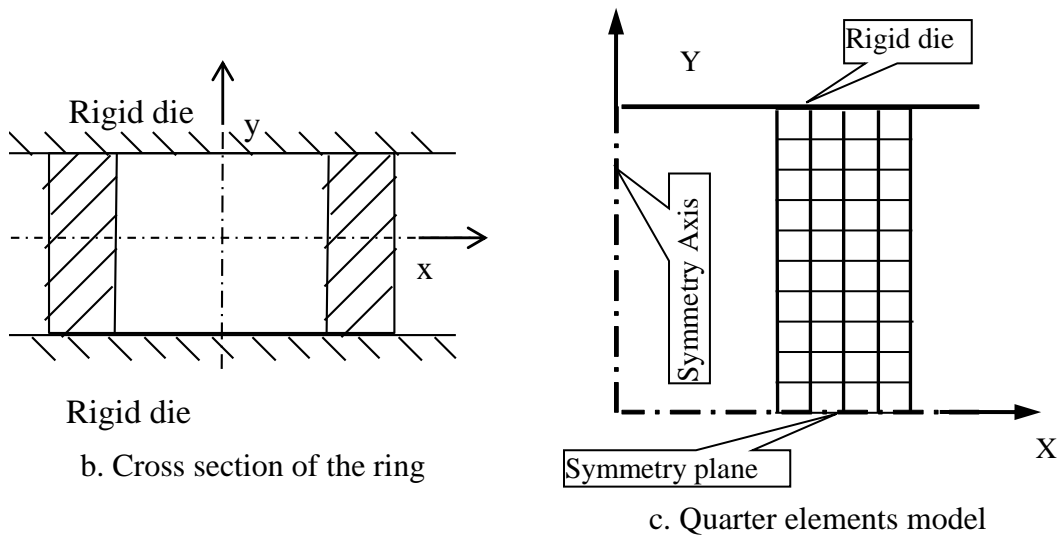
Figure 32. Establishment of Finite element model

Thus in the ANSYS geometry modeling, the cylindrical ring was represented by a rectangle block. As mentioned in previous section, this test did not just take the dimension of the specimen into consideration, but the dimensional ratio of the specimen was also accounted for. The compression result was then represented by the ratio of deformation in two directions. The FCC is an iso-friction contour plot. After each simulation run, the axis deformation and radius deformation were delivered for data processing.

As the deformation would be quite sensitive to the initial geometry, the standard geometry of the ring specimen was used for comparing is this research. The standard ratio, the outer-diameter (*OD*): internal-diameter (*ID*): height (*H*) is 6:3:2, is similar to many test cases in literatures. Specifically, in this research, the *OD* is 0.75in, *ID* is 0.375in, and *H* is 0.25in. After converting the 3D model to a 2D axisymmetric model, the height of rectangle is 0.125in, and the width as 0.1875in and it is offset from the axis as

0.1875in, representing a quarter of the cross-section. In ANSYS, the axisymmetric element has the y axis as the axis of the revolution. The offset from the y-axis was the dimension of the internal radius of the ring.

As the square elements were considered to save numerical calculation, the geometry is divided into 40 elements along the height and into 60 elements along the width to make each element a square. The die's deformation is not considered, and ideally, would be rigid, so a horizontal line is used to represent it. Among the four element techniques that could have been chosen from, trial runs showed that the element technique influences the convergence of the calculation, and the full integration provides the best convergence performance compared to reduced integration, enhanced strain, and simplified enhanced strain integration in this simulation.

4.3.2   Boundary condition setting

In the quarter model, as shown in Figure 32c, the top right of the cross-section was used, so the symmetric boundary condition was set on the bottom of the rectangle. The actual value of the force was not of concern and result of interest was the ratio of deformation during the processing, so the loading was defined by the displacement of the top die in the ANSYS. 60% of the axial reduction ratio was applied as the ultimate loading. As mentioned in previous section, the axial symmetrical model was used; the PLANE 182 was used to define the element of the ring specimen, and took "Full integration" for the element technology, "Axisymmetric" for the element behavior, and "Pure displacement" for the element formulation. Figure 33 shows the loading in ANSYS, with "S" marks for symmetrical plane, and triangle marks for loading point. Also in

63

Figure 33, the top straight line was restricted the displacement in x axis, so that the die can only move in y axis when simulating the compression process.
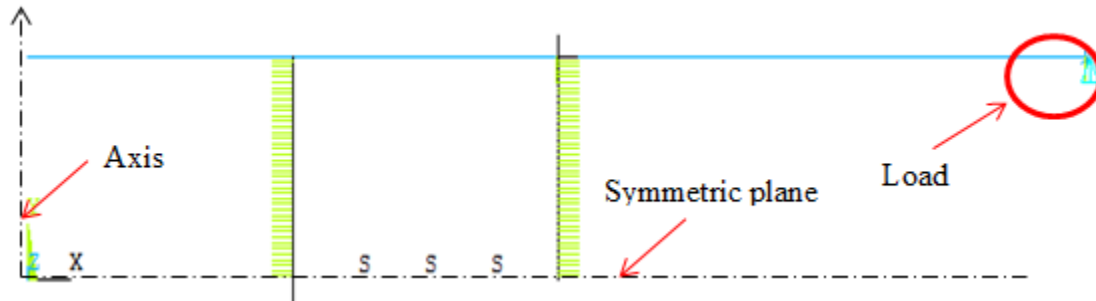
Figure 33. Load in ANSYS

Contact character is another important input in setting up of the simulation. In the ring compression test, the die should be stiffer than the specimen, so it was set as the 'target'. The interface on specimen side was the 'contact'. As the simulation model was simplified to the 2D model by defining it as an axisymmetric structure, the top straight line and the top line of the rectangle represent the interface area between die and the specimen. Thus, when these lines were selected in the contact pairs, they were defined as surface to surface contact. This was the place where the contact elements were generated. Also, for numerical purpose, the vertical lines which represent internal cylinder surface and outer cylindrical surface are combined with the top straight line and are the another contact pair in case the cylindrical surface move cross the die in the simulation. The contact on the top of the specimen and normal direction vector of the contact elements are shown in Figure 34. The long horizontal line at the top is the die, and assigned with target element; while vertical short lines on it are the normal direction vectors of the contact pair. In Figure 35, it shows the contact between die and cylindrical surface. The

definition of the die is the same as Figure 34. The two long vertical lines represent the internal and outer cylindrical surface and they are assigned with contact element, while the short horizontal lines are the normal direction of the contact pairs. In these contact pair, contact element was 'CONTACT 172', and target element was 'TARGET 169'. Such combination of 'CONTACT 172' and 'TARGET 169' enabled the surface to surface option for the contact, which was used in this research.
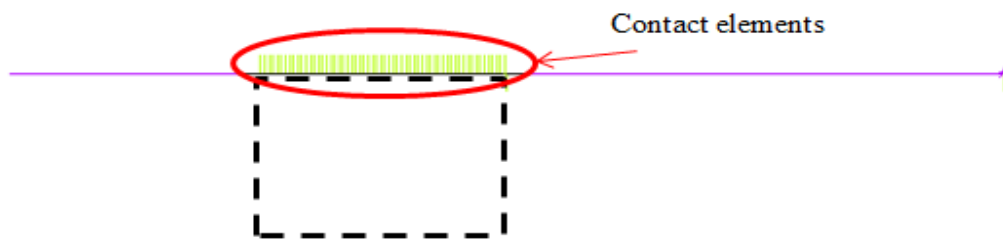
Figure 34. Contact on top surface and their normal vectors
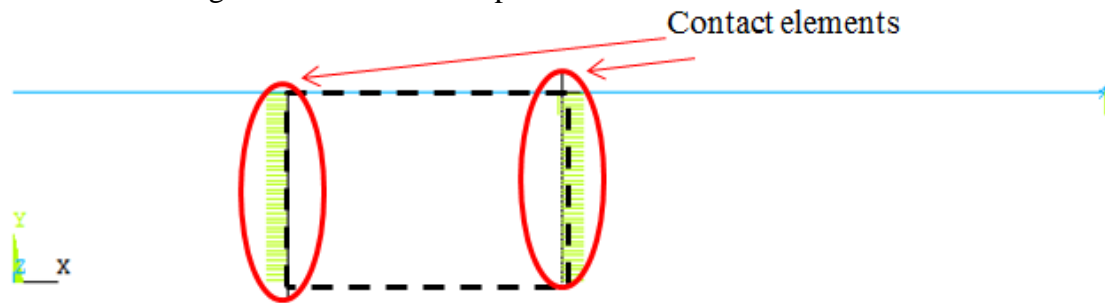
Figure 35. Contact between die and cylindrical surface

Considering the convergence of the solution, the stiffness factor of contact elements were set as 0.01, which meant the interface was soft. Contact elements would be deformed easily in the normal direction. With soft normal stiffness assigned, the contact elements and target elements in the same contact pair required less force to penetrate each other with nodes or edges of elements. The penetration accompanied with the soft stiffness matrix only served the numerical calculation, and had no physical significance.

The softened specimen interface made the numerical calculation easier. In the data analysis, the deformation of specimen interface caused by the normal stiffness would not be considered. As the die was treated as a rigid interface, the position change of the die interface represents the deformation of the specimen. In ANSYS, the interface friction condition was defined by the Coulomb's friction law, and in each run μ needed to be specified. In this research, the range of μ was varied from 0 to 0.57.

4.3.3   Solver specification

The ring compression has large deformation during the plastic deformation, so the non-linear large deformation switch is turned on in the solver. Some of runs may not be easy to converge, so the options related to sub-step are left undecided to be determined by the system automatically. When the system determines the sub-steps automatically, the number of sub-steps is determined by the convergence, and default force and moment convergence values are 0.005. As the final results become the history of deformations, it is required to store every sub-step during the simulation, in the solver setting.

4.4   Verification of the baseline FEA model

4.4.1   Experiments for the verification on baseline FEA model

In Robinson's work (Robinson, Ou, and Armstrong 2004, 54-59), the Poisson's ratio is 0.3, and μ is adopted from 0 to 0.57 discontinuously. While in the compression process, as most of the loading period, the stress is over the yield strength, and the material behavior displays as plasticity. The ideal plasticity material is incompressible, and the Poisson ratio is 0.5. FEA experiments in this section will sort out how the

Poisson's ratio should be set in ANSYS. Also, through experiments in this section, the influence of material properties on the deformation was demonstrated.

With the baseline FEA model established in the previous section and material model, experiments with Poisson's ratio at 0.05 (low Poisson's ratio), and 0.45 (high Poisson's ratio) at several friction levels were tested. μ=0.57 (high friction), μ=0.1 (middle friction), μ=0.05 (low friction) and μ=0 (no friction) were used. As shown in Figure 32, the displacement of the node on the left down corner of the rectangle (the center of the internal cylinder surface) in X direction, and the displacement of the node on the right upper corner of the rectangle (the upper interface) in Y direction were the output for the FCC plot.

The experiment of demonstrating the material properties effects on FCC took the clay constitutive relation from Robinson's research (Robinson, Ou, and Armstrong 2004, 54-59), and LY12 to compare. All settings in the FEA were the same as to each other but the material model changed. The friction applied on the contact pair was μ=0.57.

4.4.2   Results and discussions on baseline FEA model validation

In this section, a set of comparison simulation runs are presented with the aim of verifying the previous theoretical deduction on the influence of Poisson's effect on the ring compression test, the finite model and boundary conditions discussed in the previous section are applied in ANSYS. From Figure 36 to Figure 38, x-axis is the percentage of the height reduction, and y-axis is the percentage of the ring's internal diameter reduction.

In Figure 36 and Figure 37, each curve represents the deformations of the ring specimens under specific constant μ and Poisson's ratio v. Also Figure 36 and Figure 37

67

show that both high Poisson's ratio (0.45) and low Poisson's ratio (0.05) are applied for

each friction conditions in the experiments.
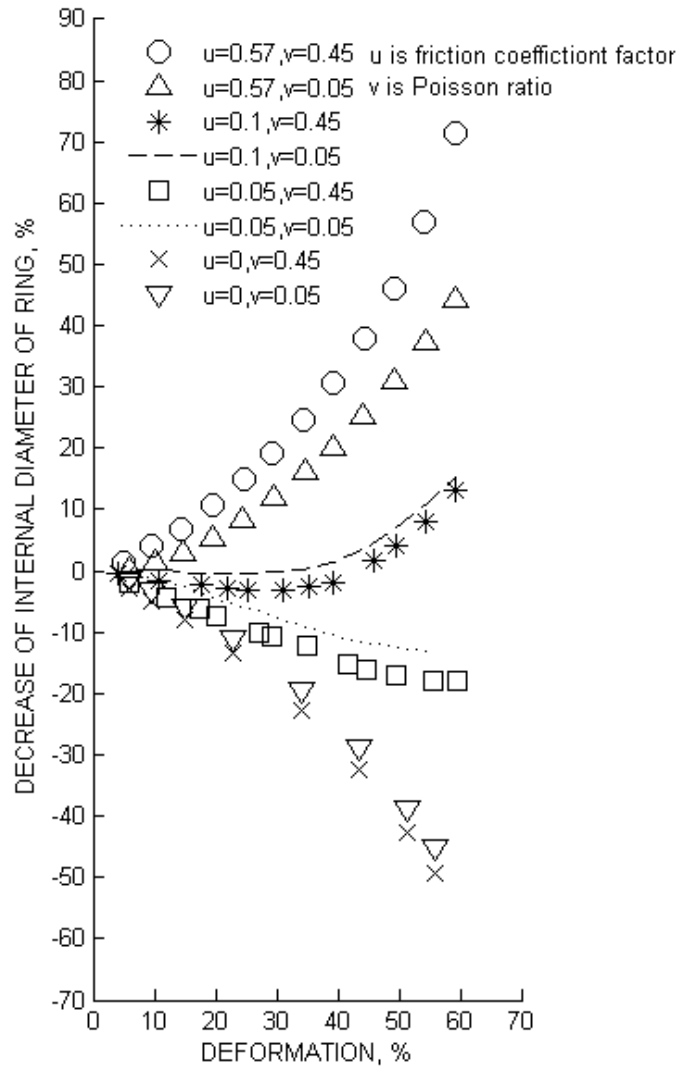
Figure 36. Deformation of ring specimen under the effect of the Poisson's ratio
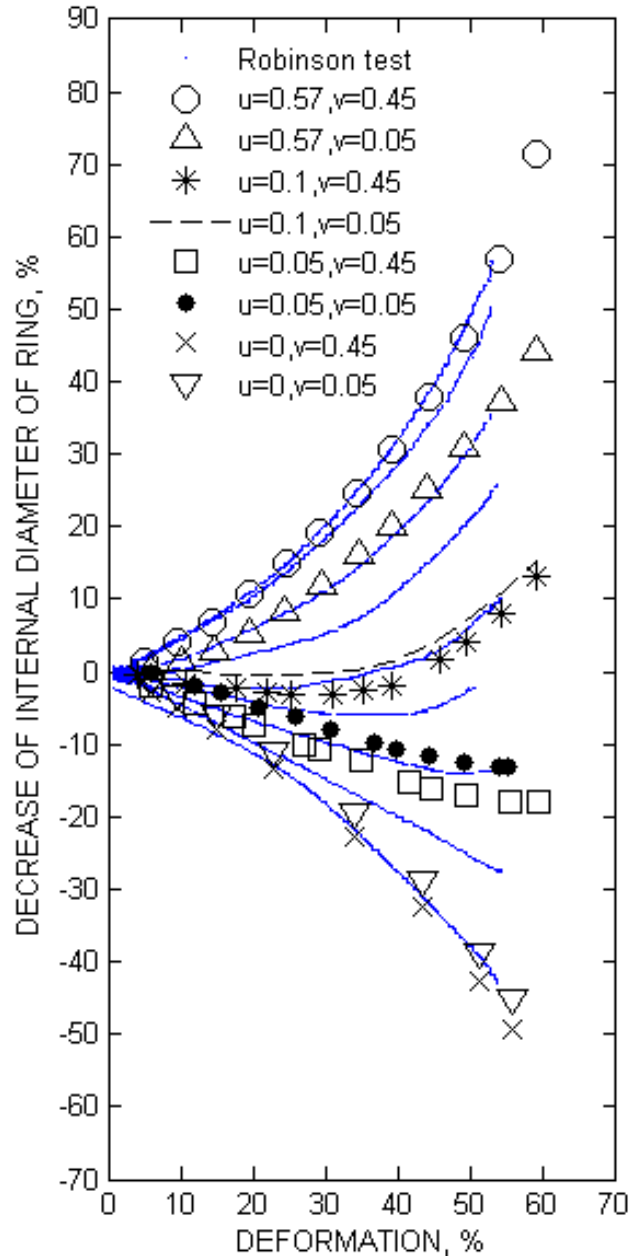
Figure 37. Robinson test with various Poisson's effect

When the μ is set to be 0.57, which is extremely high, the general pattern of the

internal diameter of the ring is shrinking. Those two curves corresponding to μ=0.57 have

a positive relation between x-axis and y-axis. It means that the internal diameter will

reduce all the way along with the reduction of the height. Meanwhile, their slopes are different and the difference keeps growing. In this case, the internal diameter of the specimen with Poisson's ratio at 0.45 had more dimensional decrease compared to the specimen with lower Poisson's ratio (0.05).

When the μ is 0.05 (extremely low), the general deformation pattern of the internal diameter of the ring is dilation. Those two curves corresponding to μ=0.05 have negative relations between x-axis and y-axis. It means that the internal diameter will expand when the height reduces. The difference between two curves is also growing. The internal diameter of the specimen with Poisson's ratio of 0.45 is increasing more than the specimen with lower Poisson's ratio (0.05).

When the interface friction μ is equal to 0.1, which is medium low, the general deformation pattern of the internal diameter of the ring is dilating first, and then shrinking. Those two curves corresponding to it have a parabolic-like shape. They all start at the origin. The difference between parabolas increases first, then decreases. The internal diameter of the specimen with Poisson's ratio of 0.45 dilates faster in the first stage and shrinks faster in the second stage.

In Figure 37, deformation curves from Figure 36 are plotted in the FCM from Robinson's research for comparison. It can be seen that when the Poisson's ratio is 0.45, the FCM would match Robinson's experiments well. When the Poisson's ratio is relatively low, v=0.05, the deformation curve generated in the FEA is quite different from the deformation curves from Robinson's research, especially when the interface is rough.

Theoretically, when the specimen is under large strain, for instance when under plastic deformation, the Poisson's ratio was considered as 0.5, because in transversal plane, the elastic deformation did not exist; the plastic material is uncompressible. It is worthy to note that this experiment indicates that in ANSYS, the deformation defined by Poisson's ratio would influence the deformation ratio without considering the elastic period or plastic period in a large compression simulation. Even if the yield strength is an input, the solver will use the same Poisson's ratio in both elastic and plastic deformation. The elastic deformation would be relatively small compared to the plastic deformation. So the Poisson's ratio in ANSYS would be proper if set as a large value in the ring compression simulation. The simulation results in Figure 37 match the theory and physical experiment well. It also shows a good match between the deformations of simulation with Poisson's ratio 0.45 and simulation results from Robinson's result (Robinson, Ou, and Armstrong 2004, 54-59).

Figure 38 shows a good match between deformations from all the friction levels simulated in current ANSYS simulation and Robinson's simulation. The simulation model is acceptable, and Poisson's ratio is set as close to 0.5 as possible. In this research, we picked the Poisson's ratio as 0.48.
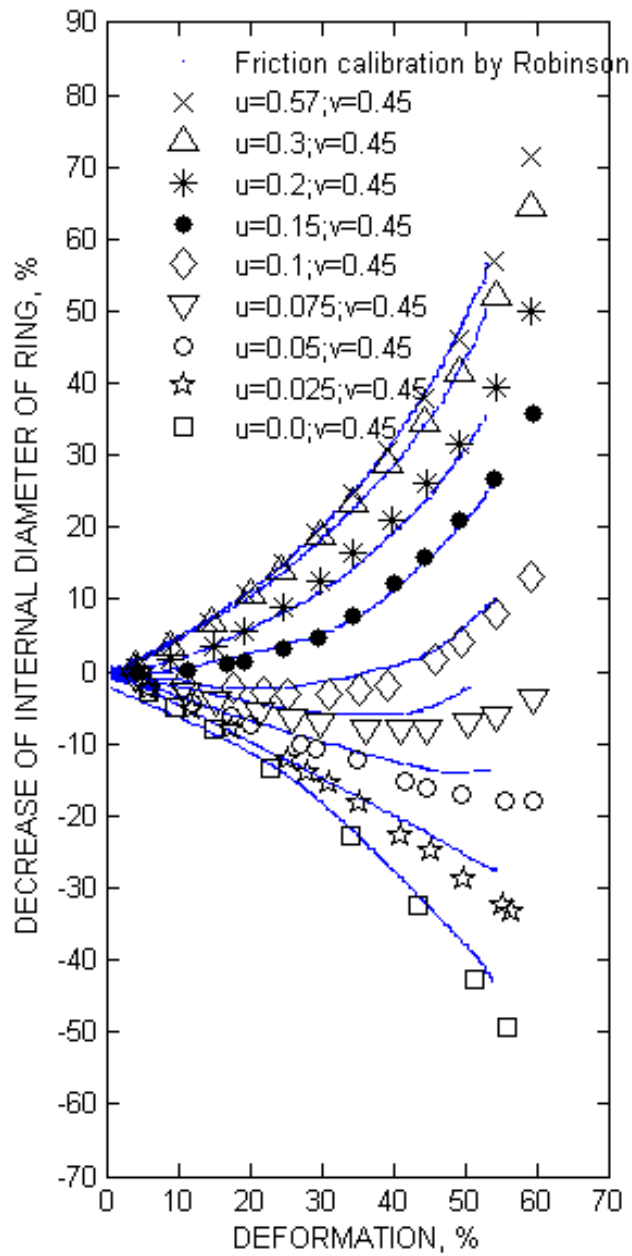
Figure 38. Deformation of ring specimen with the Poisson's ratio as 0.45

In the literature review, the possible influence of material properties on the behavior of ring compression was discussed. It is assume that the behavior of the ring in the compressing test would only be affected by the material properties and the interface

72

condition. In Figure 39, the comparison between the deformation results is shown based on the T. Robinson's material and self-defined material properties. The compared material is LY12. Here the elastic modulus used is 10.6Gpa, tangent modulus is 4000ksi, and yield strength is 47ksi. Difference between deformations is quite obvious in Figure 39. The higher the μ and compression volume becomes, the greater the difference is. This simulation proves the importance of the material mechanical properties in determining the shape of the product in the upset forging.
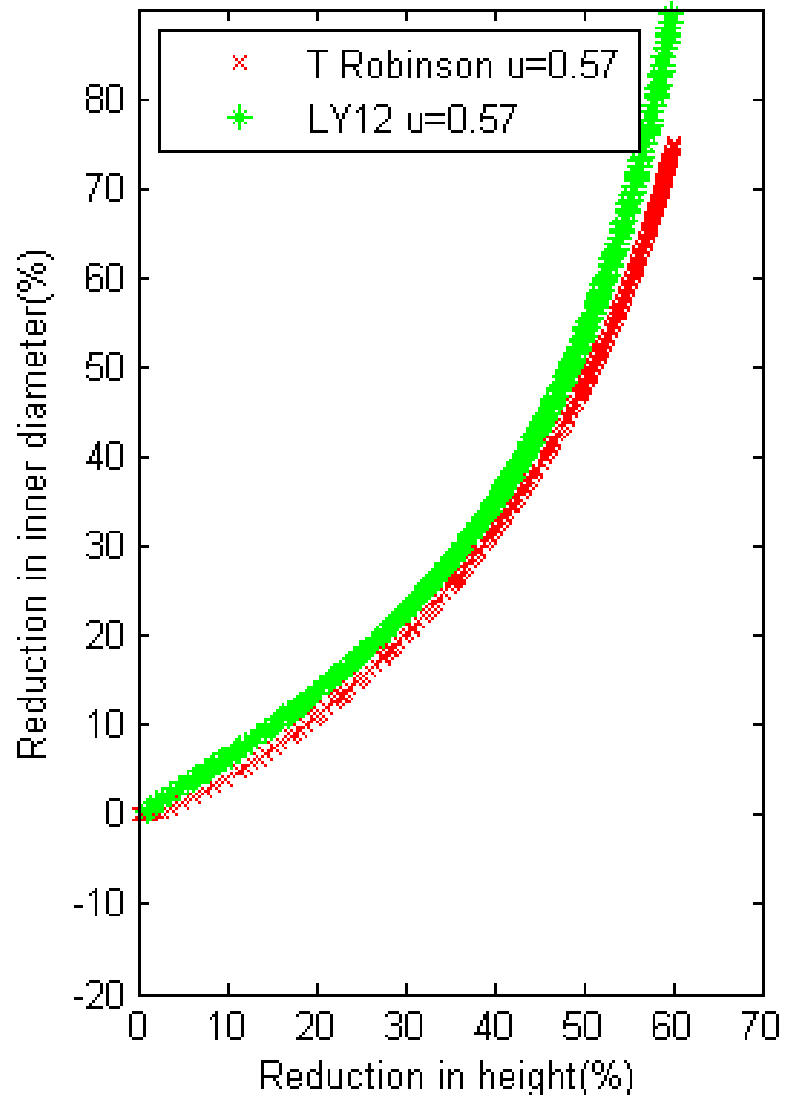
Figure 39. deformations of ring specimen with different materials

4.5   Checking barreling and material folding phenomena

4.5.1   The setting of the experiments for barreling

Now we check if barreling is observed and how the shape of the test samples is affected by different friction conditions. An experiment was set to observe the changing of boundaries in the compression process.

Three ring compression simulations were used in this experiment with three different μ factors. All other boundary conditions setting were kept the same. $\mu=0$ represented the low friction, $\mu=0.1$ represented the middle friction, and $\mu=0.57$ represented the high friction. For each run, all the nodes on the boundary were recorded in three intermediate states and one starting state, so that the profiles could be reconstructed later and compared.

4.5.2 Results and discussions on barreling and material folding

From Figure 40 a to c, simulations with a series of different μ ($\mu=0$, $\mu=0.1$, and $\mu=0.57$) on the interface are presented with boundaries highlighted. The x axis represents the distances from the revolution axis of the specimen to the boundaries of the intersection the ring. The y axis represents the distances from the symmetrical plane to the intersections of the ring in the direction of revolution axis. Each figure consists of four subplots. Each subplot represents one of the intermediate compressing statuses, while the last subplots show the boundaries when the ring specimens are compressed by 60%. In each subplot, the solid lines represent the original position and shape of the quarter ring specimen model; the dot lines are the boundaries of compressed specimen; Y axis is the axis of the ring specimens. The small dot lines represent the deformed contact surface on the top of the material; and the large dot lines represent the deformed cylindrical surfaces during the compression process. Step by step this series of subplots

display the progress of boundaries as they slide, extend and bend. By comparing the Figure 40 a to c, it is shown that the internal diameters extend to maximum dimension when the μ is zero, and shrink to the smallest dimension when the μ is set to be the largest value, 0.577. The die surfaces in these drawing are not plotted. They are supposed to adhere to the top of the compressed specimen all the time without any change as it is rigid.

When ideally smooth contact with $\mu=0$ is applied in the simulation in Figure 40 a, no folding phenomena is observed. The interface of specimen slides outward along the die plate. Both internal and outer cylindrical surfaces of the ring specimen are perfect cylinders all the time without bulging. The contact interface of the ring with top die expands in area and slide along the die surface.
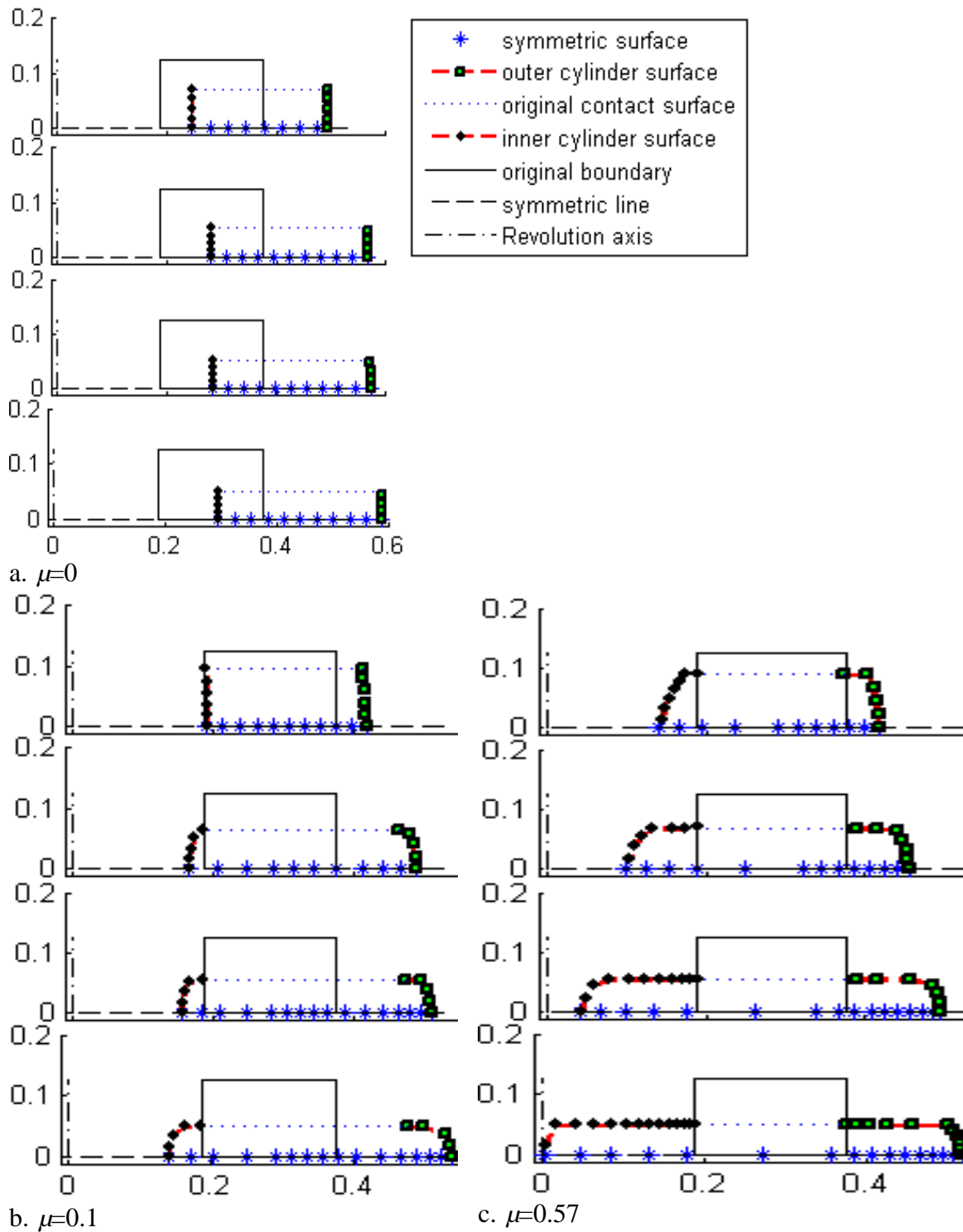
Figure 40. Boundaries of the specimens with various μ factors

a. $\mu=0$

b. $\mu=0.1$

c. $\mu=0.57$

Observing the boundaries change in the specimen with μ=0.577, whose interface is rough, in Figure 40 c, only bulging phenomenon affects the shape of the geometrical cross-section. The original contact edge of the top specimen neither slides along the die surface, nor shrinks or expands on itself, from beginning to end during the test; it is ideally stuck to the die surface. According to the friction calibration map, when μ is set to 0.577, the reduction of the internal diameter grew faster as the ring got compressed. Observing from Figure 40c, at some point, the internal cylindrical surface and outer cylindrical surface of the ring specimen does not only bend or bulge, but started to touch the die surface gradually. Such phenomena greatly increase the contact area. During the plastic deformation, the internal stress increases with a slower rate compare with the elastic deformation. In this case, the load required for further deformation does not increase a lot, while the contact area increases fast; such situation leads to the dropping of the contact stress. This is similar to Guerin's research (Guérin et al. 1999, 193-207; Wagener and Wolf 1995, 22-26), in which he mentioned that the contact pressure on the interface drops at some point of the compression procedure. At the same time Hoon Noh (Hoon Noh, Ho Min, and Bok Hwang 2011, 947-955) mentioned is his work that the material on the wall would fold towards the die. It also supports the correctness of the simulation phenomena of this research.

Figure 40b shows a case of the boundary change when low μ was applied; here the μ takes 0.10 for instance. Bulging phenomenon is observed, and the interface of specimen slide outward along the die plate. At the beginning, the internal diameter at the mirror plane moves outwards and the material near the interface bulges inwards. The

profile of the internal cylinder in the current finite element model becomes 'S' shaped curve. At this point, the material sliding tendency dominates the material folding phenomenon. As the reduction percentage grows, the material folding obtains the advantage over the outward sliding, and the profile of the internal cylinder became top of 'C' shaped curve. Finally, the original edge of contact area slides and extends, while the additional contact area generated due to the folding phenomenon. The deformation curve corresponding to such friction would be a concave curve in FCC plot, in which the beginning of the curve represents the internal diameter extension and the following segment represents the internal diameter reduction. It can be deduced that for various interfacial conditions, the changes of the internal diameters of the rings are the outcome of the combination of sliding and material folding by comparing Figure 40a with c. When the interface is smooth, there are only sliding affects. While the interface is sticky, only the material folding phenomenon occurs.

Furthermore, similar phenomenon can be observed in physical experiments as a proof for the correctness of the FEA simulation. In professor's Jami Shah's (Shah and Kuhn 1986, 255-261) physical experiments with cylinder compression, specimen with the same diameter, 1 in, at various heights, were compressed. Figure 41, lists specimen from his experiments. From left to right in the photo, it shows specimen at two different heights with their original specimen and compressed specimen. By observing compressed cylinders in Figure 41, an obvious pattern, a clear circular boundary, could be seen on each of the top surface of specimens. In the center, the profile of the circle area is quite different from the area out of the circular boundary. Some of the circular area may not

79

exactly be at the center due to the buckling phenomena in the long thin cylinder which is subjected to uniaxial load. In Figure 42, the photo is taken when the compressed are overlapped on the top of the uncompressed specimens. The left photo in Figure 42 is taken when the left two specimens Figure 41 are overlapped. The right photo in Figure 42 is taken when the right two specimens Figure 41 are overlapped. It shows that the circular boundary on the top of the compressed specimens matches the diameters of the original cylindrical specimens in each compression process.
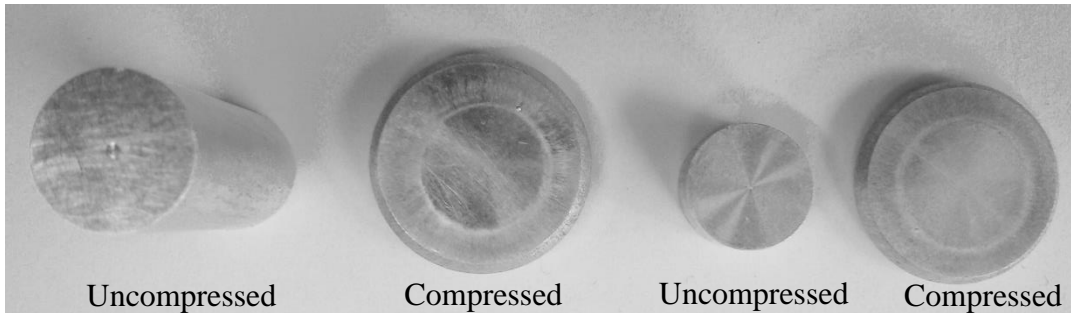
Figure 41. Compressed and uncompressed cylinders

Figure 42. Overlapped the compressed and uncompressed specimens

The area out of the circular boundary looks rough, which looks the same as the un-machined cylindrical surface. So it can be assumed that the area increasing of contact interfaces in the cylinder compression experiments is generated from the un-machined cylinder surface. This boundary matches the material folding phenomenon indicated in the simulations in this research. This phenomenon in the physical experiments of cylinder compression can be a support for the material folding phenomenon in the ring compression simulation.

When taking the boundary changes observed in this experiment into account, it would be necessary to modify the previous simulation model by assigning the machined and un-machined surface with different value of μ respectively. Normally, the external and outer cylinder surfaces of the ring were un-machined surfaces, and took μ=0.57 for both surfaces. For the initial contact surface, the μ would vary from case to case.

4.6   Application of multiple μ factors onto the interface

The purpose of this section is to verify the feasibility of applying multi-stage μ factor to approach the constant m factor, and it consists of four simulation runs. Three runs applied three different constant μ factors, that is, μ_1=0.055, μ_2=0.02, and μ_3=0.03, and additional run applied these three μ factors stage by stage. Other FEA settings were the same. The internal diameter change and axial reduction were used to comparing the results of these four runs.

In Figure 43, four curves are shown in the FCC plot. The x axis is the height reduction ratio of the specimens, y axis is the inter radius reduction ratios. Three of the

81

curves in Figure 43 are deformation curves with constant factor, and the rest was with multi-stage μ factors. In Figure 43, the FCC for μ equal to 0.055, 0.03, and 0.02 are presented. These three μ are also applied to three equally divided compression stages in a single compression. The compression range is from 0 to 60% of specimen height, so divided stages of compression used here are 0 to 20%, 20% to 40% and 40% to 60%. From 0 to 20% of axial compression, the μ is assigned as 0.055. From 20% to 40% of axial compression, the μ was assigned as 0.03. From 40% to 60% of axial compression, the μ was assigned as 0.02.

The Figure 43 shows that in the period of 0 to 20% of axial compression the deformation of the combined friction FCC overlaps to the FCC with constant μ=0.055, which is obvious that they have the exact same conditions during this period. The deformation of the combined friction FCC parallels to the FCC with constant μ=0.03 in the period of 20% to 40% of axial compression, where they share the same μ. The deformation of the combined friction FCC parallels to the FCC with constant μ=0.02 in the period of 40% to 60% of axial compression, where they share the same μ. This figure indicates that when the μ changes, the new deformation curve in the FCC frame was generated simply by shifting the segment of standard friction calibration curve at the new μ to current deformation. The segment curve is parallel to the FCC at the same μ. This means that the test variables relate to the tendency of deformation of FCC, in other words, the test set ups such as friction factor, material properties are related to the slopes of FCC. The strategy to approach the constant m friction calibration curve by μ can be finding

better matches on curves' slopes. Thus the slopes of FCC are used as the response when carrying out statistical analysis.

Figure 43 also shows cross point of deformation curves generated by three steps and the FCC when μ is 0.03. On the combined curve, the friction coefficient on the cross point is 0.02. This means that because a certain final deformation status can be achieved in several ways, the μ cannot be determined, when we only have the deformation information at the final point. In previous studies, researchers carried out the ring compression test, measured the final dimension of the specimen, put it in the friction calibration map and claimed the μ was found. According to the observation in Figure 43, such conclusions were not exactly right. With only one deformation information, the conclusions made in those studies were only one of the possible μ factors.
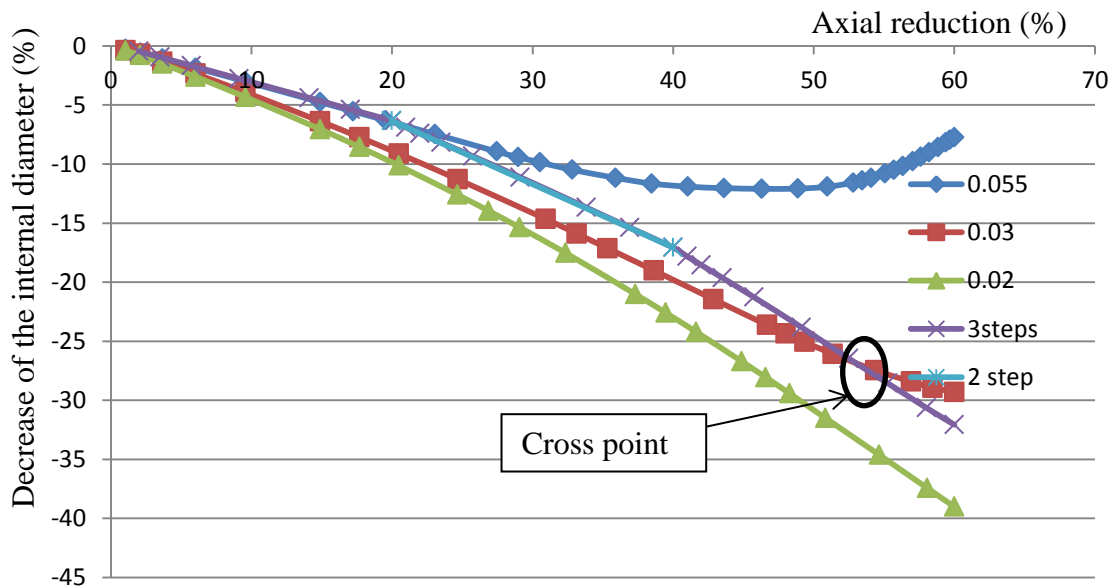
Figure 43. Deformation curves subjected to four different setting on μ factor

4.7   Summary of FEA simulation modeling

Through the validation experiments in this chapter, a baseline of FEA model was established and modified. The Poisson's ratio is set as 0.48. It was determined that the frictions are not only applied on the original die-workpiece contact but also are applied on both internal and outer cylinder surface. The response of the ring compression test should be the slopes of the FCC curves. With all this preparation, the DOE experiments are designed and carried out which are presented in the next chapter.

5. Discussion on Obtaining Multi-stage Factors

5.1   Analysis Procedure

The factors, levels and experiment plans were discussed in Chapter 3, and response of the experiments were discussed in Chapter 4. This chapter presents the analysis done on the response results.

5.1.1 Data treatment on the slope of FCC

The slope at each point on the FCC was used as the responses of each run for statistical analysis. These slopes were organized into15 combinations of factor levels as inputs so the DOE analysis can be carried out. It required four steps to organize slopes data for statistical analysis. Firstly, FCC was generated by simulating with different material properties. Secondly, the curve functions were established for each FCC through curve fitting. Thirdly, slopes were calculated by differential calculation of each curve functions at desired deformations. Fourthly, mathematical relations between mechanical properties of materials and deformations were generated through statistical analysis at particular μ factor for desired axial deformation of the ring.

Figure 44 shows the first step, 15 deformation curves, which correspond to the simulation results for the 15 material properties listed in Table 3, while μ=0.57. These curves record deformations in the same way as FCC are plotted, with x axis as the percentage of reduction of the ring specimens and y axis as the percentage of decrease of the internal diameters.
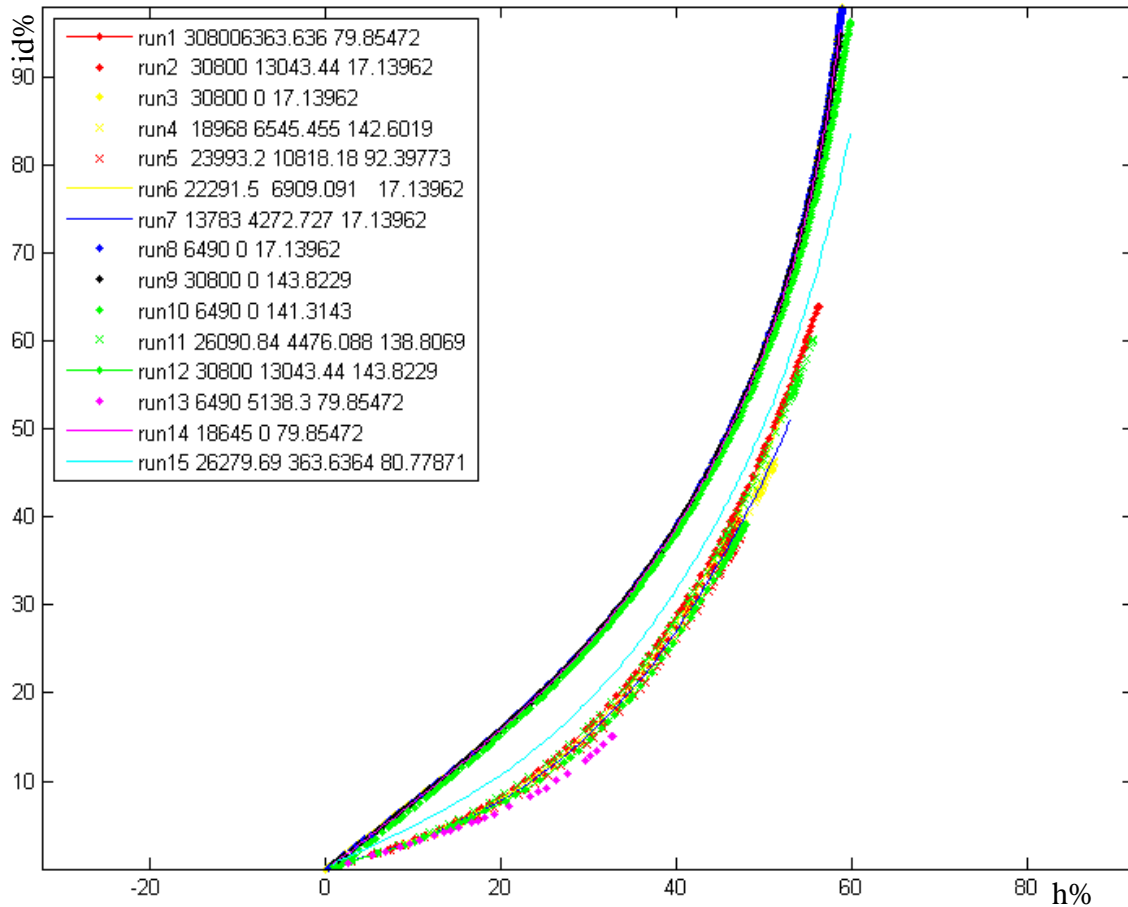
Figure 44. Deformation data of simulation runs for μ=0.57 for different materials

In the second step, data are treated for curve fitting. One of the treatments is to remove data at high deformation section from some curves. It is because that in some simulation the FCC could grow close to 100% decrease of internal diameter at the end of the compression. The trends of those ending segments are quite different from most other parts of curves, which tend to become flat. The 100% decrease of internal diameter means the internal cylinder is closed. When the internal cylinder is almost closed, there was almost no room for the internal cylinder surface to deform further inwards, and

resulting in sudden stiffness increase. Those FCC went flat at the ending segments. Therefore, when doing curve fitting, data points from the end flat segments were removed. Then functions which represented the data left were calculated through curve fitting. Polynomial, Fourier, and Gauss functions were calculated at several degrees and the best curve fitting function was selected for the minimum residual value for each curve respectively. Some deformation curves in the appendix were using piecewise functions and consisted of more than one form of function. For curve fitting for each run with μ=0.57, results of curve fitting are shown in Table 4. These functions descripts the curves shown in Figure 45, where height reduction ratio of the ring are 'x', and where the internal radius reduction ratio are 'y'

Table 4 Curve fittings for each simulation run

Run #	Equation
Run1	$f(x) = 8.385 * e^{-\left(\frac{x-1.206}{0.1665}\right)^2} + 192.3 * e^{-\left(\frac{x-3.281}{2.354}\right)^2} + 13.09 * e^{-\left(\frac{x+0.5962}{1.295}\right)^2}$
Run2	$f(x) = 0.0002683x^3 - 0.001825x^2 + 0.3469x - 0.05535$
Run3	$f(x) = 1686 * e^{-\left(\frac{x-4.539}{1.859}\right)^2} + 37.59 * e^{-\left(\frac{x-0.5591}{1.318}\right)^2} + 7.433 * e^{-\left(\frac{x+1.136}{0.8452}\right)^2}$
Run4	$f(x) = 2.395 * 10^8 * e^{-\left(\frac{x-21.51}{5.263}\right)^2} + 0 * e^{-\left(\frac{x-0.933}{0.0004816}\right)^2} + 25.14$ $* e^{-\left(\frac{x-0.2152}{1.681}\right)^2}$
Run5	$f(x) = 0.0001939x^3 + 0.003393x^2 + 0.2077x + 0.2653$
Run6	$f(x) = 6.599 * e^{-\left(\frac{x-1.097}{0.09706}\right)^2} - 7704 * e^{-\left(\frac{x-1.457}{1.814}\right)^2} + 7821 * e^{-\left(\frac{x-1.473}{1.826}\right)^2}$
Run7	$f(x) = 0.0001954x^3 + 0.003182x^2 + 0.2185x + 0.2068$

Run8	$f(x) = 0.00022x^3 + 0.00136x^2 + 0.2487x + 0.1331$
Run9	$f(x) = 0.0002645x^3 - 0.001473x^2 + 0.3356x - 0.0708$
Run10	$f(x) = 0.0002151x^3 + 0.001703x^2 + 0.2404x + 0.1558$
Run11	$f(x) = 161.3 * e^{-\left(\frac{x-2.001}{1.636}\right)^2} - 22.95 * e^{-\left(\frac{x-0.8998}{0.6332}\right)^2} + 14.63 * e^{-\left(\frac{x+0.8759}{1.063}\right)^2}$
Run12	$f(x) = 0.0002616x^3 - 0.001301x^2 + 0.3326x - 0.1683$
Run13	$f(x) = 0.0002146x^3 + 0.001808x^2 + 0.2397x + 0.1731$
Run14	$f(x) = 2966 * e^{-\left(\frac{x-5.731}{2.417}\right)^2} + 3827 * e^{-\left(\frac{x+0.2011}{1.045}\right)^2} - 3802 * e^{-\left(\frac{x+0.2025}{1.042}\right)^2}$
Run15	$f(x) = 0.0002117x^3 + 0.00201x^2 + 0.2376x + 0.135$

It is mentioned in Chapter 3 that the final reduction ratio was determined to be 60%, however, there were some simulation runs couldn't reach that final reduction ratio because of convergence difficulty. Friction calibration curves with constant μ factor from these simulations were extended to the full compression process with fitted curve equations. Then completed fitted curves at μ=0.57 for 15 mechanical properties combination are plotted in Figure 45. It is plotted the same way as in

Figure 44. Those plots at other μ factors are listed in the APPENDIX II from Figure 52 to Figure 66. 15 μ factors are used in this research, which are 0, 0.02, 0.03, 0.04, 0.05, 0.06, 0.07, 0.08, 0.10, 0.12, 0.15, 0.20, 0.30, 0.40, and 0.57.
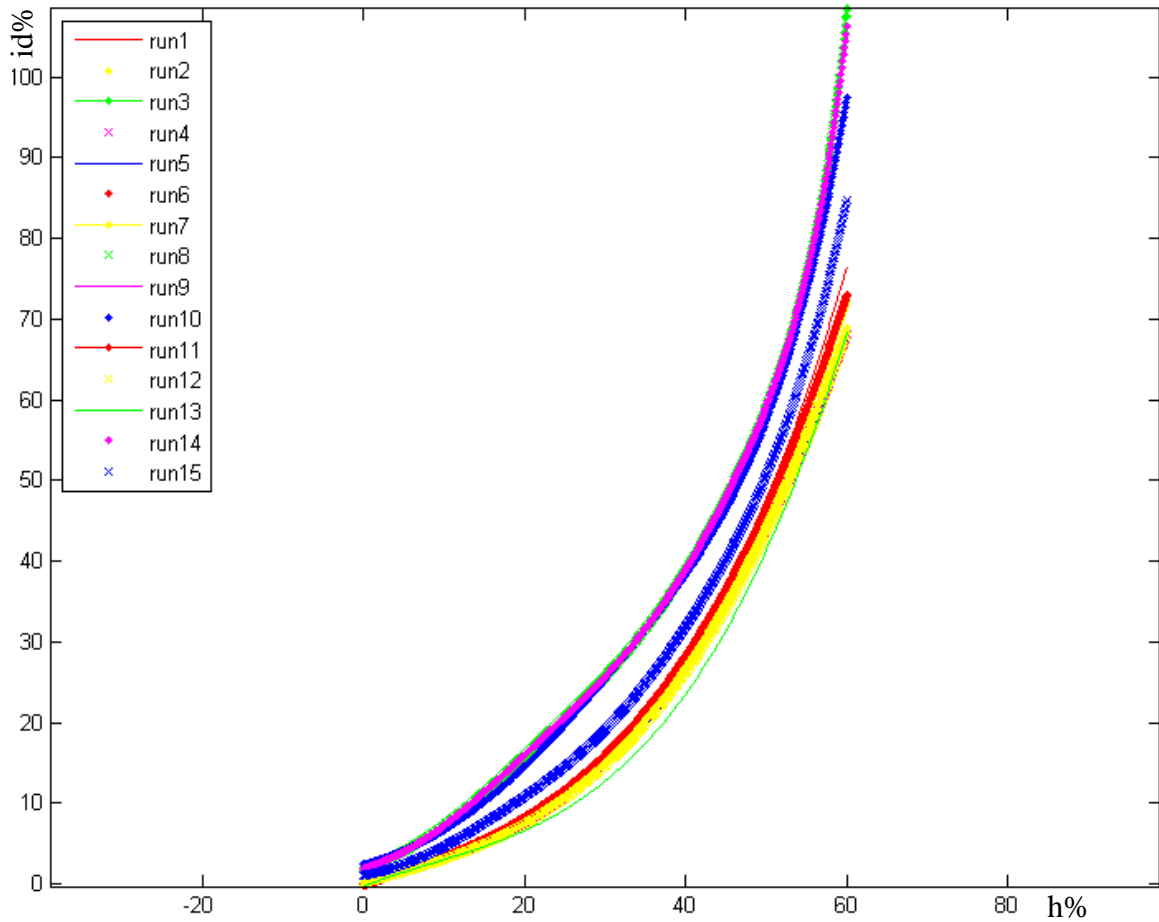
Figure 45. Curve fitting for simulation runs for μ=0.57

In third step, data of slopes, which are the responses used in the statistical analysis for all 15 combination of mechanical properties, when μ=0.57, is shown in Table 5. Differential calculation data of fitted curves were selected for every 5% reduction in height until 55% reduction because the flat segments of simulation data curve were within last 5% of curves, and they were removed when analyzing.

Table 5 The slopes of deformation curves at different reduction levels

	Slopes										
	Reduction levels										
combination	5%	10%	15%	20%	25%	30%	35%	40%	45%	50%	55%
1	0.485	0.680	0.853	0.969	1.029	1.090	1.239	1.554	2.050	2.673	3.978
2	0.348	0.391	0.473	0.596	0.759	0.962	1.205	1.489	1.812	2.176	2.581
3	0.543	0.793	0.916	0.908	0.921	1.084	1.347	1.600	1.904	2.572	4.081
4	0.438	0.607	0.785	0.949	1.081	1.181	1.285	1.473	1.877	2.683	4.129
5	0.256	0.334	0.440	0.576	0.741	0.935	1.158	1.410	1.691	2.001	2.341
6	0.460	0.643	0.825	0.972	1.067	1.131	1.237	1.500	2.018	2.789	3.734
7	0.265	0.341	0.446	0.580	0.744	0.937	1.159	1.411	1.692	2.002	2.342
8	0.279	0.342	0.439	0.567	0.729	0.924	1.153	1.414	1.708	2.035	2.395
9	0.341	0.385	0.470	0.594	0.758	0.961	1.205	1.487	1.810	2.172	2.574
10	0.274	0.339	0.437	0.567	0.729	0.923	1.150	1.409	1.701	2.024	2.380
11	0.523	0.764	0.928	0.961	0.932	1.021	1.334	1.68	1.888	2.602	4.466
12	0.339	0.385	0.470	0.594	0.758	0.961	1.203	1.484	1.805	2.164	2.563
13	0.274	0.340	0.439	0.570	0.732	0.928	1.155	1.414	1.706	2.030	2.386
14	0.521	0.766	0.917	0.936	0.931	1.059	1.332	1.615	1.909	2.559	4.070
15	0.273	0.341	0.440	0.572	0.735	0.929	1.156	1.414	1.704	2.026	2.379

90

In the fourth step, data in Table 5 was used as input for the "Design Expert". For each particular compression test, statistical relations were generated between material properties and internal diameter of the ring.

5.1.2   Statistical analysis of the data

The response variables are tangent values of points on the FCM and they are used as input when conducting statistical analysis with "Design of Experts". Table 6 shows the input data in "Design of Experts",when the ring height is reduced by 55% with μ=0.57. Definition of 'A', 'B', and 'C' are in section 3.3.7. Data at other reduction ratios and other factors μ are available by dealing with FCC curves listed in Appendix II with the treatment shown in 5.1.1, and are the intermediate data in this research.

Table 6 DOE input data

	Coded parameters			
	Elastic modulus	Tangent modulus	Yield strength	Slope
Runs	Factor1 A:A	Factor2 B:B	Factor3 C:C	Response R1
1	1	-0.3	-0.5	3.97849
2	1	0.434778	-1	2.58059
3	1	-1	-1	4.08054
4	0.026573	-0.28	0.000256	4.12947
5	0.44	0.19	-0.4	2.34059
6	0.3	-0.24	-1	3.73412
7	-0.4	-0.53	-1	2.34202
8	-1	-1	-1	2.39505
9	1	-1	0.00999	2.57396
10	-1	-1	-0.01001	2.38007
11	0.612574	-0.50763	-0.03	4.46605
12	1	0.434778	0.00999	2.56327

13	-1	-0.43479	-0.5	2.386
14	0	-1	-0.5	4.07028
15	0.628111	-0.96	-0.49263	2.37971

The ANOVA, which is a variance analysis, used the input data in Table 6. Their contributions to the response are presented as weightings in equations relating factors and response. The forms of the equations are suggested through Box-Cox analysis, that is, the power transformation analysis, from the "Design Experts".

The case used for demonstration is the analysis when the height reduction is 55%, and the μ is 0.57. The power of the response in the equation is determined as -1, according to the suggestion from Box-Cox analysis. The physical significance of the slopes on the deformation curve is the ratio of ring's internal diameter decrease ratio to height reduction ratio. Factors represent the selected materials' mechanical properties.

The response is expressed by the following equation, in which material mechanical properties are variables 'A', 'B', and 'C'.

$$\frac{1}{R1} = 0.40 - 0.061 * A + 0.14 * B - 4.41 * 10^{-3} * C - 0.057 * A * B + 5.583 * 10^{-3}$$
$$* A * C - 2.156 * 10^{-4} * B * C + 0.044 * A^2 - 0.048 * B^2 + 8.012$$
$$* 10^{-3} * C^2$$

where A, B, C are coded factors, whose levels are from -1 to 1. "A" represents the Elastic Modulus, "B" represents the Tangent Modulus, and "C" represents Yield Strength. R1 is the response, which is the slope on the deformation curve.

When carrying out statistical analysis on mechanical properties, the significance of each factor is obtained by a significance test, F-test of the ANOVA. Results show that

when the specimens are under high friction factors, and high deformations, the Tangent

Modulus is the most significant factors frequently. When specimens were under low

friction factors, and low deformations, there would even have no significant factor for

slopes; μ=0 is a typical one where the material properties have no influence on the

deformation. It matches the physical phenomenon that the plastic deformation is

dominant in the high deformed material.

Similarly, the coded factors functions are generated when the height of rings are

reduced from 5% to 50%, as shown in AppendixIII. Then, going through the same data

processing through the whole range of the μ=0 to 0.57, the relationship between material

properties and FCM' slopes are established. Equations are listed in the APPENDIX III.

When μ equals to 0, all specimen deformations are same to various material properties.

The slopes of FCC curves are listed in Table 7.

Table 7 Slopes on the deformation curve when interface is smooth

Deformation	5%	10%	15%	20%	25%	30%	35%	40%	45%	50%	55%
Slope	-0.54	-0.58	-0.63	-0.69	-0.76	-0.85	-0.95	-1.07	-1.21	-1.38	-1.58

With the equations of the relationship between mechanical properties and

deformation, when a certain material is compressed under a certain *m* factor, a matrix of

possible slopes can be generated by substituting the material mechanical properties into

the equations. At the same time, the slopes from the desired deformation curves (*m*-based

FCC) and the slopes from that matrix are compared at each axial reduction ratio level of the ring specimen. Calculated slopes in the matrix are selected when they are close to the slope of m-based FCC at the same reduction ratio. The μ factor which is associated with the selected slopes is the suggested μ factor for the axial reduction ratio. When the μ factors are determined at all reduction ratios, the list of suggested μ is completed. Such list is going to be applied in the FEA simulation to simulate the friction condition defined by m factor.

5.2   Case study—application of the multi-stages strategy

In this section, a case study is made with the data in Bin Guo's paper 2008(Guo et al. 2010, 94-97) to demonstrate the application of the method proposed in this research. The process is shown in

Figure 46 as a flowchart and the final result is a set of μ which can be used to describe the friction condition as constant shear friction factor m does. Such set of μ can be used in FEA simulation to predict the deformation of workpiece in the upset forging process subjected to the same working condition.
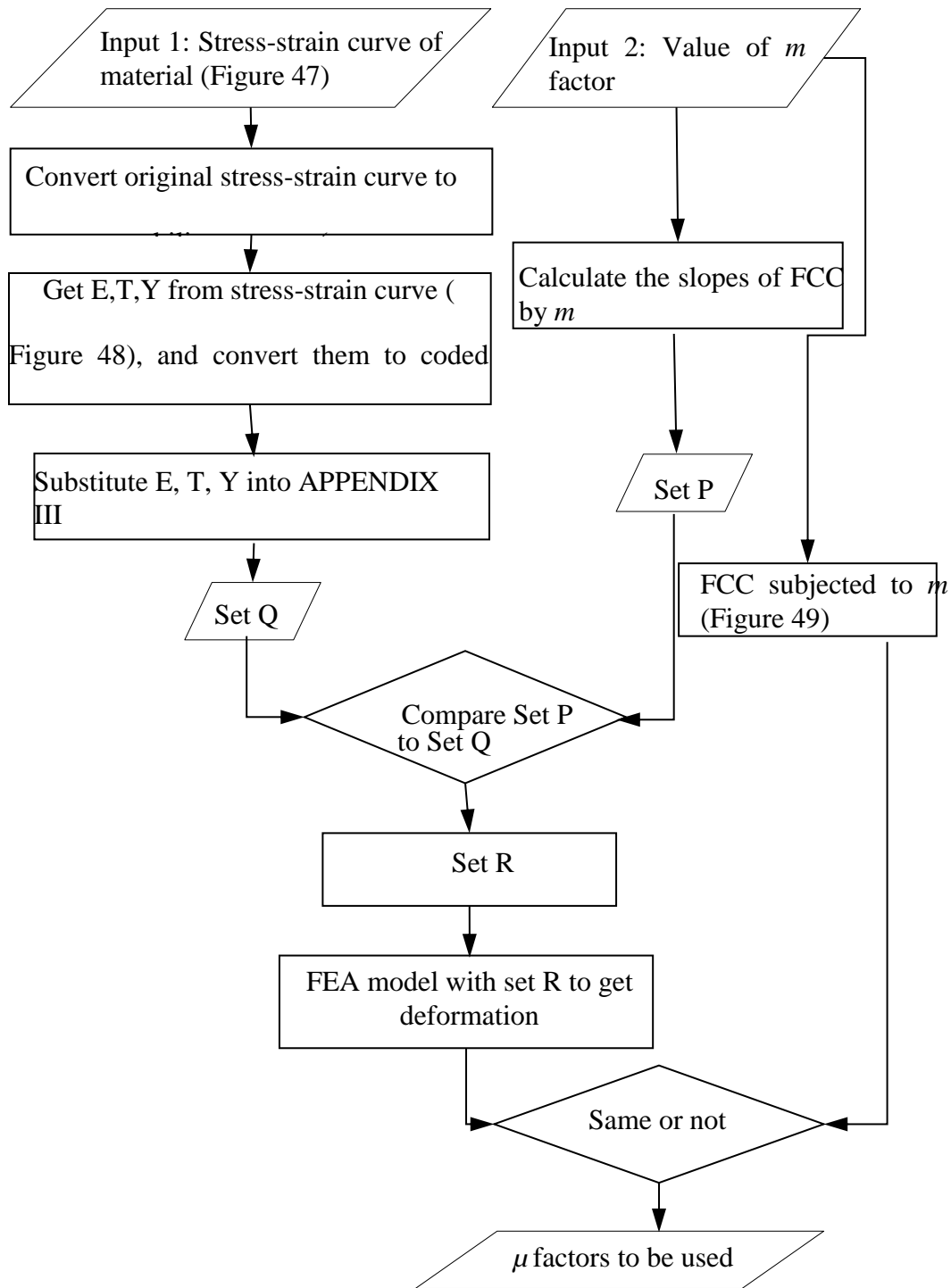
Figure 46. Flow chart of the process of finding the μ factors to describe the m factor

The input data for the process are *m* factor and stress-strain curve of the material compressed. FCM by *m* factors is from Guo's research (Guo et al. 2010, 94-97). Also the stress-strain curve of the material used is present. So there is sufficient input information to conduct the applications of the method shown in this research. The process is carried out in five steps as shown in this section.

5.2.1   Calculation of elastic modulus, tangent modulus, yield strength

In this step, it is going to convert the original stress-strain curve of the material into bilinear curve and get the elastic modulus (E), tangent modulus (T), and yield point (Y) from the bilinear stress-strain curve.

The material used in this case is the LY12 from Guo's study (Guo et al. 2010, 94-97), and the constitutive curve is shown in Figure 47. As it is shown in

Figure 48, four points (0.001699 32.68)--r, (0.004417 232)--s, (0.05879 413.4)--t, and (0.1223 413.4)--p are picked from the constitutive curve. From left to right, the first two data points are used to construct the elastic deformation period. Because the elastic strain less than 0.01, so the two data are selected within the stain range of 0--0.01, and have them divided away from each other reasonable. The last two data points are used to construct the stress-strain curve for plastic deformation. Because on the actual stress-strain curve the elastic deformation transfer to plastic deformation smoothly, data picked for bilinear curve are going to avoid points on the transferring section. The intersect point of the straight lines constructed by first two points and last two points is the yield point.

As these values on the chart are true stresses and true strains, they are converted to engineering stresses and engineering strains for calculating the elastic modulus, tangent modulus and yield points. Then the values of them are 73.9GPa for elastic modulus, 450.7MPa for tangent modulus, and 415.0Mpa for yield strength. To maintain the consistency of the unit of measurement with the previous calculations and equations which are based on ANSI, the units of elastic modulus, tangent modulus and yield strength are converted. Then the Elastic Modulus is 10720.50ksi, Tangent Modulus is 65.37ksi, and Yield Strength is 60.19ksi.
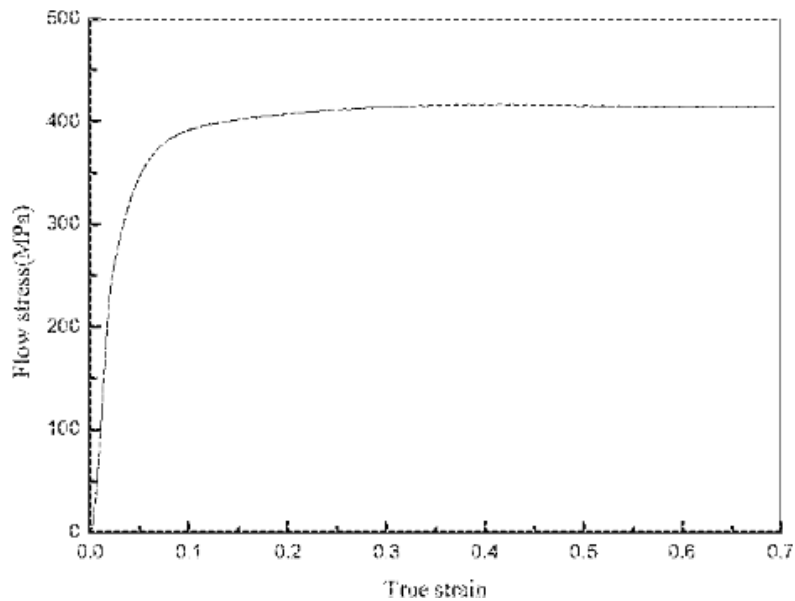
Figure 47. Constitutive curve of LY12
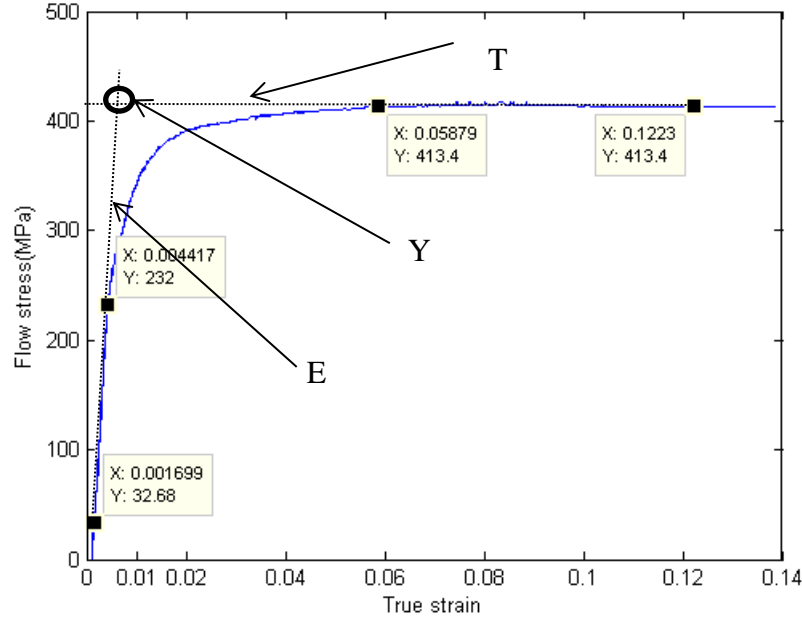
Figure 48. E, T,& Y from LY12

Then the actual material properties, 'a=10720.50', 'b=65.37', and 'c=60.19' are converted into coded material properties so that they can be applied in equations representing the material properties and slopes. The coded material properties are calculated by following equations which are deduced by the range and level of each factor.

$$A = (a - 6490) * \frac{2}{30800-6490} - 1;$$

$$B = b * \frac{2}{13000} - 1;$$

$$C = (c - 17.13962) * \frac{2}{268-17.13962} - 1;$$

The 'A', 'B', and 'C' are coded parameter which are defined in section 3.3.7, which are the variables in equations shown in APPENDIX III, are used to calculate the response, slopes of points on the FCC. A is -0.65, B is -0.9899, and C is -0.657.

5.2.2 Get slopes of FCC by *m* factor

Calculate the slopes of FCC by *m* factor at each selected height reduction level. Noted such set of slopes as "set P" in a array set, and it is nominal slope set. Table 8 shows how the data is formed in "set P" for one selected *m* factor. It is an array, with slopes on the FCC curve stored as elements. In this case study, three friction calibration curve subjected to constant *m* factor from Figure 49 (Guo,F.,Gershenson,J.K. 2003, 393-401) are used; the high friction *m*=1; the low friction *m*=0; and medium friction *m*=0.15.

Table 8 The storage form of "set P"

Height reduction levels h%	5%	10%	15%	20%	……	55%
Slopes on the m FCC						
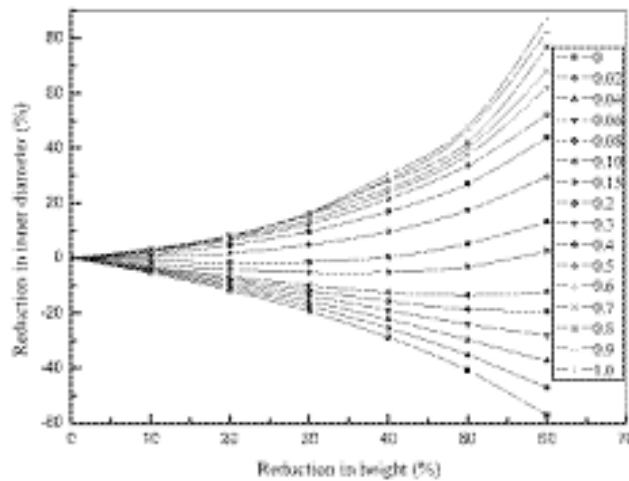
Figure 49. FCC based on *m* in Guo's research

5.2.3   Calculation of the slopes of FCC subjected to μ factors

Slopes of FCC subjected to the *m* factor at each selected height reduction level are calculated, and noted them as "set P". The coded factors (E, T, and Y) from the first step are applied into the equations from the APPENDIX III so that a matrix of slopes at each μ factor and reduction level is obtained and the substitution process is shown in Figure 50. Record such matrix as "set Q", and it is the potential slopes set. The data form of "set Q" is shown in Table 9. The column is the reduction level. The row is the μ factor level. Each the element in the matrix is the slope of the FCCs subjected to constant μ factor at selected reduction level. The μ factors used are from 0 to 0.57. For example, substitute -0.65, -0.9899, -0.657 into the equation which is constructed when the μ factor is 0.57, and selected reduction level is 55%

$$\frac{1}{R1} = 0.40 - 0.061 * A + 0.14 * B - 4.41 * 10^{-3} * C - 0.057 * A * B + 5.583 * 10^{-3} * A * C - 2.156 * 10^{-4} * B * C + 0.044 * A^2 - 0.048 * B^2 + 8.012 * 10^{-3} * C^2$$

from APPENDIX III. The R1 is the value of the slope on the FCC corresponding to it which is 290.2 here. It means, when the μ factor is 0.57, and selected reduction level is 55%, the deformation curve's slope is 290.2. Slopes at other reduction levels and other μ factors are calculated similarly refer to APPENDIX III.

Input: E, T, Y in the form of coded value (A, B, C)

Equations from
APPENDIX III

Select one μ factor

Select one height reduction level

All reduction levels

No

Yes

"set Q"

All μ factor levels

No

Yes

Finish
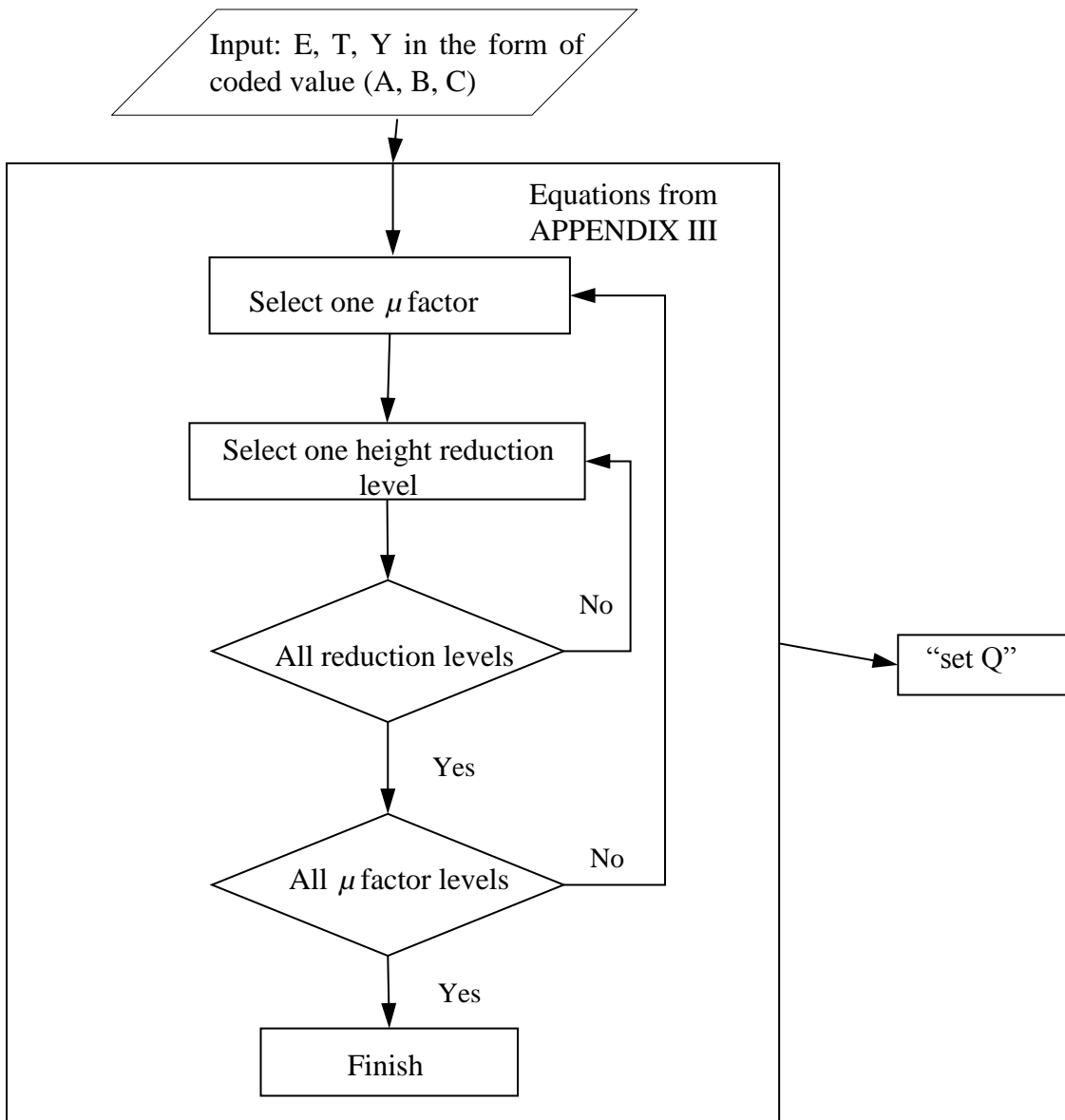
Figure 50 The calculating flow chart for the matrix of possible slopes

Table 9 Slopes on the deformation curves stored in "set Q"

Height reduction level h% / μ factor	5%	10%	15%	……	55%
0					
0.01					
0.02					
……					
0.57					

5.2.4   Selection of μ factor at each reduction level

Compare "set P" to "set Q". At each reduction level, there will be one value from "set Q" closest to the value from "set P" and record the μ factor corresponding to it in "set R". After going through all selected reduction levels, the candidate μ factors for each reduction levels are recorded in "set R". Then the suggested friction μ candidates for different m value are shown in the Table 10.

Table 10 μ candidates

Deformation period	Assigned μ when m=0	Assigned μ when m=0.15	Assigned μ when m=1	Modified μ when m=1
5%	0	0.05	0.15	0.15
10%	0	0.08	0.15	0.20
15%	0	0.09	0.15	0.20
20%	0	0.10	0.20	0.20
25%	0	0.09	0.57	0.57
30%	0	0.09	0.40	0.40
35%	0	0.07	0.30	0.30
40%	0	0.07	0.30	0.30
45%	0	0.06	0.57	0.57
50%	0	0.06	0.57	0.57
55%	0	0.55	0.30	0.57

5.2.5 Verification the conversion of friction coefficient factors

After applying friction candidates from Table 10 in the ANSYS simulations with the code shown in APPENDIX I, the comparisons of deformation curves are constructed between deformation curve from multiple μ and the FCM by m factors as shown in Figure 51.

a. m=0

b. m=0.15

c. m=1.0
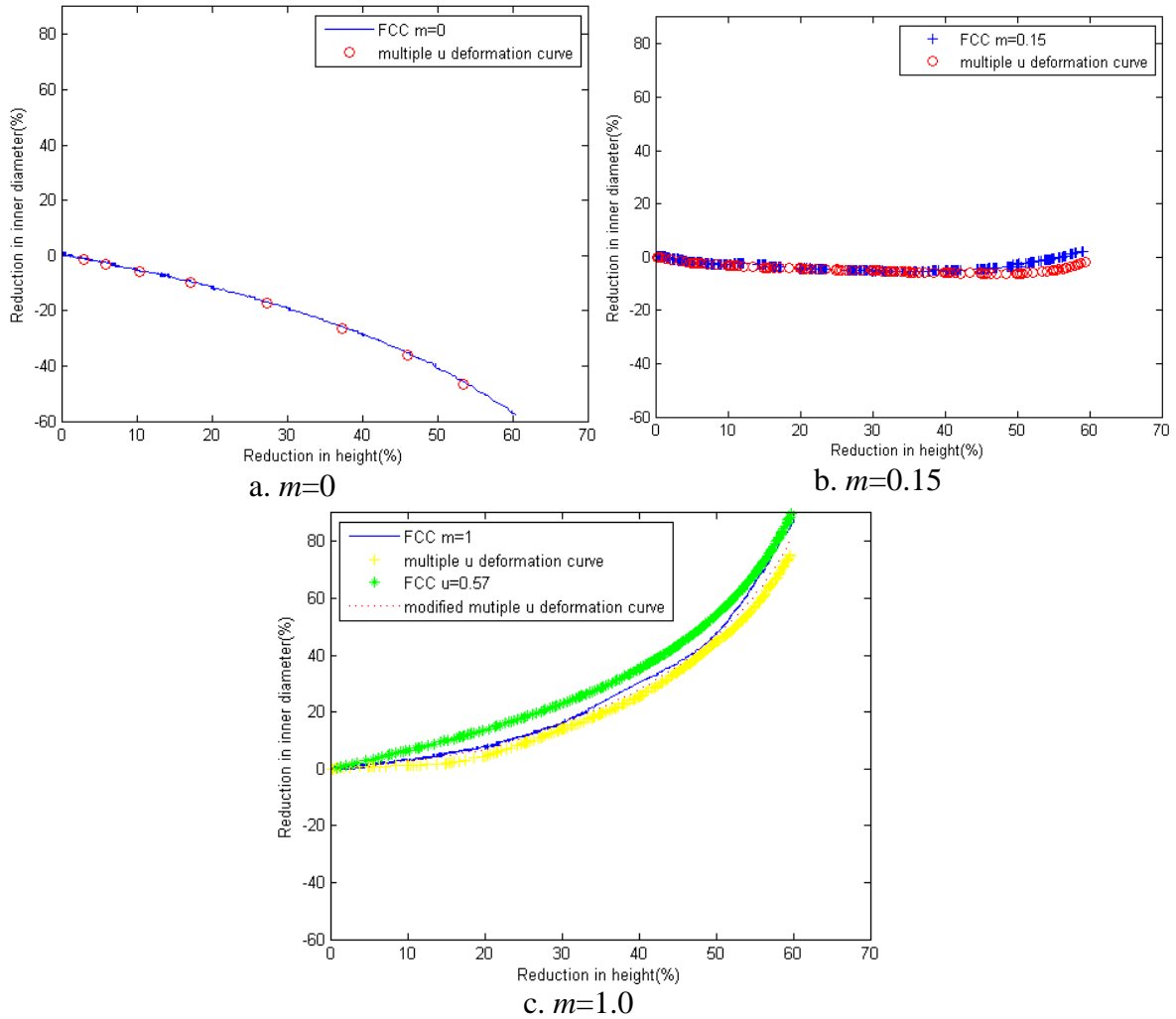
Figure 51. The relationship between reductions in internal diameter and height at

different m for LY12 (Aluminum alloy)

In Figure 51, it plots the deformation curve obtained using the multiple μ factors determined for LY12, by the method proposed in this thesis, and in each subplot, they compared with the FCC with constant m factor. It shows good matches in the three typical FCC selected. x axis are the axial reduction ratio of the ring specimen, y axis are the reduction ratio of the internal diameter of the ring specimen. In Figure 51 a, the $m=0$ (ideally smooth), and the $u=0$ represent exactly the same friction condition, so that two curves are exactly overlapped. In Figure 51b, the normal interface friction factor $m=0.15$ is applied. Two curves are in slightly parabolic shape, and they almost overlaps to each other. It means that the deformation of the ring specimen with combined μ factors and that with constant $m=0.15$ are almost the same. Their internal diameters of the rings first expanded and then shrank. In Figure 51c, four curves are presented. The FCC for $m=1$, the FCC for $\mu=0.57$, and two curves by applying multiple μs are plotted. One of the deformation curves is generated with list of μ factors gained by the method proposed in this thesis directly, and the other is generated with that list after slight modifying on it. Both $m=1$ and $\mu=0.57$ are supposed to represent the sticking interface. However, in Figure 51, it shows that the curve generated by $m=1$ is closer to the deformation curve for multiple μ than that of for $\mu=0.57$. When μ factors are modified at some deformation periods, the deformation curve moves even closer toward the FCC by $m=1$.

5.3   Summary of the DOE on simulation of ring compression test

In this chapter, the complete procedure of using multi-stage friction coefficient factor to simulate the constant shear friction factor is demonstrated, and it's verified

104

through a case study. It shows that the deformation from the multi-stage μ factors and the constant m factors matches well in the ring compression tests.

It also indicates that to have better matching, the procedure for generate the suggested μ list can be improved in two ways. The curve fitting model of the objective deformation curve, the FCM by m factor, can be improved with better fitting model, so that more accurate desired slopes can be obtained. More control intermediate reduction ratio can be used for precise control on the deformation simulation.

6. Guideline of the using the multi-stage μ factor method

This section describes the method of converting constant shear friction factor *m* to friction coefficient factor μ. It involves three steps

1. Data collecting

Two types of information are needed: one is the mechanical properties of the material; the other is the *m* factor of the particular forging process, the *m*-based FCC corresponding to it.

One should obtain the mechanical properties of the material used in the manufacturing, either through test or from handbook. To find the *m* factor, one should compress a ring specimen, measure the changes in height and internal diameter, and refer it to the *m*-based FCM. Then one can record the *m*-based FCC for the *m* factor.

2. Data analysis

The data acquired in the first step is used differently. For the *m*-based FCC, one should calculate the slope of the curve at 11 reduction levels and store them in an array "set P".

The mechanical properties are treated as following. Firstly, get the elastic modulus (E), tangent modulus (T), and yield strength (Y). Secondly, one should convert the actual values of E, T, and Y into codes values and substitute them into equations in APPENDIX III. Thirdly, one should calculate the slopes of FCC at each possible μ factor and at each reduction level, and store them in a matrix, "set Q", in the form shown in Table 9.

106

3. Data comparison

The "set P" and "set Q" should be compared at each reduction level, so that the slopes from "set Q" which are closest to the values in "set P" at the same reduction level are selected. Then one check the μ factor corresponding to the selected slopes in "set Q", and store them in "set R". The elements in "set R" would be the best candidate μ factor at each reduction level. When apply suggested μ factor from "set R" in time sequence, it will simulate the friction condition described by m factor.

7. Conclusions

A FEA model, running with commercial software ANSYS is established for simulating the deformation of the ring compression test. In this model, the internal and outer cylindrical surfaces of the ring, which do not contact initially with the die, as well as the original interface between ring specimen and plate die are applied with friction factors. This is because those initially separated surface may touch the die due to the material folding phenomenon. Also, the Poisson's ratio is set constantly as 0.5 for any materials. When adopted the same input parameters of T. Robinson's experiment in the established model, the simulating results is agreement with Robinson's experimental results, indicating that the established FEA model works well.

It is shown that the final shape of the compressed ring specimen can be simulated by applying some different μ friction factors stage by stage, and the slopes of FCC curve and reduction ratio are parameters that represent the deformation of the ring specimen. Also the material mechanical properties are proved to be another important factor in the ring compression test.

Some formulas between the deformation parameters, material mechanical properties, and μ factors are generated through the statistical analysis to the simulating results of the ring compression test. Based on these formulas, a method to substitute the m factor with μ factors for particular material by selecting and applying the μ factor in time sequence is found. For a certain material, a matrix, which obtains possible slopes of FCC under all concerned μ factors at selected height reduction level, is generated through the statistical analysis on simulations. Then the possible set of μ factors are selected by

comparing the slopes of *m*-based FCC to the matrix of possible slopes of FCC at each height reduction level. The slope from the matrix with minimum difference to the slopes on the *m*-based FCC is associated with the μ factor which can describe the same friction condition as *m* does at the particular reduction level. Through such substitution, the deformation of the specimen with the selected μ factor matches that of the specimen when the *m* factor is applied. This method overcomes the shortage of FEA method in the compressing process: the *m* factor which is widely adopted in cold forging is not used to describe friction condition in FEA. By converting the *m* factor into μ factor, the cold forging can be simulated, so that the processing can be predicted.

8.   Bibliography

ASM International. 2002. *Atlas of Stress-Strain Curves* ASM International.

Avitzur, B. 1964. "Forging of Hollow Discs." *Israel J.Technol* 2 (3): 295-304.

Avitzur, Betzalel. 1968. *Metal Forming: Processes and Analysis*. New York: McGraw-Hill.

Bay, Niels. 1987. "Friction Stress and Normal Stress in Bulk Metal-Forming Processes." *Journal of Mechanical Working Technology* 14 (2): 203-223.

Behrens, A. and H. Schafstall. 1998. "2D and 3D Simulation of Complex Multistage Forging Processes by use of Adaptive Friction Coefficient." *Journal of Materials Processing Technology* 80–81 (0): 298-303.

Boothroyd, G. and Leo Alting. 1994. *Manufacturing Engineering Processes*. Vol. 40. New York: Marcel Dekker.

Cristino, V. A. M., P. A. R. Rosa, and P. A. F. Martins. 2011. "Surface Roughness and Material Strength of Tribo-Pairs in Ring Compression Tests." *Tribology International* 44 (2): 134-143.

Danckert, Joachim and Tarras Wanheim. 1988. "Analysis of the Ring Test Method for the Evaluation of Frictional Stresses in Bulk Metal Forming Processes." *CIRP Annals - Manufacturing Technology* 37 (1): 217-220.

Davim, J. Paulo and MyiLibrary. 2012. *Statistical and Computational Techniques in Manufacturing*. New York: Springer.

de Sanctis, A. M., A. Forcellese, S. M. Roberts, and P. J. Withers. 1997. "Frictional Behaviour of Al359/SiC/20p Composite Under Isothermal and Non-Isothermal Hot-Working Conditions as a Function of Surface Roughness." *Journal of Materials Processing Technology* 72 (2): 195-200.

DePierre, V. and AT Male. 1969. "Mathematical Calibration of the Ring Test for Friction Studies in Flat Forging Operations."Univ. of Manchester England, .

Dixit, Prakash Mahadeo, Uday S. Dixit, and SpringerLink (Online service). 2008. *Modeling of Metal Forming and Machining Processes: By Finite Element and Soft Computing Methods*. London: Springer.

Finite element method. https://en.wikipedia.org/wiki/Finite_element_method., https://en.wikipedia.org/wiki/Finite_element_method.

Guérin, J. D., H. Bartys, A. Dubois, and J. Oudin. 1999. "Finite Element Implementation of a Generalized Friction Model:: Application to an Upsetting–sliding Test." *Finite Elements in Analysis and Design* 31 (3): 193-207.

Guide, ANSYS User's. 2007. "Ver. 11.0." *ANSYS Inc*.

Guo, Bin, Feng Gong, Chunju Wang, and Debin Shan. 2010. "Experimental Research and Numerical Simulation of LY12 and HPb62-2 Ring Compression." In *Advanced Tribology*, edited by Jianbin Luo, Yonggang Meng, Tianmin Shao and Qian Zhao, 94-97: Springer Berlin Heidelberg.

Guo,F.,Gershenson,J.K. 2003. "Comparison of Modular Measurement Methods Based on Consistency Analysis and Sensitivity Analysis." *ASME Conference Proceedings* Volume 3b: 15th International Conference on Design Theory and Methodology: 393-401.

Hansen, PH, Niels Bay, and Peter Christensen. 1988. "Analysis of the Ring Compression Test using a General Friction Model and the Upper Bound Elemental Technique." .

Hartley, R. S., T. J. Cloete, and G. N. Nurick. 2007. "An Experimental Assessment of Friction Effects in the Split Hopkinson Pressure Bar using the Ring Compression Test." *International Journal of Impact Engineering* 34 (10): 1705-1728.

Hatzenbichler, Thomas, Otto Harrer, Stefan Wallner, Florian Planitzer, Mario Kuss, Roman Pschera, and Bruno Buchmayr. 2012. "Deviation of the Results obtained from Different Commercial Finite Element Solvers due to Friction Formulation." *Tribology International* 49 (0): 75-79.

Hayhurst, D. R. and M. W. Chan. 2005. "Determination of Friction Models for Metallic Die–workpiece Interfaces." *International Journal of Mechanical Sciences* 47 (1): 1-25.

Hoon Noh, Jeong, Kyung Ho Min, and Beong Bok Hwang. 2011. "Deformation Characteristics at Contact Interface in Ring Compression." *Tribology International* 44 (9): 947-955.

Joun, M. S., H. G. Moon, I. S. Choi, M. C. Lee, and B. Y. Jun. 2009. "Effects of Friction Laws on Metal Forming Processes." *Tribology International* 42 (2): 311-319.

koteco.co. "Hydraulic Press.", http://www.koteco.co.kr/m21_11.htm.

Kuhn, HA, T. Erturk, and PW Lee. 1973. "A Fracture Criterion for Cold Forming(Combined Stress and/Or Strain Prediction)." *(American Society of Mechanical Engineers, 1973.) ASME, Transactions, Series H- Journal of Engineering Materials and Technology,* 95: 213-218.

Li, L. X., D. S. Peng, J. A. Liu, Z. Q. Liu, and Y. Jiang. 2000. "An Experimental Study of the Lubrication Behavior of A5 Glass Lubricant by Means of the Ring Compression Test." *Journal of Materials Processing Technology* 102 (1–3): 138-142.

Lin, S. Y. 1999. "Investigation of Die–Workpiece Interface Friction with Lubrication during the Upsetting Process." *International Journal of Advanced Manufacturing Technology* 15 (9): 666-673.

———. 1995. "An Investigation of Die-Workpiece Interface Friction during the Upsetting Process." *Journal of Materials Processing Technology* 54 (1–4): 239-248.

Lin, Z. C. and S. Y. Lin. 1990. "An Investigation of a Coupled Analysis of a Thermo-Elastic-Plastic Model during Warm Upsetting." *International Journal of Machine Tools and Manufacture* 30 (4): 599-612.

Lin, Zone-Ching and Chun-kung Chen. 2005. "Inverse Calculation of the Friction Coefficient during the Warm Upsetting of Molybdenum." *International Journal of Mechanical Sciences* 47 (7): 1059-1078.

———. 2006. "Inverse Calculation of the Friction Coefficient for Upsetting a Cylindrical Mild Steel by the Experimental Load." *Journal of Materials Processing Technology* 178 (1–3): 297-306.

Mahrenholtz, D. and N. L. Dung. 1987. "Mathematical Modelling of Metal Forming Processes by Numerical Methods." Sttugart, Springer-Verlag, 1987.

MALE, A. T. 1964. "A Method for the Determination of the Coefficient of Friction of Metals Under Conditions of Bulk Plastic Deformation." 93: 38-46.

Male, Alan T. and Vincent DePierre. 1970. "The Validity of Mathematical Solutions for Determining Friction from the Ring Compression Test." *Journal of Lubrication Technology* 92 (3): 389.

Mielnik, Edward M. 1991. *Metalworking Science and Engineering*. New York: McGraw-Hill.

Montgomery, Douglas C. 2009. *Design and Analysis of Experiments*. Hoboken, NJ: Wiley.

Po ̈hlandt, Klaus and Kurt Lange. 1985. *Handbook of Metal Forming*. New York: McGraw-Hill.

Polakowski, NH. 1949. "The Compression Test in Relation to Cold Rolling." *J.Iron Steel Inst* 163: 250-276.

Rao, J. Babu, Syed Kamaluddin, J. Appa Rao, M. M. M. Sarcar, and N. R. M. R. Bhargava. 2009a. "Deformation Behavior of Al–4Cu–2Mg Alloy during Cold Upset Forging." *Journal of Alloys and Compounds* 471 (1–2): 128-136.

———. 2009b. "Finite Element Analysis of Deformation Behavior of Aluminium–Copper Alloys." *Materials & Design* 30 (4): 1298-1309.

Robinson, T., H. Ou, and C. G. Armstrong. 2004. "Study on Ring Compression Test using Physical Modelling and FE Simulation." *Journal of Materials Processing Tech* 153: 54-59.

Rudkins, N. T., P. Hartley, I. Pillinger, and D. Petty. 1996. "Friction Modelling and Experimental Observations in Hot Ring Compression Tests." *Journal of Materials Processing Tech* 60 (1): 349-353.

Sahi, M., R. Rahouadj, R. Herbach, and D. Choulier. 1996. "The Influence of Viscoplasticity in the Interpretation of the Ring Test." *Journal of Materials Processing Technology* 58 (2–3): 286-292.

Schroeder, William and DA Webster. 1949. "Press-Forging Thin Sections: Effect of Friction, Area and Thickness on Pressure Required." *J.Appl.Mech* 16: 289-294.

Shah, Jami J. and Howard A. Kuhn. 1986. "An Empirical Formula for Workability Limits in Cold Upsetting and Bolt Heading." *Journal of Applied Metalworking* 4 (3): 255-261.

Shaw, MC and JP Avery. 1983. "Forming Limits." *Journal of Vibration Acoustics Stress and Reliability in Design* 105: 247.

Sofuoglu, H. and H. Gedikli. 2002. "Determination of Friction Coefficient Encountered in Large Deformation Processes." *Tribology International* 35 (1): 27-34.

Sofuoglu, H., H. Gedikli, and J. Rasty. 2001. "Determination of Friction Coefficient by Employing the Ring Compression Test." *JOURNAL OF ENGINEERING MATERIALS AND TECHNOLOGY-TRANSACTIONS OF THE ASME* 123 (3): 338-348.

Sofuoglu, Hasan and Jahan Rasty. 1999. "On the Measurement of Friction Coefficient Utilizing the Ring Compression Test." *Tribology International* 32 (6): 327-335.

Szeliga, Danuta, Jerzy Gawad, and Maciej Pietrzyk. 2006. "Inverse Analysis for Identification of Rheological and Friction Models in Metal Forming." *Computer Methods in Applied Mechanics and Engineering* 195 (48–49): 6778-6798.

United States. Dept. of Defense. 1966. *Metallic Materials and Elements for Aerospace Vehicle Structures*. United States:.

Valberg, Henry S. 2010. *Applied Metal Forming: Including FEM Analysis* Cambridge University Press.

Wagener, HW and J. Wolf. 1995. "Friction in Cold Forging of Steel.".

weiku.com. "Forging Hummer C41-55kg.", http://www.weiku.com/products/10427534/Forging_Hammer_C41_55kg.html.

Yang, Tung-Sheng. 2007. *A Refined Friction Modeling for Lubricated Metal Forming Process*. Vol. 27 Springer Netherlands.

APPENDIX I The ANSYS INPUT FILE FOR MULTI-STAGE μ FACTOR

!*************************It is an example code when μ factors are 0.05, 0.08, 0.09, 0.10, 0.09, 0.09, 0.07, 0.07, 0.06, 0.06, 0.055, 0.055, and this set of μ factors is used to describe the constant shear friction m=0.15

```
!BinBuo m=0.15 combine ,0.57   Elastic Modulus was 10720.50ksi, Tangent Modulus
was 65.37ksi, and Yield strength was !60.19ks
FINISH  ! Make sure we are at BEGIN level
/CLEAR,NOSTART  ! Clear model since no SAVE found
/NOPR
KEYW,PR_SET,1
KEYW,PR_STRUC,1
/PREP7
ET,1,PLANE182
KEYOPT,1,1,0
KEYOPT,1,3,1
KEYOPT,1,6,0

MPTEMP,,,,,,,,
MPTEMP,1,0
MPDATA,EX,1,,10720.50
MPDATA,PRXY,1,,0.48
TB,BISO,1,1,2,
TBTEMP,0
TBDATA,,60.19,65.37,,,,
MPTEMP,,,,,,,,
MPTEMP,1,0

MPDATA,MU,2,,0.57
MPDATA,MU,3,,0.05
MPDATA,MU,4,,0.57
*SET,TOTALHEIGHT,0.25
*SET,Height,TOTALHEIGHT/2
*SET,OUTDIAMETER , Height*6
*SET,OUTRADIUS , OUTDIAMETER/2
*SET,INTERNALRADIUS,OUTRADIUS/2
*SET,WIDTH,OUTRADIUS-INTERNALRADIUS
blc4,INTERNALRADIUS,0,WIDTH,Height
K,5,0,HEIGHT
K,6,OUTDIAMETER,HEIGHT
K,7,OUTDIAMETER-0.003125,HEIGHT
LSTR,5,6
```

```
LSTR,5,7
LESIZE,1, , ,60, , , , ,1
LESIZE,3, , ,60, , , , ,1
LESIZE,2, , ,40, , , , ,1
LESIZE,4, , ,40, , , , ,1
AMESH,1
gplot
!*
!*
!*
CM,_NODECM,NODE
CM,_ELEMCM,ELEM
CM,_KPCM,KP
CM,_LINECM,LINE
CM,_AREACM,AREA
CM,_VOLUCM,VOLU
/GSAV,cwz,gsav,,temp
MP,MU,3,0.05
MAT,3
MP,EMIS,3,7.88860905221e-031
R,3
REAL,3
ET,2,169
ET,3,172
R,3,,,0.1,0.1,0,
RMORE,,,1.0E20,0.0,1.0,
RMORE,0.0,0,1.0,,1.0,0.5
RMORE,0,1.0,1.0,0.0,,1.0
KEYOPT,3,3,0
KEYOPT,3,4,0
KEYOPT,3,5,0
KEYOPT,3,7,0
KEYOPT,3,8,0
KEYOPT,3,9,0
KEYOPT,3,10,2
KEYOPT,3,11,0
KEYOPT,3,12,0
KEYOPT,3,2,0
KEYOPT,2,2,0
KEYOPT,2,3,0
! Generate the target surface
LSEL,S,,,5
CM,_TARGET,LINE
```

```
TYPE,2
LATT,-1,3,2,-1
TYPE,2
LMESH,ALL
! Create a pilot node
KSEL,S,,,6
KATT,-1,3,2,-1
KMESH,6
! Generate the contact surface
LSEL,S,,,3
CM,_CONTACT,LINE
TYPE,3
NSLL,S,1
ESLN,S,0
ESURF
*SET,_REALID,3
ALLSEL
ESEL,ALL
ESEL,S,TYPE,,2
ESEL,A,TYPE,,3
ESEL,R,REAL,,3
LSEL,S,REAL,,3
/PSYMB,ESYS,1
/PNUM,TYPE,1
/NUM,1
EPLOT
ESEL,ALL
ESEL,S,TYPE,,2
ESEL,A,TYPE,,3
ESEL,R,REAL,,3
LSEL,S,REAL,,3
CMSEL,A,_NODECM
CMDEL,_NODECM
CMSEL,A,_ELEMCM
CMDEL,_ELEMCM
CMSEL,S,_KPCM
CMDEL,_KPCM
CMSEL,S,_LINECM
CMDEL,_LINECM
CMSEL,S,_AREACM
CMDEL,_AREACM
CMSEL,S,_VOLUCM
CMDEL,_VOLUCM
```

119

```
/GRES,cwz,gsav
CMDEL,_TARGET
CMDEL,_CONTACT
!*
!*
/REPLO
!*
CM,_NODECM,NODE
CM,_ELEMCM,ELEM
CM,_KPCM,KP
CM,_LINECM,LINE
CM,_AREACM,AREA
CM,_VOLUCM,VOLU
/GSAV,cwz,gsav,,temp
MP,MU,2,0.57
MAT,2
MP,EMIS,2,7.88860905221e-031
R,4
REAL,4
ET,4,169
ET,5,172
R,4,,,0.1,0.1,0,
RMORE,,,1.0E20,0.0,1.0,
RMORE,0.0,0,1.0,,1.0,0.5
RMORE,0,1.0,1.0,0.0,,1.0
KEYOPT,5,3,0
KEYOPT,5,4,0
KEYOPT,5,5,0
KEYOPT,5,7,0
KEYOPT,5,8,0
KEYOPT,5,9,0
KEYOPT,5,10,2
KEYOPT,5,11,0
KEYOPT,5,12,0
KEYOPT,5,2,0
KEYOPT,4,2,0
KEYOPT,4,3,0
! Generate the target surface
LSEL,S,,,6
CM,_TARGET,LINE
TYPE,4
LATT,-1,4,4,-1
TYPE,4
```

```
LMESH,ALL
! Create a pilot node
KSEL,S,,,7
KATT,-1,4,4,-1
KMESH,7
! Generate the contact surface
LSEL,S,,,2
LSEL,A,,,4
CM,_CONTACT,LINE
TYPE,5
NSLL,S,1
ESLN,S,0
ESURF
*SET,_REALID,4
ALLSEL
ESEL,ALL
ESEL,S,TYPE,,4
ESEL,A,TYPE,,5
ESEL,R,REAL,,4
LSEL,S,REAL,,4
/PSYMB,ESYS,1
/PNUM,TYPE,1
/NUM,1
EPLOT
ESEL,ALL
ESEL,S,TYPE,,4
ESEL,A,TYPE,,5
ESEL,R,REAL,,4
LSEL,S,REAL,,4
CMSEL,A,_NODECM
CMDEL,_NODECM
CMSEL,A,_ELEMCM
CMDEL,_ELEMCM
CMSEL,S,_KPCM
CMDEL,_KPCM
CMSEL,S,_LINECM
CMDEL,_LINECM
CMSEL,S,_AREACM
CMDEL,_AREACM
CMSEL,S,_VOLUCM
CMDEL,_VOLUCM
/GRES,cwz,gsav
CMDEL,_TARGET
```

```
CMDEL,_CONTACT
DL,1, ,SYMM
FINISH
/SOL
ANTYPE,0
NLGEOM,1
TIME,1
OUTRES,ERASE
OUTRES,ALL,ALL
DK,6, ,-0.05*HEIGHT, ,0,UY, , , , , ,
DK,7, ,-0.05*HEIGHT, ,0,UY, , , , , ,
SOLVE
MP,MU,3,0.08
DK,6, ,-0.10*HEIGHT, ,0,UY, , , , , ,
DK,7, ,-0.10*HEIGHT, ,0,UY, , , , , ,
SOLVE
MP,MU,3,0.09
DK,6, ,-0.15*HEIGHT, ,0,UY, , , , , ,
DK,7, ,-0.15*HEIGHT, ,0,UY, , , , , ,
SOLVE
MP,MU,3,0.10
DK,6, ,-0.20*HEIGHT, ,0,UY, , , , , ,
DK,7, ,-0.20*HEIGHT, ,0,UY, , , , , ,
SOLVE
MP,MU,3,0.09
DK,6, ,-0.25*HEIGHT, ,0,UY, , , , , ,
DK,7, ,-0.25*HEIGHT, ,0,UY, , , , , ,
SOLVE
MP,MU,3,0.09
DK,6, ,-0.30*HEIGHT, ,0,UY, , , , , ,
DK,7, ,-0.30*HEIGHT, ,0,UY, , , , , ,
SOLVE
MP,MU,3,0.07
DK,6, ,-0.35*HEIGHT, ,0,UY, , , , , ,
DK,7, ,-0.35*HEIGHT, ,0,UY, , , , , ,
SOLVE
MP,MU,3,0.07
DK,6, ,-0.40*HEIGHT, ,0,UY, , , , , ,
DK,7, ,-0.40*HEIGHT, ,0,UY, , , , , ,
SOLVE
MP,MU,3,0.06
DK,6, ,-0.45*HEIGHT, ,0,UY, , , , , ,
DK,7, ,-0.45*HEIGHT, ,0,UY, , , , , ,
```

```
SOLVE
MP,MU,3,0.06
DK,6, ,-0.50*HEIGHT, ,0,UY, , , , , ,
DK,7, ,-0.50*HEIGHT, ,0,UY, , , , , ,
SOLVE
MP,MU,3,0.055
DK,6, ,-0.55*HEIGHT, ,0,UY, , , , , ,
DK,7, ,-0.55*HEIGHT, ,0,UY, , , , , ,
SOLVE
MP,MU,3,0.055
DK,6, ,-0.60*HEIGHT, ,0,UY, , , , , ,
DK,7, ,-0.60*HEIGHT, ,0,UY, , , , , ,
SOLVE
FINISH
/POST26
/UI,COLL,1
NUMVAR,200
SOLU,191,NCMIT
STORE,MERGE
FILLDATA,191,,,,1,1
REALVAR,191,191
!*
NSOL,2,102,U,Y, DefHeight
STORE,MERGE
!*
NSOL,3,1,U,X, DefRad
STORE,MERGE
PRVAR,2,3,
!*
!***********************************
*GET, PPP, VARI, 0, NSETS, , ,
*CREATE,scratch,gui
*DEL,_P26_EXPORT
*DIM,_P26_EXPORT,TABLE,PPP,2
VGET,_P26_EXPORT(1,0),1
VGET,_P26_EXPORT(1,1),2
VGET,_P26_EXPORT(1,2),3
*cfopen,BinGuo_m015dif057,txt,casestudyBinGuo
*VWRITE,'TIME','DefHeight','DefRad'
%14C %14C %14C
*VWRITE,_P26_EXPORT(1,0),_P26_EXPORT(1,1),_P26_EXPORT(1,2)
%14.5G %14.5G %14.5G
*cfclos
```

123

```
*END
/INPUT,scratch,gui
!***************************
```
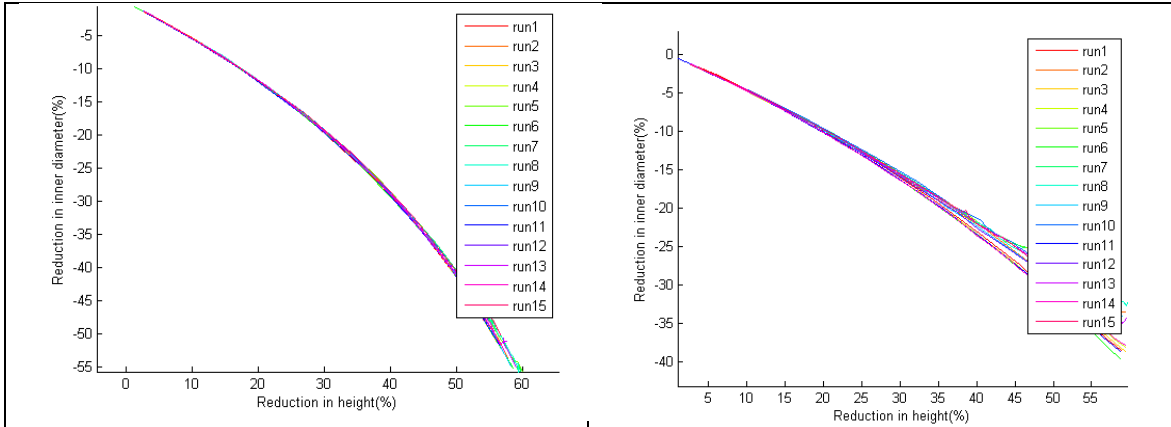
APPENDIX II FCM FOR EACH FRICTION LEVELS

Figure 52. μ=0
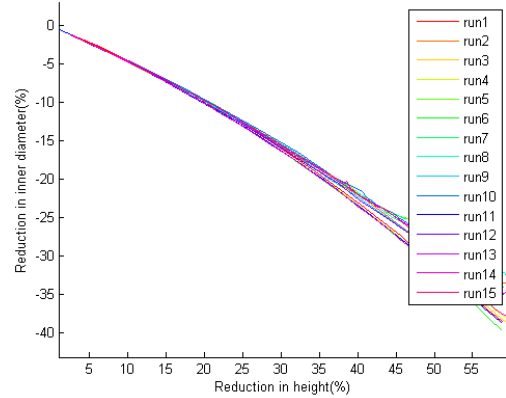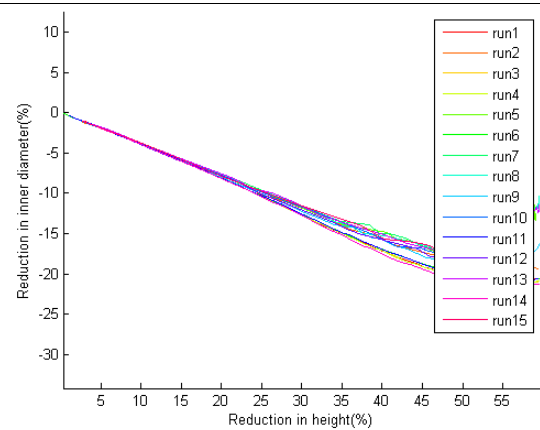
Figure 53. μ=0.02
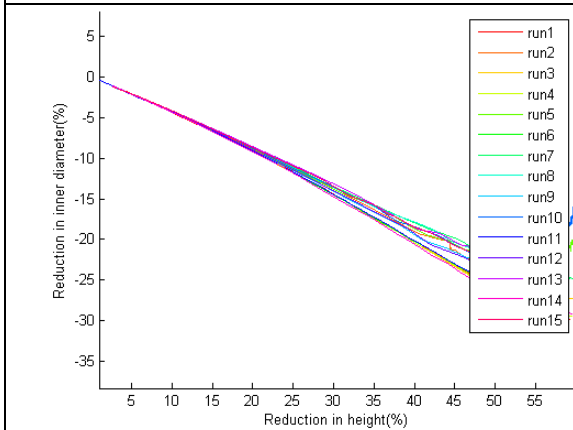

Figure 54. μ=0.03

Figure 55. μ=0.04

Figure 56. μ=0.05

Figure 57. μ=0.06

Figure 58. μ=0.07

Figure 59. μ=0.08

Figure 60. μ=0.10

Figure 61. μ=0.12

Figure 62. μ=0.15

Figure 63. μ=0.20

Figure 64. μ=0.30
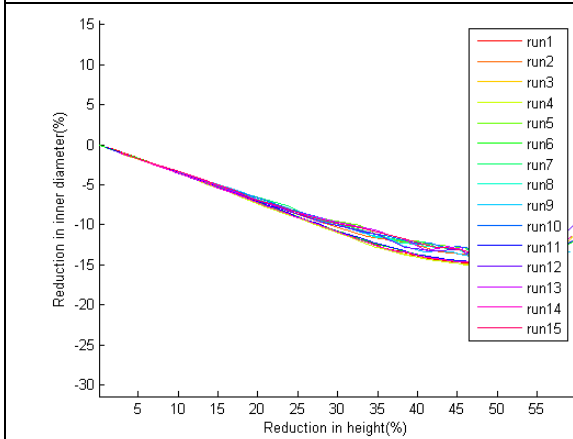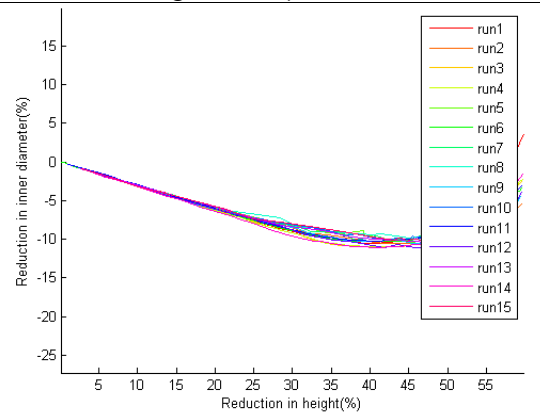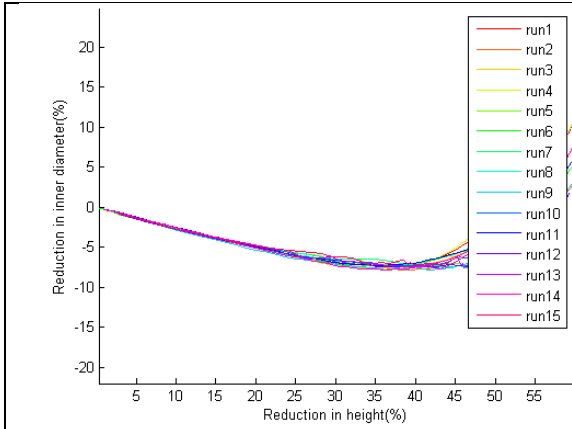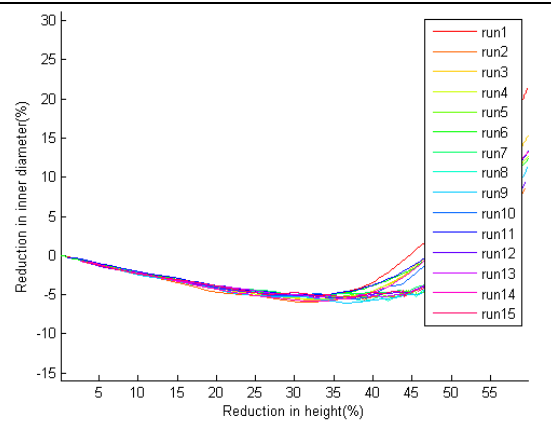

Figure 65. μ=0.40
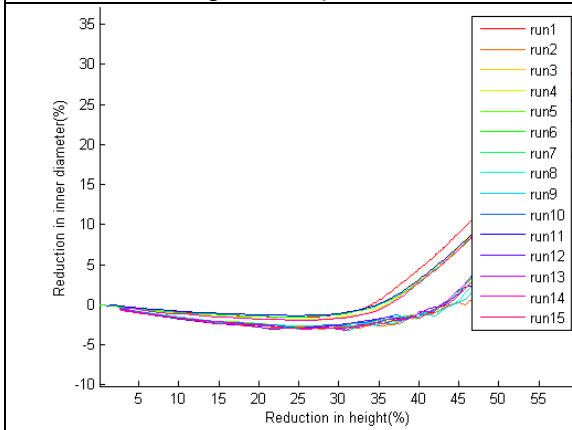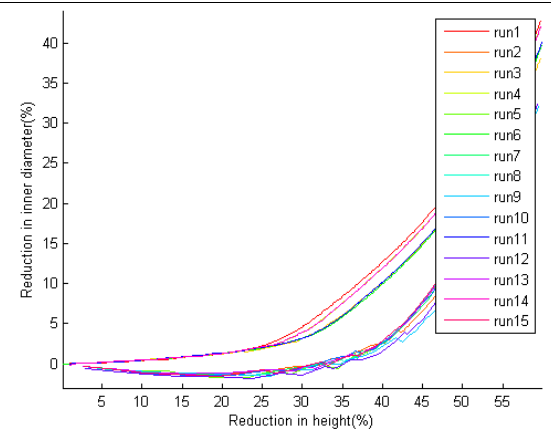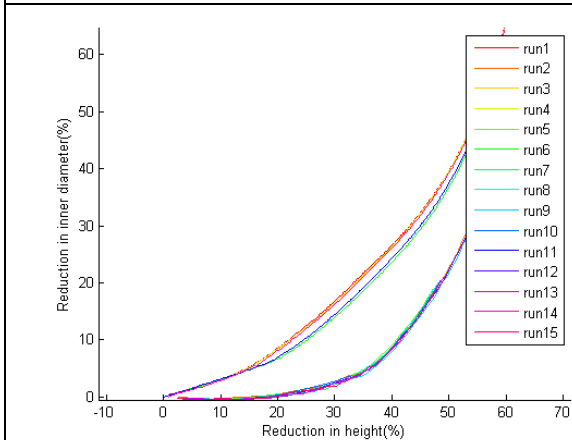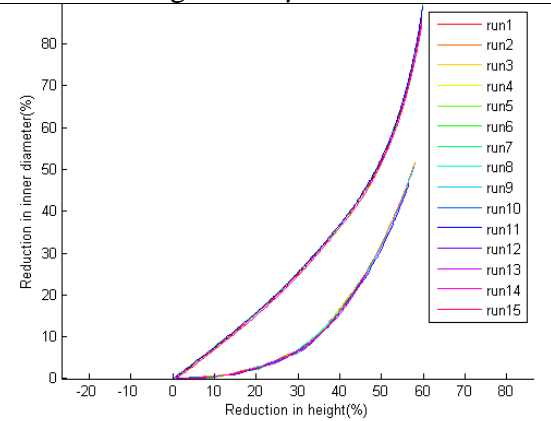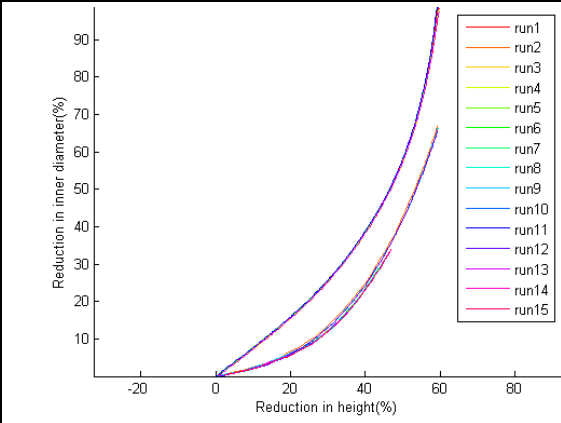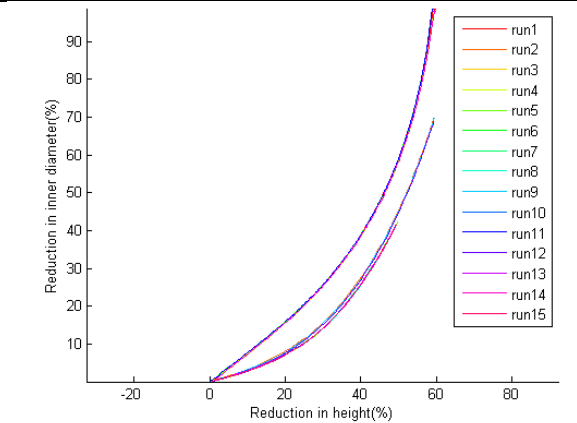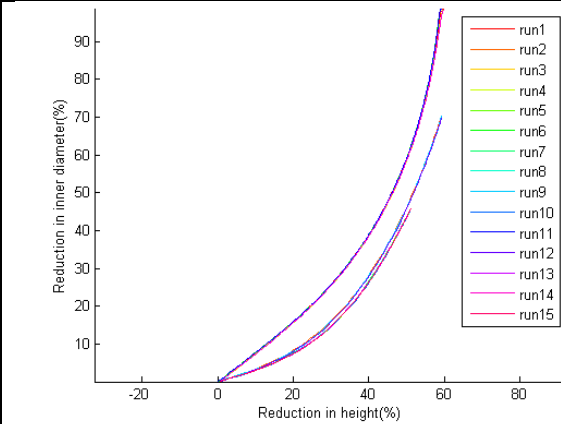
Figure 66. μ=0.57

APPENDIX III EQUATIONS FOR MATERIAL PROPERTIES AND

DEFORMATION SLOPES

R1 are slopes of the FCC for selected μ factor and selected height reduction levels.

A, B, C are coded elastic modulus, tangent modulus, and yield strength.

The section organized equations in the following way: first fix the μ factor, and list equations at all reduction level (h%). Then after all reduction level are calculated, move to the next μ factor.

When the μ=0.57,

Reduction level 5%

$$(R1)^{-1/2} = 1.81 - 0.26 * A + 0.51 * B - 0.27 * c - 0.29 * A * B + 0.060 * A * C - 0.014 * B * C + 0.11 * A^2 + 0.018 * B^2 + 0.051 * C^2.$$

Reduction level 10%

$$(R1)^{-1} = 2.74 - 0.53 * A + 1.39 * B - 0.11 * C - 0.63 * A * B + 0.18 * A * C - 0.064 * B * C + 0.28 * A^2 - 0.28 * B^2 + 0.11 * C^2$$

Reduction level 15%

$$(R1)^{-3} = 10.86 - 2.90 * A + 7.84 * B - 0.79 * C - 3.09 * A * B + 1.09 * A * C - 0.35 * B * C + 1.25 * A^2 - 2.5 * B^2 + 0.31 * C^2$$

Reduction level 20%

$$(R1)^{-3} = 5.17 - 0.86 * A + 2.80 * B - 0.32 * C - 0.76 * A * B + 0.40 * A * C - 0.15 * B * C + 0.37 * A^2 - 1.44 * B^2 + 0.041 * C^2$$

Reduction level 25%

$$(R1)^{-3} = 2.51 - 0.17 * A + 0.81 * B - 0.16 * C + 0.015 * A * B + 0.16 * A * C - 0.012 * B * C - 0.043 * A^2 - 0.58 * B^2 - 0.061 * C^2$$

Reduction level 30%

$$(R1)^{-3} = 1.23 - 0.029 * A + 0.29 * B - 0.12 * C - 0.021 * A * B + 0.12 * A * C + 0.022 * B * C - 0.058 * A^2 - 0.14 * B^2 - 0.051 * C^2$$

Reduction level 35%

$$(R1)^{-3} = 0.61 - 0.11 * A + 0.22 * B - 0.020 * C - 0.17 * A * B + 0.020 * A * C - 1.065 * 10^{-3} * B * C + 0.071 * A^2 + 0.014 * B^2 + 3.868 * 10^{-4} * C^2$$

Reduction level 40%

$$(R1)^{-3} = 0.33 - 0.090 * A + 0.13 * B + 0.015 * C - 0.1 * A * B - 8.187 * 10^{-3} * A * C - 0.011 * B * C + 0.049 * A^2 + 0.021 * B^2 + 0.021 * C^2$$

Reduction level 45%

$$(R1)^{-3} = 0.19 - 0.029 * A + 0.054 * B - 3.114 * 10^{-3} * C - 0.017 * A * B + 9.48 * 10^{-3} * A * C - 5.064 * 10^{-3} * B * C - 5.21 * 10^{-3} * A^2 + 1.107 * 10^{-3} * B^2 + 9.38 * 10^{-3} * C^2$$

Reduction level 50%

$$ln(R1) = 0.73 + 0.066 * A - 0.18 * B + 0.027 * C + 0.036 * A * B - 0.042 * A * C + 0.011 * B * C - 0.012 * A^2 + 0.066 * B^2 + 1.137 * 10^{-3} * C^2$$

Reduction level 55%

$$\frac{1}{R1} = 0.40 - 0.061 * A + 0.14 * B - 4.41 * 10^{-3} * C - 0.057 * A * B + 5.583 * 10^{-3} * A * C - 2.156 * 10^{-4} * B * C + 0.044 * A^2 - 0.048 * B^2 + 8.012 * 10^{-3} * C^2$$

****

When the μ=0.40,

Reduction level 5%

$$(R1)^{-3} = 40.30 - 24.12 * A + 40.91 * B - 2.84 * C - 21.84 * A * B + 2.58 * A * C - 4.12 * B * C + 4.39 * A^2 + 6.63 * B^2 + 3.25 * C^2$$

131

Reduction level 10%

$$(R1)^{-3} = 24.76 - 9.99 * A + 21.10 * B - 1.81 * C - 9.31 * A * B + 2.19 * A * C - 1.49 * B * C + 2.29 * A^2 - 2.15 * B^2 + 1.22 * C^2$$

Reduction level 15%

$$(R1)^{-3} = 12.50 - 3.20 * A + 8.65 * B - 0.88 * C - 3.02 * A * B + 1.22 * A * C - 0.46 * B * C + 1.03 * A^2 - 2.96 * B^2 + 0.34 * C^2$$

Reduction level 20%

$$(R1)^{-3} = 5.80 - 0.86 * A + 3.23 * B - 0.54 * C - 0.87 * A * B + 0.72 * A * C - 0.11 * B * C + 0.40 * A^2 - 1.64 * B^2 + 0.027 * C^2$$

Reduction level 25%

$$(R1)^{-3} = 2.54 - 0.44 * A + 1.59 * B - 0.45 * C - 0.70 * A * B + 0.57 * A * C - 6.776 * 10^{-3} * B * C$$

Reduction level 30%

$$(R1)^{-3} = 1.27 - 0.099 * A + 0.47 * B - 0.14 * C - 0.17 * A * B + 0.15 * A * C + 0.032 * B * C + 0.076 * A^2 - 0.18 * B^2 - 0.036 * C^2$$

Reduction level 35%

$$(R1)^{-3} = 0.66 - 0.078 * A + 0.24 * B - 0.036 * C - 0.13 * A * B + 0.042 * A * C + 2.371 * 10^{-3} * B * C$$

Reduction level 40%

$$(R1)^{-3} = 0.34 - 0.016 * A + 0.052 * B + 7.135 * 10^{-3} * C$$

Reduction level 45%

$$(R1)^{-3} = 0.19 - 0.016 * A + 0.045 * B - 9.98 * 10^{-3} * C - 0.013 * A * B + 0.017 * A * C - 8.311 * 10^{-3} * B * C - 0.011 * A^2 + 2.643 * 10^{-3} * B^2 - 1.334 * 10^{-3} * C^2$$

Reduction level 50%

$$(R1)^{-3} = 0.11 - 0.021 * A + 0.55 * B - 9.932 * 10^{-3} * C - 0.022 * A * B + 0.013 * A * C - 4.052 * B * C$$

Reduction level 55%

$$(R1)^{-3} = 0.064 - 0.017 * A + 0.051 * B - 0.01 * C - 0.023 * A * B + 0.012 * A * C - 1.964 * 10^{-3} * B * C$$

****

When the μ=0.30,

Reduction level 5%

$$R1 = 0.27 + 0.10 * A - 0.20 * B + 9.458 * 10^{-3} * C + 0.084 * A * B + 8.895 * 10^{-3} * A * C + 2.681 * 10^{-3} * B * C - 0.13 * A^2 + 0.090 * B^2 + 0.011 * C^2$$

Reduction level 10%

$$R1 = 0.32 + 0.14 * A - 0.32 * B + 0.026 * C + 0.13 * A * B - 3.754 * 10^{-3} * A * C - 0.010 * B * C - 0.20 * A^2 + 0.18 * B^2 + 0.030 * C^2$$

Reduction level 15%

$$R1 = 0.40 + 0.11 * A - 0.33 * B + 0.048 * C + 0.11 * A * B - 0.041 * A * C - 1.175 * 10^{-3} * B * C - 0.15 * A^2 + 0.21 * B^2 + 0.025 * C^2$$

Reduction level 20%

$$(R1)^{-2} = 4.24 - 0.54 * A + 2.18 * B - 0.38 * C - 0.58 * A * B + 0.46 * A * C - 0.12 * B * C + 0.21 * A^2 - 1.06 * B^2 - 0.035 * C^2$$

Reduction level 25%

$$(R1)^{-3} = 3.21 - 0.53 * A + 1.70 * B + 0.015 * C$$

Reduction level 30%

$$(R1)^{-3} = 1.44 - 0.17 * A + 0.58 * B - 2.543 * 10^{-3} * C$$

Reduction level 35%

$$R1 = 1.12 + 0.10 * A - 0.18 * B - 5.612 * 10^{-3} * C + 0.091 * A * B + 0.023 * A * C - 0.014 * B * C - 0.094 * A^2 + 0.058 * B^2 - 6.402 * 10^{-3} * C^2$$

Reduction level 40%

$$(R1)^{-3} = 0.36 - 0.069 * A + 0.093 * B - 7.922 * 10^{-4} * C - 0.062 * A * B - 0.013 * A * C + 7.709 * 10^{-3} * B * C + 0.065 * A^2 + 1.598 * 10^{-3} * B^2 - 6.565 * 10^{-3} * C^2$$

Reduction level 45%

$$(R1)^{-3} = 0.19 - 0.011 * A + 0.026 * B - 8.861 * 10^{-3} * C - 6.457 * 10^{-3} * A * B + 0.011 * A * C - 7.887 * 10^{-3} * B * C$$

Reduction level 50%

$$(R1)^{-3} = 0.10 - 0.015 * A + 0.543 * B - 9.723 * 10^{-3} * C - 0.017 * A * B + 0.013 * A * C - 7.792 * 10^{-3} * B * C$$

Reduction level 55%

$$(R1)^{-3} = 0.059 - 0.012 * A + 0.033 * B - 3.304 * 10^{-3} * C - 9.379 * 10^{-3} * A * B + 2.498 * 10^{-3} * A * C - 2.229 * 10^{-3} * B * C + 8.981 * 10^{-3} * A^2 - 0.018 * B^2 + 3.771 * 10^{-3} * C^2$$

****

When μ=0.20,

Reduction level 5%

$$(R1)^{-\frac{1}{2}} = 0.39 - 0.46 * A + 1.79 * B - 0.62 * C - 1.04 * A * B + 0.90 * A * C - 0.08 * B * C$$

Reduction level 10%

$$(R1)^{-\frac{1}{2}} = 3.03 - 0.13 * A + 1.13 * B - 0.31 * C - 0.30 * A * B + 0.40 * A * C - 0.097 * B * C + 0.19 * A^2 - 0.91 * B^2 + 0.085 * C^2$$

Reduction level 15%

$$(R1)^{-\frac{1}{2}} = 2.42 - 0.065 * A + 0.76 * B - 0.19 * C - 0.14 * A * B + 0.21 * A * C - 0.10 * B * C + 0.14 * A^2 - 0.67 * B^2 + 0.038 * C^2$$

Reduction level 20%

$$(R1)^{-\frac{1}{2}} = 1.88 - 0.058 * A + 0.44 * B - 0.074 * C - 0.033 * A * B + 0.082 * A * C - 0.072 * B * C + 0.11 * A^2 - 0.44 * B^2 + 0.018 * C^2$$

Reduction level 25%

$$\frac{1}{R1} = 2.26 - 0.11 * A + 0.60 * B - 0.053 * C + 0.026 * A * B + 0.027 * A * C - 0.087 * B * C + 0.19 * A^2 - 0.70 * B^2 + 0.031 * C^2$$

Reduction level 30%

$$(R1)^{-2} = 2.32 - 0.11 * A + 0.72 * B - 0.082 * C + 0.015 * A * B - 5.682 * 10^{-3} * A * C - 0.052 * B * C + 0.23 * A^2 - 0.86 * B^2 + 0.065 * C^2$$

Reduction level 35%

$$(R1)^{-3} = 1.27 - 1.819 * 10^{-3} * A + 0.31 * B - 0.077 * C + 5.058 * 10^{-3} * A * B - 9.245 * 10^{-3} * A * C + 0.037 * B * C + 0.073 * A^2 - 0.41 * B^2 + 0.047 * C^2$$

Reduction level 40%

$$(R1)^{-3} = 0.54 + 0.068 * A - 0.028 * B - 0.052 * C + 0.055 * A * B + 0.021 * A * C + 0.031 * B * C - 0.041 * A^2 - 0.057 * B^2 - 0.028 * C^2$$

Reduction level 45%

$$(R1)^3 = 3.86 + 6.613 * 10^{-3} * A + 0.54 * B - 0.067 * C$$

Reduction level 50%

$$(R1)^3 = 8.24 + 0.20 * A - 0.30 * B + 0.068 * C + 0.34 * A * B - 0.66 * A * C + 0.78 * B * C$$

Reduction level 55%

$$(R1)^{-2} = 0.16 - 8.416 * 10^{-3} * A + 0.039 * B - 7.228 * 10^{-3} * C - 9.008$$
$$* 10^{-3} * A * B + 0.010 * A * C - 1.956 * 10^{-3} * B * C + 0.014$$
$$* A^2 - 0.039 * B^2 + 1.67 * 10^{-3} * C^2$$

****

When μ=0.15,

Reduction level 5%

$$(R1)^{\frac{1}{2}} = 0.17 - 0.051 * A + 0.030 * B - 0.066 * C - 0.14 * A * B + 0.14 * A$$
$$* C + 0.029 * B * C - 0.049 * A^2 + 0.32 * B^2 - 0.062 * C^2$$

Reduction level 10%

$$\ln(R1) = -4.17 - 0.33 * A - 1.31 * B + 0.60 * C - 0.24 * A * B - 0.38 * A$$
$$* C + 0.22 * B * C - 0.23 * A^2 + 2.04 * B^2 - 0.089 * C^2$$

Reduction level 15%

$$(R1 + 0.01)^{\frac{1}{2}}$$
$$= 0.21 + 0.016 * A - 0.36 * B + 0.13 * C + 0.076 * A * B$$
$$- 0.14 * A * C - 0.016 * B * C - 0.035 * A^2 + 0.21 * B^2$$
$$+ 5.472 * 10^{-3} * C^2$$

Reduction level 20%

$$\ln(R1) = -2.51 - 7.766 * 10^{-3} * A - 1.31 * B + 0.45 * C + 0.14 * A * B$$
$$- 0.44 * A * C + 2.958 * 10^{-3} * B * C - 0.21 * A^2 + 1.01 * B^2$$
$$+ 0.047 * C^2$$

Reduction level 25%

$$\ln(R1) = -1.68 + 0.032 * A - 0.74 * B + 0.13 * C - 2.336 * 10^{-3} * A * B$$
$$- 0.060 * A * C + 0.018 * B * C - 0.18 * A^2 + 0.85 * B^2$$
$$- 0.042 * C^2$$

Reduction level 30%

$$(R1)^{\frac{1}{2}} = 0.60 + 0.027 * A - 0.17 * B + 0.010 * C + 6.443 * 10^{-3} * A * B$$
$$+ 3.750 * 10^{-3} * A * C + 5.447 * 10^{-3} * B * C - 0.049 * A^2$$
$$+ 0.20 * B^2 - 0.013 * C^2$$

Reduction level 35%

$$(R1)^2 = 0.40 + 0.054 * A - 0.27 * B + 0.013 * C + 0.020 * A * B - 0.011 * A$$
$$* C + 0.029 * B * C - 0.086 * A^2 + 0.30 * B^2 - 1.991 * 10^{-3}$$
$$* C^2$$

Reduction level 40%

$$(R1)^{-1} = 0.96 + 0.055 * A - 0.015 * B - 0.041 * C + 0.030 * A * B + 0.046$$
$$* A * C - 0.016 * B * C + 4.338 * 10^{-3} * A^2 - 0.040 * B^2$$
$$- 0.014 * C^2$$

Reduction level 45%

$$(R1)^2 = 2.02 - 0.14 * A + 0.31 * B + 0.017 * C - 0.091 * A * B + 2.722$$
$$* 10^{-3} * A * C - 0.010 * B * C + 0.045 * A^2 - 0.081 * B^2$$
$$+ 0.42 * C^2$$

Reduction level 50%

$$(R1)^{-2} = 0.28 + 0.040 * A - 0.067 * B - 4.581 * 10^{-3} * C + 0.039 * A * B$$
$$- 0.010 * A * C - 9.994 * 10^{-3} * B * C + 7.096 * 10^{-4} * B^2$$
$$- 0.012 * B^2 + 1.526 * 10^{-3} * C^2$$

Reduction level 55%

$$(R1)^3 = 19.97 - 3.85 * A + 2.20 * B + 3.66 * C - 3.22 * A * B - 1.91 * A * C$$
$$+ 3.26 * B * C - 0.11 * A^2 - 1.22 * B^2 - 1.56 * C^2$$

****

When μ=0.12,

Reduction level 5%

$(R1 + 0.18)^2$

$$= 6.865 * 10^{-3} + 1.649 * 10^{-3} * A - 0.014 * B + 3.040 * 10^{-3} * C + 8.560 * 10^{-4} * A * B - 1.360 * 10^{-3} * A * C + 2.171 * 10^{-3} * B * C - 2.323 * 10^{-3} * A^2 + 0.016 * B^2 - 4.353 * 10^{-4} * C^2$$

Reduction level 10%

$$R1 = -0.045 + 9.872 * 10^{-3} * A - 0.055 * B - 7.359 * 10^{-3} * C$$

Reduction level 15%

$$R1 = -0.057 + 0.068 * A - 0.12 * B - 2.946 * 10^{-3} * C + 0.057 * A * B - 9.902 * 10^{-3} * A * C - 4.841 * 10^{-3} * B * C - 0.016 * A^2 + 0.024 * B^2 - 0.022 * C^2$$

20%

$$R1 = 0.011 + 0.012 * A - 0.070 * B + 9.640 * 10^{-3} * C + 3.553 * 10^{-3} * A * B - 2.956 * 10^{-3} * A * C - 0.012 * B * C + 8.249 * 10^{-3} * A^2 + 0.073 * B^2 - 0.019 * C^2$$

Reduction level 25%

$$R1 = 0.11 - 0.071 * A - 0.024 * B + 0.024 * C - 0.081 * A * B + 3.200 * 10^{-3} * A * C - 0.018 * B * C + 0.026 * A^2 + 0.15 * B^2 - 0.014 * C^2$$

Reduction level 30%

$$(R1)^{-\frac{1}{2}} = 2.57 + 0.39 * A + 0.33 * B - 0.26 * C + 0.33 * A * B + 0.17 * A * C + 3.977 * 10^{-3} * B * C - 5.778 * 10^{-3} * A^2 - 0.81 * B^2 + 0.077 * C^2$$

Reduction level 35%

$$(R1)^{-\frac{1}{2}} = +1.93 - 0.086 * A + 0.43 * B - 0.073 * C - 0.083 * A * B + 0.089 * A * C + 0.024 * B * C + 0.068 * A^2 - 0.38 * B^2 + 8.753 * 10^{-3} * C^2$$

Reduction level 40%

$$R1 = 0.63 - 0.071 * A - 0.043 * B + 0.024 * C - 0.069 * A * B - 0.020 * A * C - 0.018 * B * C - 0.027 * A^2 + 0.27 * B^2 + 0.016 * C^2$$

Reduction level 45%

$$(R1)^3 = 1.72 - 1.00 * A + 1.38 * B - 0.074 * C - 1.06 * A * B + 0.11 * A * C + 0.013 * B * C + 0.033 * A^2 + 0.086 * B^2 + 0.12 * C^2$$

Reduction level 50%

$$(R1)^{-3} = 0.28 + 0.034 * A - 0.069 * B - 0.011 * C$$

Reduction level 55%

$$(R1)^3 = 10.58 - 1.61 * A + 5.52 * B - 2.07 * C - 2.80 * A * B + 1.70 * A * C - 0.20 * B * C + 0.50 * A^2 + 0.35 * B^2 - 0.83 * C^2$$

****

When μ=0.10,

Reduction level 5%

$$(R1 + 0.24)^{\frac{1}{2}}$$
$$= 0.18 + 0.11 * A + 0.017 * B - 0.13 * C - 0.081 * A * B + 0.075 * A * C + 0.056 * B * C$$

Reduction level 10%

$$R1 = -0.064 - 0.047 * A + 0.043 * B - 0.019 * C - 0.077 * A * B + 0.023 * A * C + 2.244 * 10^{-3} * B * C - 7.233 * 10^{-3} * A^2 + 0.11 * B^2 - 0.028 * C^2$$

Reduction level 15%

$$R1 = -0.12 + 0.022 * A - 0.070 * B - 0.019 * C + 0.042 * A * B - 0.017 * A * C - 4.88 * 10^{-3} * B * C$$

Reduction level 20%

$$\ln(R1 + 0.14)$$
$$= -3.28 + 0.31 * A - 0.84 * B + 0.67 * C + 1.08 * A * B - 0.74$$
$$* A * C + 0.37 * B * C - 0.11 * A^2 - 1.10 * B^2 + 0.81 * C^2$$

Reduction level 25%

$$R1 = 0.025 - 0.039 * A + 0.062 * B - 1.502 * 10^{-3} * C - 0.049 * A * B$$
$$- 4.663 * 10^{-3} * A * C + 6.070 * 10^{-3} * B * C + 1.250 * 10^{-3}$$
$$* A^2 + 2.731 * 10^{-3} * B^2 + 7.535 * 10^{-3} * C^2$$

Reduction level 30%

$$(R1)^{\frac{1}{2}} = 0.29 - 0.038 * A - 0.015 * B - 0.013 * C - 0.084 * A * B + 4.111$$
$$* 10^{-3} * A * C - 0.017 * B * C - 0.020 * A^2 + 0.14 * B^2$$
$$- 0.033 * C^2$$

Reduction level 35%

$$(R1)^{-\frac{1}{2}} = 3.50 - 0.90 * A + 1.77 * B - 0.033 * C - 0.087 * A * B + 0.19 * A$$
$$* C + 0.16 * B * C + 0.16 * A^2 - 0.43 * B^2 + 0.087 * C^2$$

Reduction level 40%

$$(R1)^{\frac{1}{2}} = 0.55 + 0.010 * A - 0.15 * B + 0.030 * C + 9.943 * 10^{-3} * A * B$$
$$- 0.039 * A * C + 1.624 * 10^{-3} * B * C - 0.010 * A^2 + 0.18$$
$$* B^2 - 0.025 * C^2$$

Reduction level 45%

$$(R1)^3 = 0.64 - 0.42 * A + 0.29 * B + 0.098 * C - 0.39 * A * B - 0.062 * A$$
$$* C - 0.022 * B * C + 0.058 * A^2 + 0.55 * B^2 - 0.099 * C^2$$

Reduction level 50%

$$(R1)^2 = 1.95 - 0.84 * A + 1.05 * B + 0.089 * C - 0.72 * A * B - 0.066 * A$$
$$* C - 0.050 * B * C + 0.12 * A^2 + 0.47 * B^2 - 0.030 * C^2$$

Reduction level 55%

$$(R1)^{-2} = 0.31 + 0.066 * A - 0.11 * B - 0.014 * C + 0.031 * A * B - 2.312 \\ * 10^{-4} * A * C + 0.026 * B * C - 0.043 * A^2 + 0.027 * B^2 \\ + 0.014 * C^2$$

****

When μ=0.09,

Reduction level 5%

$$R1 = -0.20 - 0.011 * A - 0.044 * B + 0.062 * C + 0.031 * A * B - 0.073 * A \\ * C + 0.032 * B * C - 0.046 * A^2 + 0.026 * B^2 + 0.046 * C^2$$

Reduction level 10%

$$R1 = -0.16 - 1.341 * 10^{-3} * A + 0.013 * B - 0.016 * C$$

Reduction level 15%

$$R1 = -0.12 - 7.150 * 10^{-3} * A + 0.036 * B - 9.607 * 10^{-3} * C$$

Reduction level 20%

$$R1 = -0.092 - 2.789 * 10^{-3} * A + 0.036 * B - 8.969 * 10^{-3} * C - 0.019 * A \\ * B + 0.021 * A * C + 3.557 * 10^{-3} * B * C$$

Reduction level 25%

$$(R1 + 0.1)^{\frac{1}{2}} = 0.19 + 0.019 * A - 0.066 * B + 0.039 * C$$

Reduction level 30%

$$(R1 + 0.07)^{\frac{1}{2}} = 0.20 + 0.052 * A - 0.18 * B + 0.038 * C$$

Reduction level 35%

$$(R1 + 0.001)^{-\frac{1}{2}} = 0.25 + 0.054 * A - 0.24 * B + 5 * 10^{-3} * C$$

Reduction level 40%

$$R1 = 0.23 + 0.019 * A - 0.15 * B - 0.012 * C - 0.018 * A * B + 0.015 * A * C$$
$$- 0.027 * B * C - 0.017 * A^2 + 0.19 * B^2 - 0.060 * C^2$$

reduction level 45%

$$R1 = 0.63 + 0.011 * A - 0.13 * B + 0.028 * C$$

reduction level 50%

$$R1 = 1.17 - 0.24 * A + 0.31 * B + 0.024 * C - 0.28 * A * B + 0.088 * A * C$$
$$- 0.055 * B * C + 0.12 * A^2 + 0.18 * B^2 - 0.048 * C^2$$

reduction level 55%

$$(R1)^{-2} = 0.30 + 0.23 * A - 0.42 * B + 0.028 * C + 0.28 * A * B - 0.16 * A$$
$$* C + 0.069 * B * C - 0.17 * A^2 - 0.041 * B^2 + 0.043 * C^2$$

****

When μ=0.08,

Reduction level 5%

$$R1 = -0.26 + 0.023 * A - 0.028 * B - 5.913 * 10^{-3} * C$$

Reduction level 10%

$$R1 = -0.18 - 0.020 * A + 9.265 * 10^{-3} * B + 4.981 * 10^{-3} * C - 0.014 * A$$
$$* B - 7.544 * 10^{-3} * A * C + 6.207 * 10^{-4} * B * C + 3.029$$
$$* 10^{-3} * A^2 + 4.150 * 10^{-3} * B^2 - 2.549 * 10^{-3} * C^2$$

Reduction level 15%

$$R1 = -0.15 - 0.030 * A + 0.048 * B - 0.015 * C - 0.025 * A * B + 6.160$$
$$* 10^{-3} * A * C - 5.046 * 10^{-3} * B * C$$

Reduction level 20%

$$R1 = -0.15 - 9.962 * 10^{-3} * A + 0.057 * B - 0.033 * C - 0.022 * A * B$$
$$+ 0.016 * A * C - 1.952 * 10^{-3} * B * C$$

Reduction level 25%

$$R1 = -0.13 + 0.011 * A + 0.018 * B - 0.013 * C$$

Reduction level 30%

$$R1 = 0.087 + 0.026 * A - 0.038 * B + 6.208 * 10^{-3} * C$$

Reduction level 35%

$$R1 = 1.37 * 10^{-3} + 0.031 * A - 0.11 * B + 0.022 * C$$

reduction level 40%

$$\ln(R1) = -2.23 + 0.084 * A - 1.06 * B + 0.045 * C$$

reduction level 45%

$$(R1)^{\frac{1}{2}} = 0.71 - 0.16 * A + 0.025 * B + 0.045 * C - 0.15 * A * B - 0.067 * A * C - 8.566 * 10^{-3} * B * C + 0.013 * A^2 + 0.19 * B^2 - 0.11 * C^2$$

reduction level 50%

$$(R1)^{-\frac{1}{2}} = 1.01 + 0.20 * A - 0.17 * B + 8.417 * 10^{-3} * C + 0.22 * A * B + 8.091 * 10^{-3} * A * C + 0.023 * B * C - 0.020 * A^2 - 0.22 * B^2 + 0.13 * C^2$$

reduction level 55%

$$(R1)^2 = 2.82 - 1.16 * A + 1.92 * B - 0.28 * C - 1.52 * A * B + 0.39 * A * C - 0.16 * B * C + 0.31 * A^2 + 0.68 * B^2 - 0.55 * C^2$$

****

When μ=is 0.07,

Reduction level 5%

$$R1 = -0.23 + 0.10 * A - 0.065 * B - 0.062 * C + 0.044 * A * B + 0.064 * A * C + 1.941 * 10^{-3} * B * C - 0.050 * A^2 - 0.073 * B^2 - 0.041 * C^2$$

Reduction level 10%

$$R1 = -0.29 - 0.059 * A + 0.020 * B + 0.045 * C - 0.018 * A * B - 0.047 * A * C - 4.746 * 10^{-3} * B * C + 0.030 * A^2 + 0.058 * B^2 + 0.026 * C^2$$

Reduction level 15%

$$R1 = -0.26 - 0.080 * A + 0.068 * B + 0.038 * C - 0.039 * A * B - 0.042 * A * C - 2.921 * 10^{-3} * B * C + 0.036 * A^2 + 0.058 * B^2 + 0.037 * C^2$$

Reduction level 20%

$$R1 = -0.19 - 0.012 * A + 0.046 * B - 0.010 * C$$

Reduction level 25%

$$R1 = -0.16 - 7.551 * 10^{-3} * A + 0.074 * B - 0.046 * C - 0.052 * A * B + 0.042 * A * C + 2.054 * 10^{-3} * B * C$$

Reduction level 30%

$$R1 = -0.12 + 0.061 * A - 0.021 * B + 0.050 * C + 8.559 * 10^{-3} * A * B + 0.047 * A * C - 4.971 * 10^{-4} * B * C - 0.033 * A^2 - 0.042 * B^2 - 0.015 * C^2$$

Reduction level 35%

$$R1 = -0.089 + 0.037 * A - 0.073 * B - 6.197 * 10^{-3} * C + 9.136 * 10^{-3} * A * B + 4.821 * 10^{-3} * A * C - 0.013 * B * C - 0.019 * A^2 + 0.014 * B^2 - 0.013 * C^2$$

reduction level 40%

$$R1 = -0.013 - 0.055 * A - 0.078 * B + 0.068 * C - 0.030 * A * B - 0.065 * A * C - 0.036 * B * C + 0.021 * A^2 + 0.12 * B^2 + 4.551 * 10^{-3} * C^2$$

reduction level 45%

$$R1 = 0.18 - 0.21 * A + 0.015 * B + 0.13 * C - 0.13 * A * B - 0.12 * A * C - 0.070 * B * C + 0.075 * A^2 + 0.26 * B^2 + 0.028 * C^2$$

reduction level 50%

$$(R1)^{\frac{1}{2}} = 0.77 - 0.28 * A + 0.19 * B + 0.083 * C - 0.22 * A * B - 0.063 * A * C - 0.066 * B * C + 0.076 * A^2 + 0.26 * B^2 + 0.022 * C^2$$

reduction level 55%

$$(R1)^{-2} = 0.61 + 0.71 * A - 0.88 * B + 0.034 * C + 0.72 * A * B - 0.16 * A * C + 0.21 * B * C - 0.14 * A^2 - 0.56 * B^2 + 0.049 * C^2$$

****

When μ=0.06,

Reduction level 5%

$$R1 = -0.22 - 0.039 * A + 0.062 * B + 9.834 * 10^{-3} * C + 0.034 * A * B - 0.032 * A * C - 0.015 * B * C$$

Reduction level 10%

$$R1 = -0.37 + 0.027 * A - 0.040 * B - 3.395 * 10^{-3} * C + 0.024 * A * B + 0.022 * A * C + 0.012 * B * C$$

Reduction level 15%

$$(R1 + 0.36)^{\frac{1}{2}} = 0.095 + 0.044 * A - 9.876 * 10^{-3} * B - 0.056 * C - 1.119 * 10^{-3} * A * B + 0.11 * A * C + 0.014 * B * C - 0.010 * A^2 + 0.048 * B^2 + 0.014 * C^2$$

Reduction level 20%

$$R1 = -0.26 - 0.033 * A + 0.080 * B - 0.021 * C - 0.052 * A * B + 0.020 * A * C - 4.748 * 10^{-3} * B * C + 5.205 * 10^{-4} * A^2 + 0.018 * B^2 - 5.354 * 10^{-3} * C^2$$

Reduction level 25%

$$R1 = -0.18 - 0.045 * A + 0.11 * B - 0.021 * C - 0.067 * A * B + 6.238 * 10^{-3} * A * C + 8.253 * 10^{-3} * B * C - 3.923 * 10^{-3} * A^2 + 0.011 * B^2 - 0.011 * C^2$$

Reduction level 30%

$$R1 = -0.16 - 0.027 * A + 0.085 * B - 9.979 * 10^{-3} * C - 0.046 * A * B$$
$$- 4.769 * 10^{-3} * A * C + 5.161 * 10^{-4} * B * C - 8.194 * 10^{-3}$$
$$* A^2 + 8.921 * 10^{-4} * B^2 - 3.415 * 10^{-3} * C^2$$

Reduction level 35%

$$(R1 + 0.21)^2$$
$$= 1.588 * 10^{-3} + 6.601 * 10^{-4} * A + 4.163 * 10^{-4} * B + 3.802$$
$$* 10^{-5} * C - 3.631 * 10^{-4} * A * B - 8.565 * 10^{-5} * A * C$$
$$+ 1.358 * 10^{-3} * B * C$$

reduction level 40%

$$R1 = -0.17 + 0.049 * A - 0.099 * B - 9.76 * 10^{-3} * C + 0.038 * A * B$$
$$+ 0.025 * A * C + 0.018 * B * C$$

reduction level 45%

$$R1 = -2.841 * 10^{-3} - 0.013 * A - 0.12 * B - 6.346 * 10^{-4} * C$$

reduction level 50%

$$R1 = 0.30 - 0.20 * A + 0.071 * B - 0.14 * C - 0.22 * A * B + 0.11 * A * C$$
$$- 0.13 * B * C + 0.13 * A^2 + 0.14 * B^2 - 0.100 * C^2$$

reduction level 55%

$$R1 = 1.10 - 0.61 * A + 0.59 * B - 0.36 * C - 0.69 * A * B + 0.20 * A * C$$
$$- 0.38 * B * C + 0.27 * A^2 + 0.29 * B^2 - 0.31 * C^2$$

****

When μ=0.055,

Reduction level 5%

$$\ln(R1 + 0.38)$$
$$= -2.11 + 0.69 * A - 0.37 * B - 0.18 * C + 0.37 * A * B + 0.63$$
$$* A * C + 0.44 * B * C - 0.24 * A^2 - 0.52 * B^2 - 0.85 * C^2$$

Reduction level 10%

$$R1 = -0.34 - 0.011 * A + 0.10 * B - 0.038 * C - 0.031 * A * B + 0.028 * A * C - 0.017 * B * C - 1.464 * 10^{-3} * A^2 + 0.11 * B^2 - 0.035 * C^2$$

Reduction level 15%

$$R1 = -0.34 - 0.028 * A + 0.054 * B - 0.013 * C - 0.040 * A * B + 0.015 * A * C - 2.172 * 10^{-3} * B * C + 4.346 * 10^{-3} * A^2 + 0.034 * B^2 - 2.883 * 10^{-3} * C^2$$

Reduction level 20%

$$R1 = -0.32 - 0.025 * A - 5.189 * 10^{-3} * B + 0.014 * C - 0.022 * A * B - 1.735 * 10^{-3} * A * C + 0.013 * B * C + 0.013 * A^2 - 0.056 * B^2 + 0.028 * C^2$$

Reduction level 25%

$$(R1 + 0.49)^3$$
$$= 9.895 * 10^{-3} - 1.058 * 10^{-3} * A - 2.963 * 10^{-4} * B + 1.539 * 10^{-3} * C - 2.458 * 10^{-4} * A * B - 3.406 * 10^{-7} * A * C + 1.160 * 10^{-3} * B * C + 1.822 * 10^{-3} * A^2 - 8.430 * 10^{-3} * B^2 + 3.704 * 10^{-3} * C^2$$

Reduction level 30%

$$(R1 + 0.44)^3$$
$$= 7.886 * 10^{-3} - 1.427 * 10^{-4} * A + 3.846 * 10^{-3} * B - 3.097 * 10^{-4} * C$$

Reduction level 35%

$$R1 = -0.22 + 5.575 * 10^{-3} * A + 0.027 * B - 0.013 * C$$

reduction level 40%

$$R1 = -0.14 - 0.019 * A + 0.039 * B - 0.012 * C - 0.031 * A * B - 6.609 * 10^{-3} * A * C - 2.247 * 10^{-3} * B * C - 0.018 * A^2 + 0.040 * B^2 - 0.014 * C^2$$

reduction level 45%

$$R1 = 0.025 + 0.044 * A + 0.029 * B - 0.12 * C - 0.074 * A * B + 0.14 * A * C$$
$$+ 7.259 * 10^{-4} * B * C - 0.084 * A^2 + 0.037 * B^2 - 0.10 * C^2$$

reduction level 50%

$$R1 = 0.21 + 0.15 * A - 0.036 * B - 0.21 * C - 0.038 * A * B + 0.29 * A * C$$
$$- 8.446 * 10^{-3} * B * C - 0.092 * A^2 - 0.026 * B^2 - 0.095 * C^2$$

reduction level 55%

$$R1 = 0.34 + 0.39 * A - 0.15 * B - 0.33 * C + 0.19 * A * B + 0.47 * A * C$$
$$- 0.12 * B * C$$

****

When μ=0.05,

Reduction level 5%

$$ln(R1 + 0.35)$$
$$= -1.96 - 2.36 * A + 2.41 * B + 0.43 * C - 1.15 * A * B$$
$$- 0.066 * A * C - 0.51 * B * C + 0.34 * A^2 + 0.51 * B^2 + 0.42$$
$$* C^2$$

Reduction level 10%

$$R1 = -0.41 - 0.096 * A - 0.11 * B - 8.718 * 10^{-3} * C + 0.086 * A * B$$
$$- 2.997 * 10^{-3} * A * C - 4.397 * 10^{-3} * B * C - 0.021 * A^2$$
$$- 0.050 * B^2 - 0.028 * C^2$$

Reduction level 15%

$$R1 = -0.43 + 0.12 * A - 0.12 * B - 0.023 * C + 0.10 * A * B + 5.772 * 10^{-3}$$
$$* A * C - 8.399 * 10^{-3} * B * C - 0.018 * A^2 - 0.055 * B^2$$
$$- 0.039 * C^2$$

Reduction level 20%

$$ln(R1 + 0.39) = -3.64 + 0.18 * A + 0.91 * B - 0.36 * C$$

Reduction level 25%

$(R1 + 0.37)^{\frac{1}{2}}$
$$= 0.31 - 0.085 * A + 0.25 * B - 0.067 * C - 0.11 * A * B$$
$$+ 0.079 * A * C + 2.193 * 10^{-3} * B * C$$

Reduction level 30%

$\ln(R1 + 0.35)$
$$= -2.25 - 0.91 * A + 2.35 * B - 0.57 * C - 1.06 * A * B + 0.71$$
$$* A * C + 0.010 * B * C$$

Reduction level 35%

$(R1 + 0.31)^{\frac{1}{2}}$
$$= 4.08 + 2.48 * A - 3.78 * B - 0.45 * C + 0.51 * A * B + 1.22$$
$$* A * C - 1.42 * B * C - 1.08 * A^2 + 3.08 * B^2 - 1.63 * C^2$$

reduction level 40%

$$R1 = -0.24 + 0.046 * A - 0.063 * B - 6.182 * 10^{-4} * C + 0.040 * A * B$$
$$- 4.641 * 10^{-3} * A * C + 3.946 * 10^{-3} * B * C - 0.011 * A^2$$
$$- 0.048 * B^2 - 6.649 * 10^{-3} * C^2$$

reduction level 45%

$$R1 = -0.21 + 0.15 * A - 0.17 * B - 0.045 * C + 0.11 * A * B + 0.025 * A * C$$
$$- 0.017 * B * C - 0.027 * A^2 - 0.045 * B^2 - 0.070 * C^2$$

reduction level 50%

$$R1 = 0.36 + 0.13 * A - 0.11 * B - 0.14 * C + 0.070 * A * B + 0.087 * A * C$$
$$- 0.094 * B * C + 0.016 * A^2 + 0.052 * B^2 - 0.14 * C^2$$

reduction level 55%

$$\ln(R1) = -0.99 - 1.03 * A + 1.41 * B - 0.25 * C - 1.04 * A * B + 0.22 * A$$
$$* C - 0.24 * B * C + 0.29 * A^2 + 1.20 * B^2 - 0.069 * C^2$$

****

When μ=0.04,

Reduction level 5%

149

$$(R1 + 0.41)^{\frac{1}{2}}$$
$$= 0.21 - 0.014 * A + 0.18 * B - 0.067 * C - 0.10 * A * B$$
$$+ 0.15 * A * C + 0.019 * B * C - 0.018 * A^2 + 0.096 * B^2$$
$$- 0.023 * C^2$$

Reduction level 10%

$$(R1 + 0.53)^2$$
$$= 0.018 - 2.698 * 10^{-3} * A - 6.015 * 10^{-3} * B + 4.999 * 10^{-3}$$
$$* C + 3.249 * 10^{-3} * A * B - 8.149 * 10^{-3} * A * C - 2.428$$
$$* 10^{-3} * B * C + 2.586 * 10^{-3} * A^2 - 7.271 * 10^{-3} * B^2 + 2.296$$
$$* 10^{-3} * C^2$$

Reduction level 15%

$$(R1 + 0.53)^2$$
$$= 0.015 - 2.893 * 10^{-3} * A - 2.582 * 10^{-3} * B + 3.477 * 10^{-3}$$
$$* C - 1.885 * 10^{-3} * A * B - 7.046 * 10^{-3} * A * C - 1.960$$
$$* 10^{-3} * B * C + 2.202 * 10^{-3} * A^2 - 6.238 * 10^{-3} * B^2 + 1.621$$
$$* 10^{-3} * C^2$$

Reduction level 20%

$$R1 = -0.41 - 6.917 * 10^{-3} * A + 0.029 * B - 4.111 * 10^{-3} * C$$

Reduction level 25%

$$(R1 + 0.48)^{\frac{1}{2}}$$
$$= 0.28 - 0.023 * A + 0.19 * B - 0.055 * C - 0.092 * A * B$$
$$+ 0.081 * A * C + 0.025 * B * C - 0.013 * A^2 + 0.023 * B^2$$
$$+ 3.896 * 10^{-3} * C^2$$

30%

$$(R1 + 0.49)^{\frac{1}{2}}$$
$$= 0.31 - 0.025 * A + 0.20 * B - 0.052 * C - 0.096 * A * B$$
$$+ 0.080 * A * C + 0.027 * B * C - 0.013 * A^2 + 0.015 * B^2$$
$$+ 0.015 * C^2$$

Reduction level 35%

$$R1 = -0.38 - 0.027 * A + 0.077 * B - 7.836 * 10^{-3} * C - 0.034 * A * B$$
$$+ 0.014 * A * C + 8.039 * 10^{-3} * B * C + 8.00 * 10^{-3} * A^2$$
$$- 9.741 * 10^{-3} * B^2 + 0.020 * C^2$$

Reduction level 40%

$$R1 = -0.35 - 0.017 * A + 0.021 * B - 5.71 * 10^{-3} * C - 7.234 * 10^{-3} * A * B$$
$$- 0.014 * A * C - 0.015 * B * C + 0.011 * A^2 - 0.052 * B^2$$
$$+ 0.018 * C^2$$

reduction level 45%

$$R1 = -0.27 + 5.949 * 10^{-3} * A + 1.187 * 10^{-3} * B - 0.035 * C + 2.623$$
$$* 10^{-3} * A * B + 8.294 * 10^{-4} * A * C - 0.035 * B * C - 2.241$$
$$* 10^{-3} * A^2 - 0.066 * B^2 - 5.525 * 10^{-3} * C^2$$

reduction level 50%

$$(R1 + 0.23)^{\frac{1}{2}}$$
$$= 5.09 - 1.14 * A - 4.02 * B + 3.55 * C + 1.46 * A * B - 3.68$$
$$* A * C + 0.69 * B * C - 0.54 * A^2 + 1.76 * B^2 + 0.53 * C^2$$

reduction level 55%

$$(R1 + 0.13)^{\frac{1}{2}} = 0.51 - 0.032 * A + 0.21 * B - 0.013 * C$$

****

When μ=0.03,

Reduction level 5%

$$(R1 + 0.50)^{\frac{1}{2}}$$
$$= 0.39 - 0.15 * A + 0.26 * B + 0.039 * C - 0.21 * A * B$$
$$+ 0.021 * A * C + 0.052 * B * C + 4.775 * 10^{-3} * A^2 + 0.058$$
$$* B^2 + 0.047 * C^2$$

Reduction level 10%

$$R1 = -0.48 + 0.060 * A - 0.050 * B - 0.054 * C + 0.042 * A * B + 0.032 * A$$
$$* C - 0.037 * B * C - 0.011 * A^2 - 0.014 * B^2 - 0.031 * C^2$$

151

Reduction level 15%

$$R1 = -0.52 + 0.035 * A - 0.042 * B - 0.033 * C + 0.037 * A * B + 6.593 * 10^{-3} * A * C - 0.041 * B * C$$

Reduction level 20%

$$\ln(R1 + 0.52) = -3.61 - 0.2 * A + 0.67 * B - 0.21 * C$$

Reduction level 25%

$$(R1 + 0.57)^{\frac{1}{2}} = 0.32 - 0.091 * A + 0.19 * B + 6.81 * 10^{-3} * C - 0.12 * A * B + 0.026 * A * C + 0.027 * B * C + 0.012 * A^2 + 7.406 * 10^{-3} * B^2 + 0.030 * C^2$$

Reduction level 30%

$$(R1 + 0.61)^{\frac{1}{2}} = 0.37 - 0.10 * A + 0.23 * B - 1.551 * 10^{-3} * C - 0.16 * A * B + 0.043 * A * C + 0.036 * B * C + 0.012 * A^2 + 4.451 * 10^{-4} * B^2 + 0.048 * C^2$$

Reduction level 35%

$$(R1 + 0.62)^{\frac{1}{2}} = 0.35 - 0.072 * A + 0.21 * B - 0.041 * C - 0.13 * A * B + 0.071 * A * C + 0.021 * B * C + 0.010 * A^2 - 0.026 * B^2 + 0.041 * C^2$$

reduction level 40%

$$(R1 + 0.60)^{\frac{1}{2}} = 0.30 - 2.329 * 10^{-3} * A + 0.14 * B - 0.090 * C - 0.035 * A * B + 0.089 * A * C - 0.017 * B * C + 5.166 * 10^{-3} * A^2 - 0.073 * B^2 + 5.561 * 10^{-3} * C^2$$

reduction level 45%

$(R1 + 0.59)^{\frac{1}{2}}$
$$= 0.34 - 0.051 * A + 0.13 * B - 0.038 * C + 3.412 * 10^{-3} * A$$
$$* B + 8.112 * 10^{-3} * A * C - 0.053 * B * C$$

reduction level 50%

$\ln(R1 + 0.55)$
$$= -1.32 - 0.97 * A + 1.06 * B + 0.84 * C + 0.23 * A * B - 0.90$$
$$* A * C - 0.13 * B * C$$

reduction level 55%

$\ln(R1 + 0.44)$
$$= -0.60 - 1.36 * A + 1.15 * B + 1.84 * C + 0.81 * A * B - 1.63$$
$$* A * C - 0.021 * B * C + 0.098 * A^2 - 0.65 * B^2 + 0.16 * C^2$$

****

When μ=0.02,

Reduction level 5%

$\ln(R1 + 0.51)$
$$= -2.50 - 0.40 * A + 0.84 * B + 0.86 * C - 0.96 * A * B + 1.08$$
$$* A * C - 0.12 * B * C$$

Reduction level 10%

$(R1 + 0.55)^{\frac{1}{2}} = 0.30 - 0.098 * A + 0.048 * B - 0.017 * C$

Reduction level 15%

$\ln(R1 + 0.59) = -2.56 - 0.51 * A + 0.28 * B - 0.033 * C$

Reduction level 20%

$(R1 + 0.59)^{-1}$
$$= 27.69 + 16.74 * A - 29.87 * B + 2.29 * C + 10.83 * A * B$$
$$- 12.21 * A * C + 12.24 * B * C - 11.16 * A^2 + 14.55 * B^2$$
$$- 5.14 * C^2$$

Reduction level 25%

$$(R1 + 0.63)^{\frac{1}{2}}$$
$$= 4.12 + 2.21 * A - 2.23 * B - 0.18 * C + 1.02 * A * B - 0.29$$
$$* A * C + 0.81 * B * C - 2.04 * A^2 + 3.12 * B^2 - 0.77 * C^2$$

Reduction level 30%

$$(R1 + 0.61)^{-\frac{1}{2}} = 4.18 + 1.04 * A - 2.27 * B + 0.13 * C$$

Reduction level 35%

$$\ln(R1 + 0.73)$$
$$= -2.38 - 0.57 * A + 2.04 * B - 1.02 * C - 1.33 * A * B + 1.25$$
$$* A * C - 0.12 * B * C$$

reduction level 40%

$$\ln(R1 + 0.78) = -2.46 - 0.42 * A + 1.24 * B - 0.14 * C$$

reduction level 45%

$$\ln(R1 + 0.83) = -1.95 - 0.82 * A + 1.24 * B + 0.068 * C$$

reduction level 50%

$$\ln(R1 + 0.89)$$
$$= -1.67 - 0.97 * A - 0.44 * B - 0.59 * C - 0.21 * A * B + 1.10$$
$$* A * C - 0.60 * B * C$$

reduction level 55%

$$\ln(R1 + 0.44)$$
$$= -1.25 - 0.46 * A + 0.85 * B - 0.51 * C - 0.096 * A * B$$
$$+ 1.18 * A * C - 0.89 * B * C$$